The University of British Columbia

FACULTY OF GRADUATE STUDIES

PROGRAMME OF THE

FINAL ORAL EXAMINATION

FOR THE DEGREE OF

DOCTOR OF PHILOSOPHY

of

PRABAKAR NAIDU

B.Sc. (Hons.), Indian Institute of Technology, Kharagpur (Calcutta), 1960

M.Tech., Indian Institute of Technology, Kharagpur (Calcutta), 1962

MONDAY, JULY 12TH, 1965, AT 10:30 A.M.

IN ROOM 206, CHEMICAL ENGINEERING BUILDING

COMMITTEE IN CHARGE

Chairman: J. R. MacKay

C. W. Clark	J. A. Jacobs
F. W. Dalby	R. D. Russell
G. P. Erickson	K. O. Westphal

External Examiner: A. J. H. Boerboom

FOM - Laboratory for Mass Separation

Amsterdam, The Netherlands

ION OPTICS OF THE MASS SPECTROMETER ION SOURCE

ABSTRACT

The ion beam transmission efficiency of the ion source is an important factor in determining the sensitivity of a mass spectrometer. Vauthier (1955) has shown for a simple source that the transmission efficiency is very low. The present thesis examines the transmission efficiency of a more complex source.

The first part of the thesis deals with the ion optical properties of a multiple slit ion source. The region of ion withdrawal has been sketched by computing the ion trajectories passing through the exit slit. It was found that for the more complex source the region of ion withdrawal is also much smaller than the total ionization space. It is not practical to confine the ionization region to the small volume from which ions are withdrawn. The effect of a source magnetic field has been taken into account. The perturbation of the trajectory due to the field is small, and therefore the mass discrimination due to the source magnetic field is imperceptible for heavy ions unless the field is of the order of a few webers/m^2.

The multiple slit ion source produces a divergent ion beam, only a small fraction of which penetrates the exit slit. Obviously a system producing a beam converging at the exit slit to a narrow parallel ribbon will be most efficient. In order to devise such a system a theory of the inverse problem of particle motion is developed in the second part of the thesis. A procedure was found to determine a potential distribution required to guide a group of particles along a set of prescribed paths. There are two important limitations to the choice of paths:

(a) there are certain paths which are not complete; that is a particle following such a path is turned back at certain points which we call mirror points.

(b) The particles which do not satisfy the initial conditions of uniform energy and direction may deviate considerably from their projected paths leading to what we have called an unstable situation.

Fortunately the complete paths are stable, and the incomplete paths are unstable. Of the two types of convergent paths studied, namely, exponentially decreasing and damped oscillatory paths, the system of damped oscillatory paths is stable.

GRADUATE STUDIES

Field of Study: Geophysics

Advanced Geophysics	J. A. Jacobs
Radioactive and isotopic processes in Geophysics	R. D. Russell
Modern Aspects of Geophysics	J. A. Jacobs

Related Studies:

Wave propagation	J. C. Savage
Electromagnetic theory	G. M. Volkoff
Digital computer programming	C. Froese
Introduction to quantum mechanics	F. W. Dalby

PUBLICATIONS

NAIDU, P. S. Telluric field and apparent resistivity over an inclined normal fault. (To appear in Canadian Journal of Earth Science.)

NAIDU, P. S., K. O. WESTPHAL. The inverse problem of particle motion and its application. (Read at Canadian Association of Physicists annual meeting held in June 1965).

The University of British Columbia

FACULTY OF GRADUATE STUDIES

PROGRAMME OF THE

FINAL ORAL EXAMINATION

FOR THE DEGREE OF

DOCTOR OF PHILOSOPHY

of

PRABAKAR NAIDU

B.Sc., (Hons.), Indian Institute of Technology, Kharagpur (Calcutta), 1960

M.Tech., Indian Institute of Technology, Kharagpur (Calcutta), 1962

MONDAY, JULY 5TH, 1965, AT 10:30 A.M.

IN ROOM 206, CHEMICAL ENGINEERING BUILDING

COMMITTEE IN CHARGE

Chairman: I. McT. Cowan

C. W. Clark	J. A. Jacobs
F. W. Dalby	R. D. Russell
G. P. Erickson	K. O. Westphal

External Examiner: A. J. H. Boerboom

FOM - Laboratory for Mass Separation

Amsterdam, The Netherlands

ION OPTICS OF THE MASS SPECTROMETER ION SOURCE

ABSTRACT

The ion beam transmission efficiency of the ion source is an important factor in determining the sensitivity of a mass spectrometer. Vauthier (1955) has shown for a simple source that the transmission efficiency is very low. The present thesis examines the transmission efficiency of a more complex source.

The first part of the thesis deals with the ion optical properties of a multiple slit ion source. The region of ion withdrawal has been sketched by computing the ion trajectories passing through the exit slit. It was found that for the more complex source the region of ion withdrawal is also much smaller than the total ionization space. It is not practical to confine the ionization region to the small volume from which ions are withdrawn. The effect of a source magnetic field has been taken into account. The perturbation of the trajectory due to the field is small, and therefore the mass discrimination due to the source magnetic field is imperceptible for heavy ions unless the field is of the order of a few webers/m^2.

The multiple slit ion source produces a divergent ion beam, only a small fraction of which penetrates the exit slit. Obviously a system producing a beam converging at the exit slit to a narrow parallel ribbon will be most efficient. In order to devise such a system a theory of the inverse problem of particle motion is developed in the second part of the thesis. A procedure was found to determine a potential distribution required to guide a group of particles along a set of prescribed paths. There are two important limitations to the choice of paths:

(a) there are certain paths which are not complete; that is a particle following such a path is turned back at certain points which we call mirror points.

(b) The particles which do not satisfy the initial conditions of uniform energy and direction may deviate considerably from their projected paths leading to what we have called an unstable situation.

Fortunately the complete paths are stable, and the incomplete paths are unstable. Of the two types of convergent paths studied, namely, exponentially decreasing and damped oscillatory paths, the system of damped oscillatory paths is stable.

GRADUATE STUDIES

Field of Study: Geophysics

Advanced Geophysics	J. A. Jacobs
Radioactive and isotopic processes in Geophysics	R. D. Russell
Modern Aspects of Geophysics	J. A. Jacobs

Related Studies:

Wave propagation	J. C. Savage
Electromagnetic theory	G. M. Volkoff
Digital computer programming	C. Froese
Introduction to quantum mechanics	F. W. Dalby

PUBLICATIONS

NAIDU, P. S. Telluric field and apparent resistivity over an inclined normal fault. (To appear in Canadian Journal of Earth Science.)

NAIDU, P. S., K. O. WESTPHAL. The inverse problem of particle motion and its application. (Read at Canadian Association of Physicists annual meeting held in June, 1965.)

ION OPTICS OF THE MASS SPECTROMETER ION SOURCE

by

PRABHAKAR SATYANARAYAN NAIDU

B.Sc. (Hon.), Indian Institute of Technology, Kharagpur, (Calcutta), 1960

M.Tech., Indian Institute of Technology, Kharagpur, (Calcutta), 1962

A THESIS SUBMITTED IN PARTIAL FULFILMENT OF

THE REQUIREMENTS FOR THE DEGREE OF

DOCTOR OF PHILOSOPHY

in the Department

of

GEOPHYSICS

We accept this thesis as conforming to the required standard

THE UNIVERSITY OF BRITISH COLUMBIA

May 1965

In presenting this thesis in partial fulfilment of the requirements for an advanced degree at the University of British Columbia, I agree that the Library shall make it freely available for reference and study. I further agree that permission for extensive copying of this thesis for scholarly purposes may be granted by the Head of my Department or by his representatives. It is understood that copying or publication of this thesis for financial gain shall not be allowed without my written permission.

Department of Geophysics

The University of British Columbia,
Vancouver 8, Canada

Date 15 Dec 61

Abstract

The ion beam transmission efficiency of the ion source is an important factor in determining the sensitivity of a mass spectrometer. Vauthier (1955) has shown for a simple source that the transmission efficiency is very low. The present thesis examines the transmission efficiency of a more complex source.

The first part of the thesis deals with the ion optical properties of a multiple slit ion source. The region of ion withdrawal has been sketched by computing the ion trajectories passing through the exit slit. It was found that for the more complex source the region of ion withdrawal is also much smaller than the total ionization space. It is not practical to confine the ionization region to the small volume from which ions are withdrawn. The effect of a source magnetic field has been taken into account. The perturbation of the trajectory due to the field is small, and therefore the mass discrimination due to the source magnetic field is imperceptible for heavy ions unless the field is of the order of a few webers/m^2.

The multiple slit ion source produces a divergent ion beam, only a small fraction of which penetrates the exit slit. Obviously a system producing a beam converging at the exit slit to a narrow parallel ribbon will be most efficient. In order to devise such a system a theory of the inverse problem of particle motion is developed in the second part of the thesis. A procedure was

found to determine a potential distribution required to guide a group of particles along a set of prescribed paths. There are two important limitations to the choice of paths:

(a) There are certain paths which are not complete; that is, a particle following such a path is turned back at certain points which we call mirror points.

(b) The particles which do not satisfy the initial conditions of uniform energy and direction may deviate considerably from their projected paths leading to what we have called an unstable situation.

Fortunately the complete paths are stable, and the incomplete paths are unstable. Of the two types of convergent paths studied, namely, exponentially decreasing and damped oscillatory paths, the system of damped oscillatory paths is stable.

TABLE OF CONTENTS

Table of Contents (continued)

LIST OF FIGURES

List of Figures (continued)

List of Figures (continued)

Acknowledgment

The writer wishes to express his sincere thanks to Drs. R. D. Russell and K. O. Westphal who supervised the research, and to Drs. W. F. Slawson and A. B. L. Whittles who made available certain information regarding the mass spectrometer of this laboratory. Thanks are also due to Dr. G. P. Erickson for reading the manuscript critically.

Professor J. A. Jacobs made it possible for the writer to come to the University of British Columbia, and has made the stay here both profitable and enjoyable through his stimulating lectures and through personal interest in his students.

The writer wishes to thank Dr. C. W. Clark of the Mathematics Department for his helpful discussion on the proof of the inverse problem. The writer was also considerably benefited from stimulating discussions with J. Allard.

The writer gratefully acknowledges the help received from the staff at the Computing Centre of the University of British Columbia.

Mr. John Blenkinsop has kindly proofread the manuscript.

The work was financed through the National Research Council of Canada grants to Drs. R. D. Russell and W. F. Slawson. The writer would like to express his gratitude for a National Research Council Studentship.

Chapter I

Sensitivity of mass spectrometer

1.1 Introduction

The mass spectrometer has become an important tool in the study of geological problems, as well as in many other branches of physics and chemistry. No matter what particular application with which the mass spectrometrist is involved he is interested in certain fundamental properties of his instrument. Specifically he is concerned with its ability to separate adequately ion beams of different ratios and its ability to produce ion beams of sufficient intensity for accurate measurement. This thesis is concerned more directly with the second consideration.

The sensitivity of a mass spectrometer depends largely upon the sensitivity of the measuring system and the efficiency of the ion source. The shot noise represents a fundamental limitation of the ion beam magnitude which can be measured, but practical consideration may also present further limitations. It is very much more difficult to specify the fundamental limitations of the ion source efficiency.

To a casual observer the efficiency of the source would appear to be particularly poor. For the mass spectrometer operated in this laboratory one molecule out of a million molecules reaches the magnetic analyser tube in form of an ion, which compares well with the figures quoted by Mayne (1960) as 10^{-4} to 10^{-7}. It is natural to look more deeply into the loss of such a large fraction of the sample.

The efficiency of the source may be thought of as a product of two factors: the first is the ionization efficiency, that is, the fraction of neutral molecules ionized by the electron beam; and the second is the ion beam transmission efficiency, that is, the fraction of beam ultimately entering the magnetic analyser tube. To increase the ionization efficiency, we may increase either the ionizing electron current or the prevailing gas pressure. Unlimited electron current, however, cannot be obtained from an electron gun without impairing the stability or reducing the life of the filament. On the other hand, the prevailing gas pressure cannot be increased indefinitely without enhancing the scattering of the ion beam by the neutral gas molecules and causing other problems.

The electrons may be concentrated in a tight beam by a uniform magnetic field in the direction of the electron beam and thus the scattering of the beam can be minimized. Since the electrons spiral around the magnetic lines of force, the effective path length of an electron is increased. The effective path length is given by

$$L' = \sqrt{\left(1 + \frac{V_r^2}{V_z^2}\right)} \cdot L$$

where L and L' are respectively the normal path length in the absence of magnetic field and the effective path length in the presence of magnetic field, and V_r and V_z are respectively the transverse and longitudinal velocity components. As mentioned in Appendix A it is questionable whether the increase in path length is significant.

The ion optical system of the ion source consists of a stack of parallel plates carrying long but narrow, parallel, coplaner slits (fig. 1.1). The function of the system is to draw the ions from the ion chamber, to accelerate them to the desired energy, and to inject them into the magnetic analyser tube as a narrow nondiverging beam. Such ions, according to Vauthier (1955), are drawn from a narrow strip, whose width is equal to the exit slit (fig. 1.2). Consider the ion source of the mass spectrometer of this laboratory. The width of the region of ionization (roughly equal to the width of the electron beam) is about 0.5 cm.; the width of the exit slit is 0.01 cm. The efficiency of ion beam transmission, therefore, is equal to 0.02.

1.2 Ion optics of the source (review):

The basic design of the ion source used in modern gas source mass spectrometry has not changed since its first appearance in 1947, then designed by Nier. The ion source used in this laboratory, which is a version of the Nier source, is shown in fig. 1.1. The ion optics of the complete system is not known, except the approximate analyses of the specialized versions given by Jacob (1950), Vauthier (1955), Dietz (1959), and Boerboom (1960).

Jacob (1950) considered the ion optics of a system consisting of a cathode, entrance plate, and anode plate. He measured the axial potential of the system in an electrolytic tank (Einstein and Jacob, 1948); the data according to him could be represented, close to the cathode, by

$$V = A \cdot \sinh(\kappa x)$$

where V is the potential, A and κ are the constants; and away from the cathode by

$$V = A \exp(\kappa x)$$

A closed solution of the paraxial trajectory equation (see page 15)

$$2V \cdot y'' + V'y' + V''y = 0 \qquad (1.1)$$

where the prime denotes differentiation with respect to x , was given by him. The method besides being approximate cannot be used over a wide range, because the approximation of the axial potential by an exponential function is not valid over such a wide range. Vauthier (1955) considered a single plate with a narrow slit and uniform field on its right hand side. In the paraxial equation (1.1), he dropped off the first term and the rest he integrated numerically. Obviously such a method is only approximate. Dietz (1959) considered a system consisting of a cathode, entrance plate, and deflector plates. He measured the potential distribution in the system from an analog model on conducting paper and drew the trajectories using the trigonometric method (Jacob, 1951). In regard to the use of conducting paper, it has been the experience of the present writer (Naidu, 1962) that the precision of potential measurement is limited to about ±5%. Furthermore, the trigonometric method requires the potential difference between the two consecutive refracting surfaces to be small, which is difficult to attain, particularly close to the slit, where the gradient is very large. Hence, to meet the conditions of the method, we have to take a large number of small steps, which, inevitably, introduces a large

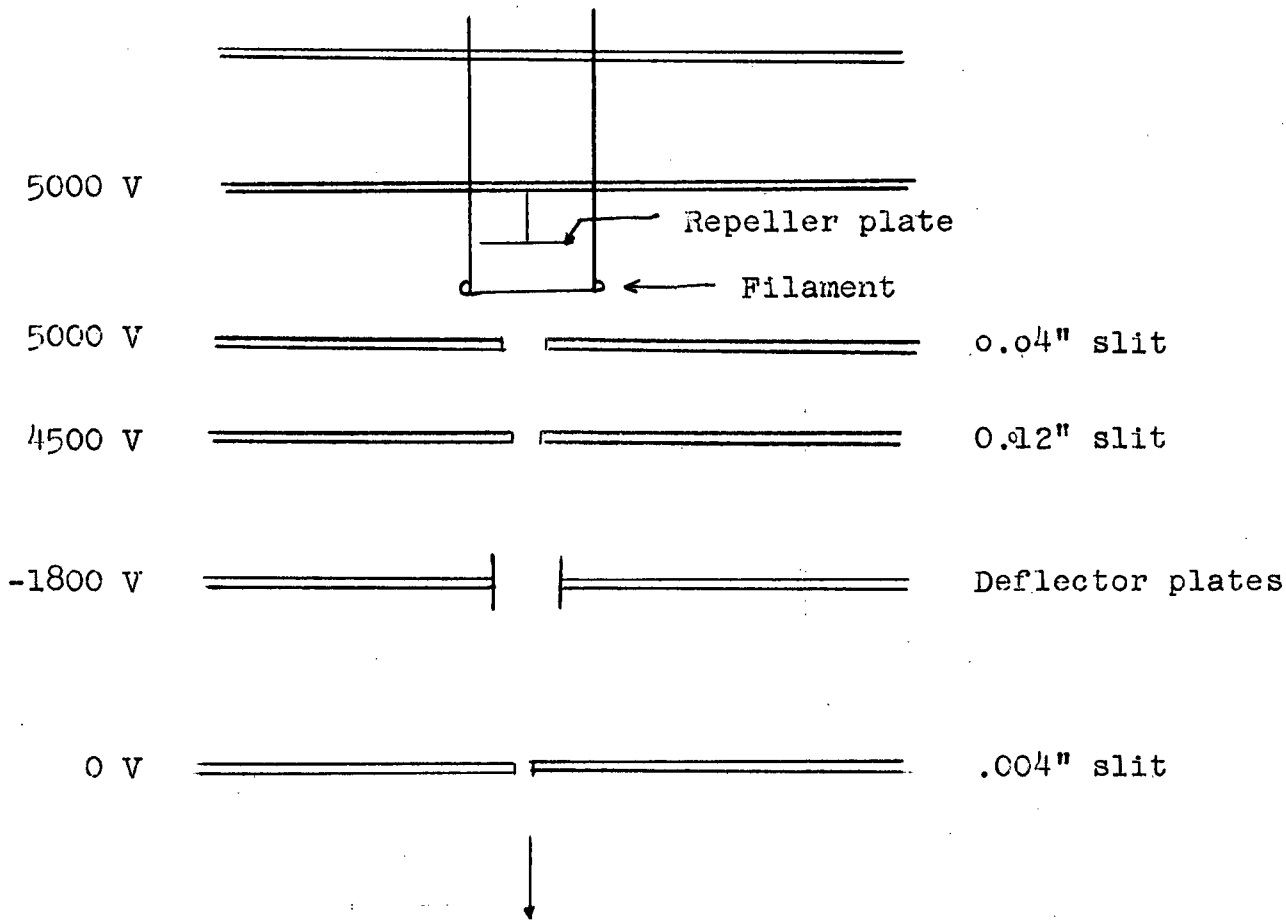

Fig. 1.1

Approximate sketch of the multiple slit ion source used in the mass spectrometer of this laboratory (adopted from J. S. Stacey's thesis, 1962).

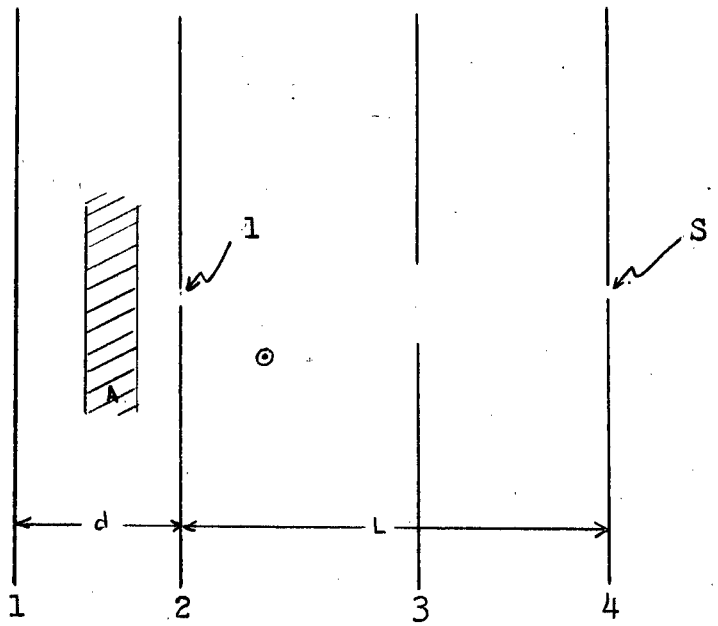

S < 1

L = 40

Fig. 1.2

Mathematical model of a multiple slit ion source. Plates extend to ∞

A . . . . Ionization space

1 . . . . Repeller plates

2 . . . . Entrance slit plate

3 . . . . Deflector plates

4 . . . . Exit slit plate

⊙ . . . . Magnetic field normal to the plane of paper

numerical error. Lastly, Boerboom considered a system of three plates, but he ignored while computing the ion trajectories the perturbation field due to the slits. Furthermore, he has not discussed the ion beam transmission efficiency of the source.

We shall compute the ion trajectories in the ion source (fig. 1.1) which is far more complex than any discussed by the previous authors. The basic problem is to find what fraction of the total number of ions formed in the ionization space (A in fig. 1.2) finds its way through the exit slit. This, naturally, demands a complete study of the system.

1.3 Statement of the problem and scope of the present work.

In the previous sections we have attempted to outline the factors limiting the sensitivity of a mass spectrometer. Poor ion beam transmission appears to be a main limiting factor. The broad purpose of the present work is to study the process of ion beam transmission, in the hope that such a study may contribute to the design of a better source. With this in mind, we set forth the following problems:

(a) To study the ion optical properties of the system shown in figure 1.2; thereby to maximize the parameters for optimum efficiency.

(b) To consider an inverse problem; that is, having specified the beam shape for maximum efficiency, to obtain the potential distribution required to guide the ions along the specified paths.

The mathematical theory of particle motion through a system

of slits representing an average source is developed in the second chapter. The potential distribution in the system is obtained analytically, and the trajectory equation is integrated numerically.

The theory of the inverse problem and its application to ion beam transmission are presented in the third chapter. A new method of estimating the effect of the thermal energy is developed.

The last chapter summarizes the main contributions of the present thesis.

Chapter II

Multiple slit ion source

Synopsis

The motion of charged particles through a system of parallel and coplaner slits in the presence of crossed electromagnetic field is considered. The equation of a trajectory in non-parametric, time independent form is derived from basic considerations. The approximations leading to a linear paraxial equation are clearly stated. The solution of the paraxial trajectory equation is approached in two different ways; that is, (a) part-by-part approach and (b) global approach. The part-by-part approach provides a physical insight into the problem and it is relatively simple but less precise; on the other hand, the global approach, though more precise, is mathematically involved. Finally the efficiency of the ion beam transmission is discussed in the light of ion optical properties of the system.

2.1 Equation of trajectory

The force exerted by an electric $\vec{E}$ and magnetic field $\vec{B}$ on a charge q and mass m moving with a velocity $\vec{v}$ is given by

$$\vec{F} = q(\vec{E} + \vec{v} \times \vec{B})$$

where we assume $v \ll c$, and where c is the velocity of light.

$$\therefore \quad m \frac{d\vec{v}}{dt} = q(\vec{E} + \vec{v} \times \vec{B}) \tag{2.1}$$

Let us consider the motion in the x,y-plane, where

$$\vec{E} = \vec{i} E_x + \vec{j} E_y \tag{2.2}$$

and

$$\vec{B} = \vec{k} B_z \tag{2.3}$$

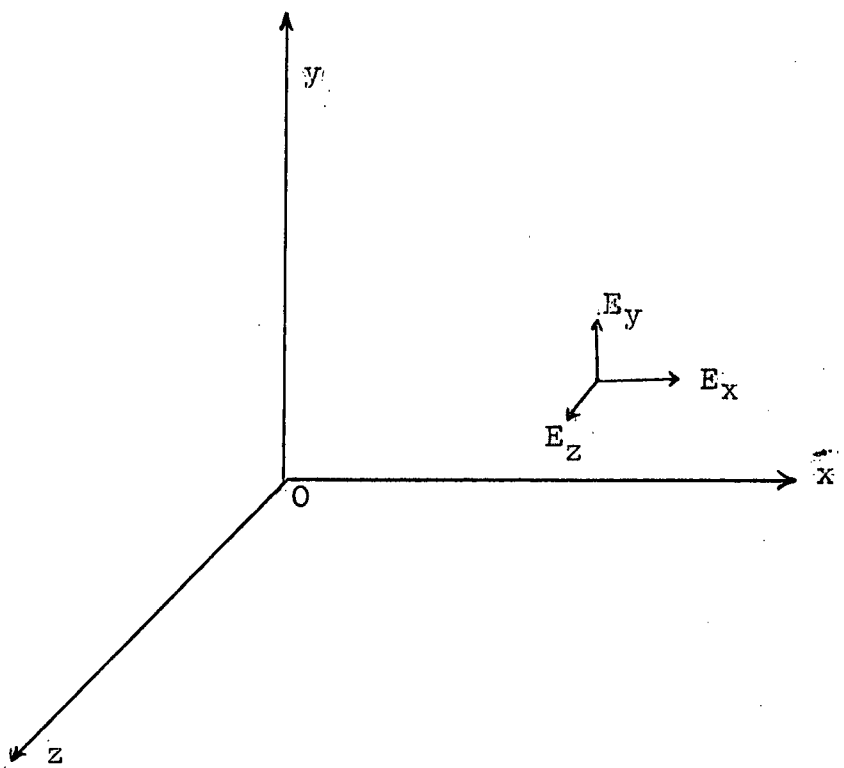

Fig. 2.0

Right-handed co-ordinate system used throughout the present work.

subscripts x, y, and z identify the x, y, and z components of the field respectively (fig 2.0). On substituting equations (2.2) and (2.3) into (2.1), we obtain the system of equations

$$\ddot{x} = q/m\,(E_x + B_z \dot{y}) \qquad (2.4)$$

and

$$\ddot{y} = q/m\,(E_y - B_z \dot{x}) \qquad (2.5)$$

where the dot(.) indicates differentiation with respect to time t. We may now express the equations (2.4) and (2.5) in non-parametric form, i.e., independent of time t. Multiplying (2.4) with $d\dot{x}$ and (2.5) with $d\dot{y}$, integrating, and adding we finally obtain

$$q \cdot \Delta V = \tfrac{1}{2} m(\dot{x}^2 + \dot{y}^2) \qquad (2.6)$$

where $q \cdot \Delta V$ is the net change in the potential energy of a particle plus the initial energy. From (2.6) we obtain

$$(\dot{x})^2 = 2q/m\,\left(\frac{\Delta V}{1+y'^2}\right)$$

$$(\dot{y})^2 = \frac{2q}{m} \cdot \left(\frac{\Delta V}{1+1/y'^2}\right)$$

where the prime stands for the differentiation with respect to x. But

$$\ddot{y} = \frac{d}{dt}(\dot{x}\,y')$$

$$= y''(\dot{x})^2 + y'\ddot{x}$$

and substituting into (2.5) we obtain

$$y'' \cdot \frac{2q}{m}\frac{\Delta V}{1+y'^2} + y'\frac{q}{m}\left(E_x + B_z\sqrt{\frac{2q}{m}\left(\frac{\Delta V y'^2}{1+y'^2}\right)}\right) =$$

$$= \frac{q}{m} \cdot \left(E_y - B_z \sqrt{\frac{2q}{m} \frac{\Delta V}{1+y'^2}} \right)$$

or

$$\frac{2\Delta V}{1+y'^2} y'' + E_x y' - E_y + B_z \sqrt{\frac{2q}{m} \Delta V (1+y'^2)} = 0 \qquad (2.7)$$

The above equation is the basic equation describing the motion of a charged particle under the influence of a two dimensional electric field and a magnetic field along the z-axis. When $B_z = 0$, the equation reduces to

$$\frac{2\Delta V}{(1+y'^2)} y'' + E_x y' - E_y = 0 \qquad (2.8)$$

Equation (2.8), for the case of an electric field, was derived by Euler (1773) using the variational principle. For the sake of simplicity we shall express E_x and E_y in terms of the potential difference .

$$\Delta V = V_0 - V + \epsilon$$
$$= \Omega$$

where V_0 is the potential at x_0, the starting point and ϵ the initial energy divided by the charge. Since

$$E_x = -\frac{\partial V}{\partial x}$$

and

$$E_y = -\frac{\partial V}{\partial y}$$

$$\therefore E_x = \frac{\partial \Omega}{\partial x}$$

$$E_y = \frac{\partial \Omega}{\partial y}$$

The new symbol Ω actually refers to the energy of the particle (it has all the properties of a potential function), and we hence continue to call it potential. Introducing these changes into the equations (2.7) and (2.8), we obtain

$$\frac{2\Omega y''}{(1+y'^2)} + \Omega_x y' - \Omega_y + B_z \sqrt{\frac{2q}{m}(1+y'^2)\Omega} = 0$$

(2.9)

and

$$\frac{2\Phi y''}{(1+y'^2)} + \Phi_x y' + \Phi_y = 0 \qquad (2.10)$$

Paraxial approximations:

Equation (2.9) may be considerably simplified if we restrict ourselves to the paraxial region, that is, the region close to the x-axis. If the potential Φ is symmetric about the x-axis, we may write

$$\Phi(x,y) = \Phi_0(x) + \Phi_1(x)y^2 + \Phi_2(x)y^4 \cdots + \Phi_n(x)y^{2n} \qquad (2.11)$$

The above equation has to satisfy the Laplace equation. On substituting (2.11) into the Laplace equation and letting the coefficients of y^m $(m = 0 \cdots 2n)$ to 0 we obtain

$$\Phi(x,y) = \Phi_0 - \frac{\Phi_0''}{2!}y^2 + \frac{\Phi_0^{IV}}{4!}y^4 + \cdots\cdots (-1)^n \frac{\Phi_0^{2n}}{(2n)!}y^{2n} \qquad (2.12)$$

where the superscripts on Φ_0 denote the order of differentiation with respect to x. Equation (2.12) may be looked upon as the Taylor's series expansion of Φ around the x-axis. Sufficiently close to the axis, we may truncate the series to first two terms, viz:

$$\Phi(x,y) = \Phi_0 - \frac{\Phi_1''}{2!}y^2$$

Therefore

$$\Phi_x = \Phi_0' - \frac{\Phi'''}{2!}y^2$$

$$\simeq \Phi_0'$$

and finally

$$\Phi_y = -\Phi_0''y$$

$$\Phi \simeq \Phi_0$$

We further assume that $(1+y'^2) \approx 1$, since $y' << 1$. Introducing these approximations into equation (2.9), we obtain*

$$2\Phi_0 y'' + \Phi_0' y' + \Phi_0'' y + B_z\sqrt{\frac{2q}{m}}\Phi_0 = 0 \qquad (2.13)$$

and when $B_z = 0$

$$2\Phi_0 y'' + \Phi_0' y' + \Phi_0'' y = 0 \qquad (2.14)$$

Equations (2.13) and (2.14) contain the physical and geometrical parameters; in order to reduce them to as few as possible, we introduce the dimensionless quantities X, Y, and Φ defined by

$$x = \omega X$$
$$y = \omega Y$$
$$\Phi_0 = K \Phi_0$$

where ω and K are the constants with the dimensions of length and potential respectively. We finally obtain the dimensionless form

$$2\Phi_0 Y'' + \Phi_0' Y' + \Phi_0'' Y + B_z \omega\sqrt{\frac{2q}{m}\frac{\Phi_0}{K}} = 0 \qquad (2.15)$$

and

$$2\Phi_0 Y'' + \Phi_0' Y' + \Phi_0'' Y = 0 \qquad (2.16)$$

where the quantity $\omega B_z\sqrt{\frac{2q}{mK}}$ is dimensionless.

It is interesting to note some of the properties of equation (2.16):

(a) since the equation is independent of K, the trajectory is independent of the actual magnitude of the potential, but dependent on the geometry of the potential distribution.

* Equation 2.13 was first derived by Boerboom (1957) using variational calculus.

(b) if we replace X by $-x$ equation (2.16) remains invariant. Physically speaking, a particle may travel in a positive or negative direction; such an ambiguity in direction will play an important role in the next chapter.

2.2 Method of solution

A closed solution of the paraxial equation can be obtained only for a few simple forms of the potential Φ_0 : for example, when the potential is of the form given by

$$\Phi_0 = ax^2+bx+c \tag{2.17}$$

Without going into the details, the solution of equation (2.16) may be given by(Shibata, 1960)

$$Y = A\cos\sqrt{a}\,z + B\sin\sqrt{a}\,z$$

where

$$z = \frac{1}{\sqrt{a}}\ln\left(\sqrt{ax^2+bx+c} + x\sqrt{a} + \frac{b}{2\sqrt{a}}\right) \qquad a>0$$

and

$$z = \frac{-1}{\sqrt{-a}}\cdot\sin^{-1}\left(\frac{ax+b}{\sqrt{b^2-4ac}}\right) \qquad a<0$$

Unfortunately, the potential even for a single slit, not to speak of a system of slits, cannot be represented by (2.17); therefore, the above method is of little use and we have to resort to numerical integration.

One could, of course, approximate any potential over a sufficiently small range by (2.17) and then apply the closed solution given above. But such a procedure, besides being as time-consuming as a numerical integration, is definitely a disadvantage over the numerical integration, in particular in studying the motion of particles which do not satisfy the paraxial conditions.

The Runge-Kutte method, though not the most accurate one--the question of error is a difficult one--is nevertheless a stable method, and that is what was mostly needed for our work. The question of round-off errors is discussed in Appendix B.

Before turning to the study of the actual slit system, an important point that was so far neglected by the previous workers (Vauthier, 1955) is discussed below. If a particle were to start at $X = o$ from rest, that is $\Phi_o = o$; it follows from the equation (2.16) that the direction $Y'(o)$ along which the particle moves and $Y(o)$, the distance from the axis, are no longer independent of each other. From (2.16) it follows that

$$Y'(o) = -\frac{\Phi_o''}{\Phi_o'} \; Y(o)$$

that is, the direction of motion is fixed for a given value of $Y(o)$. This leads to the following complications which was overlooked by the previous workers. For numerical integration the equation (2.16) is usually written in the form

$$Y''(x) = -\frac{1}{2}\,\frac{\Phi_o''(x)\,Y + \Phi_o'(x)\,Y'}{\Phi_o(x)} \qquad (2.18)$$

Using a step-by-step method, starting at $X = o$, the right hand side becomes $\frac{o}{o}$, an indeterminate form. This difficulty was overcome by Vauthier by assuming $\Phi_o(x)$ very small but not zero. The present author has found that the above assumption leads to considerable error. The indeterminateness, however, can be removed by applying L'Hospital's rule.

If a magnetic field is present, an additional complication arises, which is discussed in Appendix B.

The numerical computations were carried out on the IBM 7040 at the Computing Centre of the University of British Columbia.

2.3 Subproblems

After having derived the trajectory equation and having discussed the necessary numerical methods to solve the equation we proceed to analyse the mathematical model of a multiple slit source (fig 1.2). We adopt two different approaches, namely:

(a) The analysis by parts, that is, the model is considered part by part, in particular, the effect of each part on the ion trajectory.

(b) The global analysis, that is, the system is considered as a whole.

Although the analysis by parts is not as rigorous as the global analysis, it provides a considerable insight into the problem. The global analysis, on the other hand, is much more accurate but leads, as we shall see later, to a system of non-linear algebraic equations, the solution of which is a problem in itself. Since the physical understanding of the effect of each part upon the ion trajectory is more important than the rigour in the analysis we have emphasised on the analysis by parts.

We shall now divide the problem into five parts and treat each one of them as a separate subproblem.

(a) Entrance slit plate with uniform field on both sides of the plate (fig 2.1a).

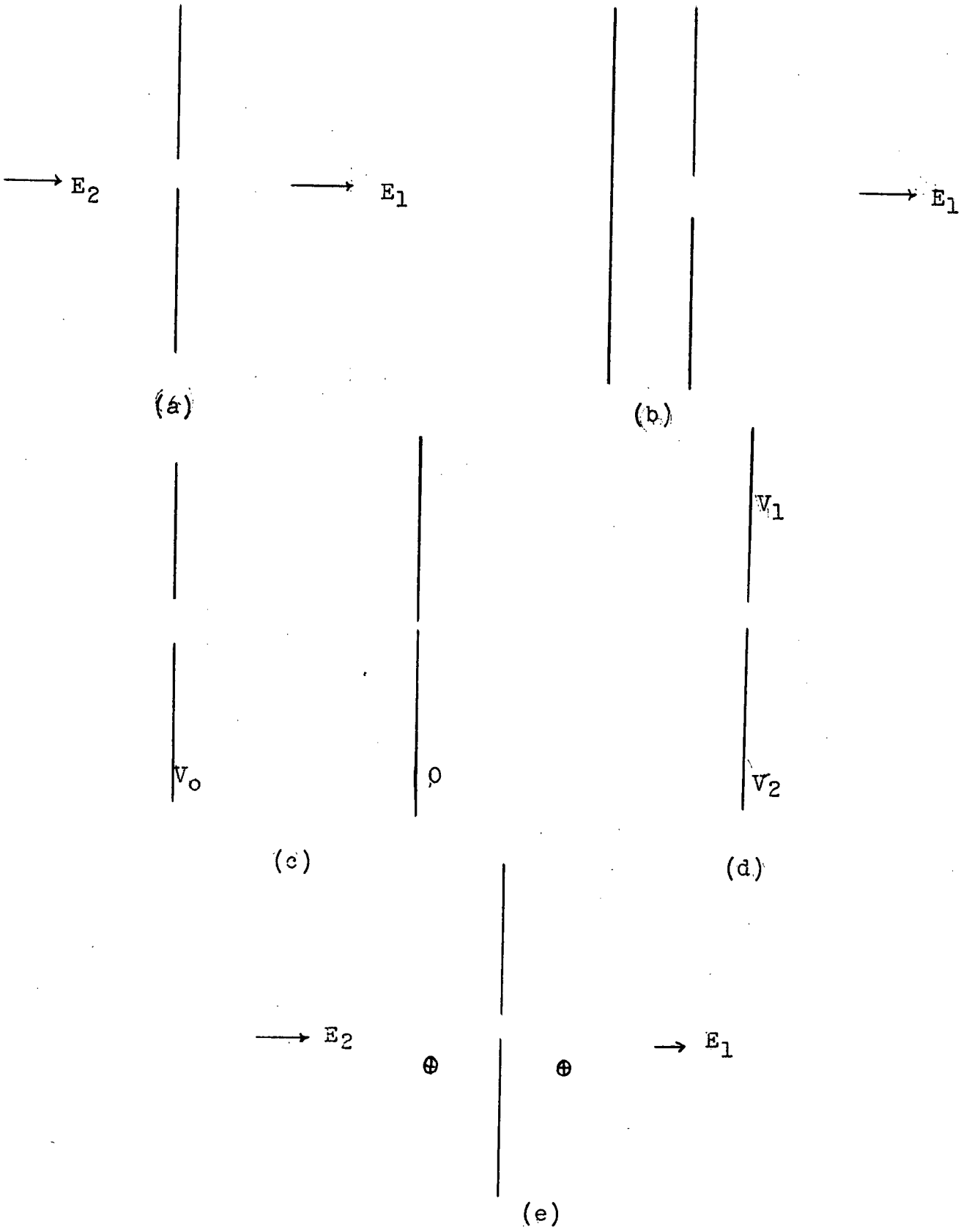

Fig. 2.1

Geometry of various subproblems.

(b) Entrance slit plate and repeller plate (fig 2.1b).

(c) Entrance slit and exit slit plate (fig 2.1c)

(d) Deflector plates (fig 2.1d)

(e) Magnetic field in the source region (fig 2.1e)

In case of each one of the above subproblems we first obtain the potential distribution using the method of conformal transformation, and then integrate the paraxial equation.

Subproblem (a)

A convenient method of solving a two dimensional boundary value problem is by the method of conformal transformation. Under a conformal transformation, the Laplace equation and homogenous boundary conditions remain invariant. A mapping function that maps the u-axis of the w-plane into two semi-infinite plates in the z-plane (see fig 2.3 for details of mapping) is given by

$$Z = P\left(w + \frac{1}{w}\right) \qquad (2.19)$$

where P is constant. If the slit width is $i \cdot 1$ $(i=\sqrt{-1})$, we obtain from (2.19)

$$P = -i/4$$

The boundary value problem now reduces to finding the solution of the Laplace equation in the w-plane, which satisfies the boundary conditions:

$$V = 0 \qquad \text{on the u-axis}$$

$$V \longrightarrow E_1 \, Re\left(P w\right)_{w \to \infty}$$

$$V \longrightarrow E_2 \, Re\left(P/w\right)_{w \to 0}$$

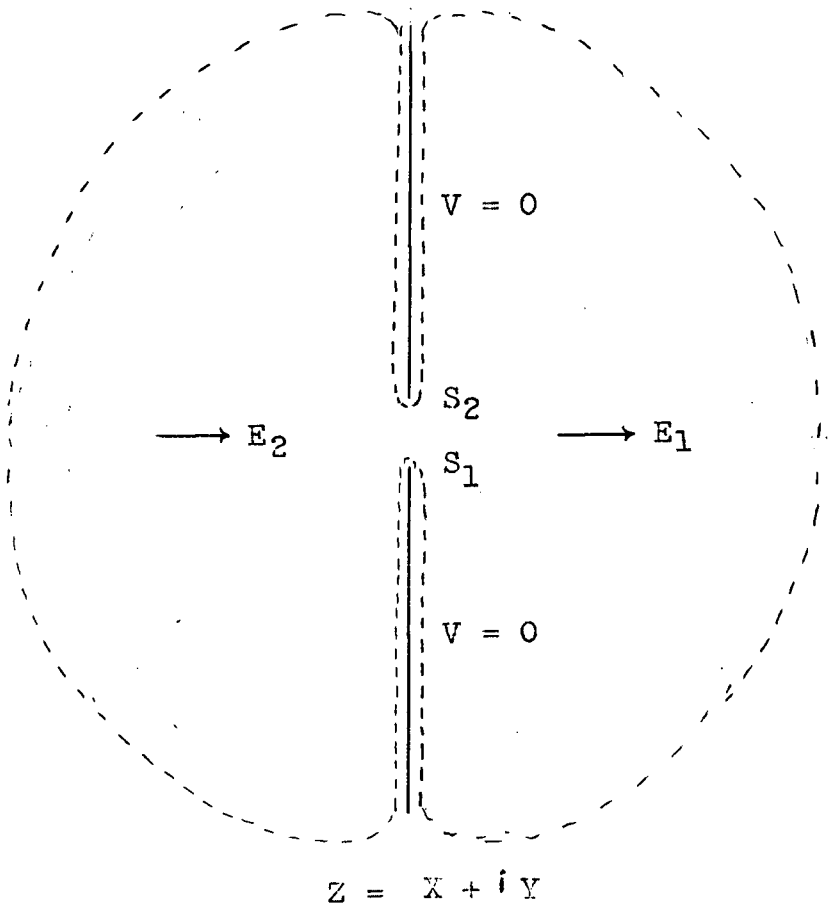

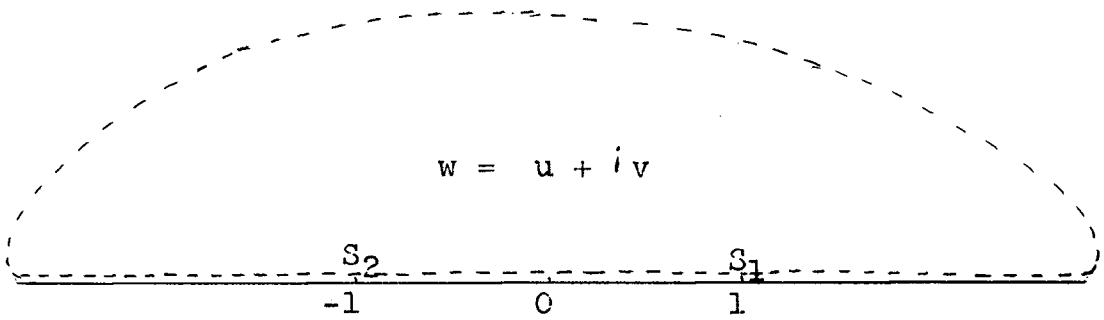

Fig. 2.2

Conformal mapping of the $w > o$ plane onto the whole of Z-plane by Schwarz-Christoffel method.

$$\frac{dz}{dw} = P \cdot (w+1)^{+1} (w-1)^{+1} w^{-2}$$

Consider a function $V(u,v)$ as defined by

$$V(u,v) = Re\left(P\left(E_1 W + \frac{E_2}{W}\right)\right) \qquad (2.20)$$

we see that the above function satisfies the Laplace equation and the boundary conditions. To map this potential onto the z-plane, we note that equation (2.19) may be expressed as

$$W = \frac{1}{2P}\left(Z \pm \sqrt{Z^2 - 4P^2}\right)$$

and

$$\frac{1}{W} = \frac{1}{2P}\left(Z \mp \sqrt{Z^2 - 4P^2}\right)$$

On substituting in (2.20) we obtain

$$V(X,Y) = \frac{1}{2}\left[E_1\, Re\left(Z + \sqrt{Z^2-4P^2}\right) + E_2 Re\left(Z - \sqrt{Z^2-4P^2}\right)\right] \qquad (2.21)$$

Allard and Russell (1963) considered a similar problem (but assumed $E_2 = 0$) and gave numerical values of potential distribution around the slit. However, they did not express the potential distribution in a convenient form as in equation (2.21). If we let $Y = 0$, we obtain the axial potential

$$V_0(X) = \frac{1}{2} E_1\left(X + \sqrt{X^2+0.25}\right) + \frac{1}{2} E_2\left(X - \sqrt{X^2+0.25}\right) \qquad (2.22)$$

We are now in a position to integrate the paraxial equation noting $\Phi(X) = V_0(0) - V_0(X)$. Two cases have been investigated:

(i) $E_2 = 0, E_1 \neq 0$ (exact value is not necessary), that is, a particle under the influence of accelerating field only.

(ii) $E_2 \neq 0, E_1 \neq 0$ that is, the particle is under the influence of the repeller field and the accelerating field.

A few typical trajectories for case (i) of the particles starting

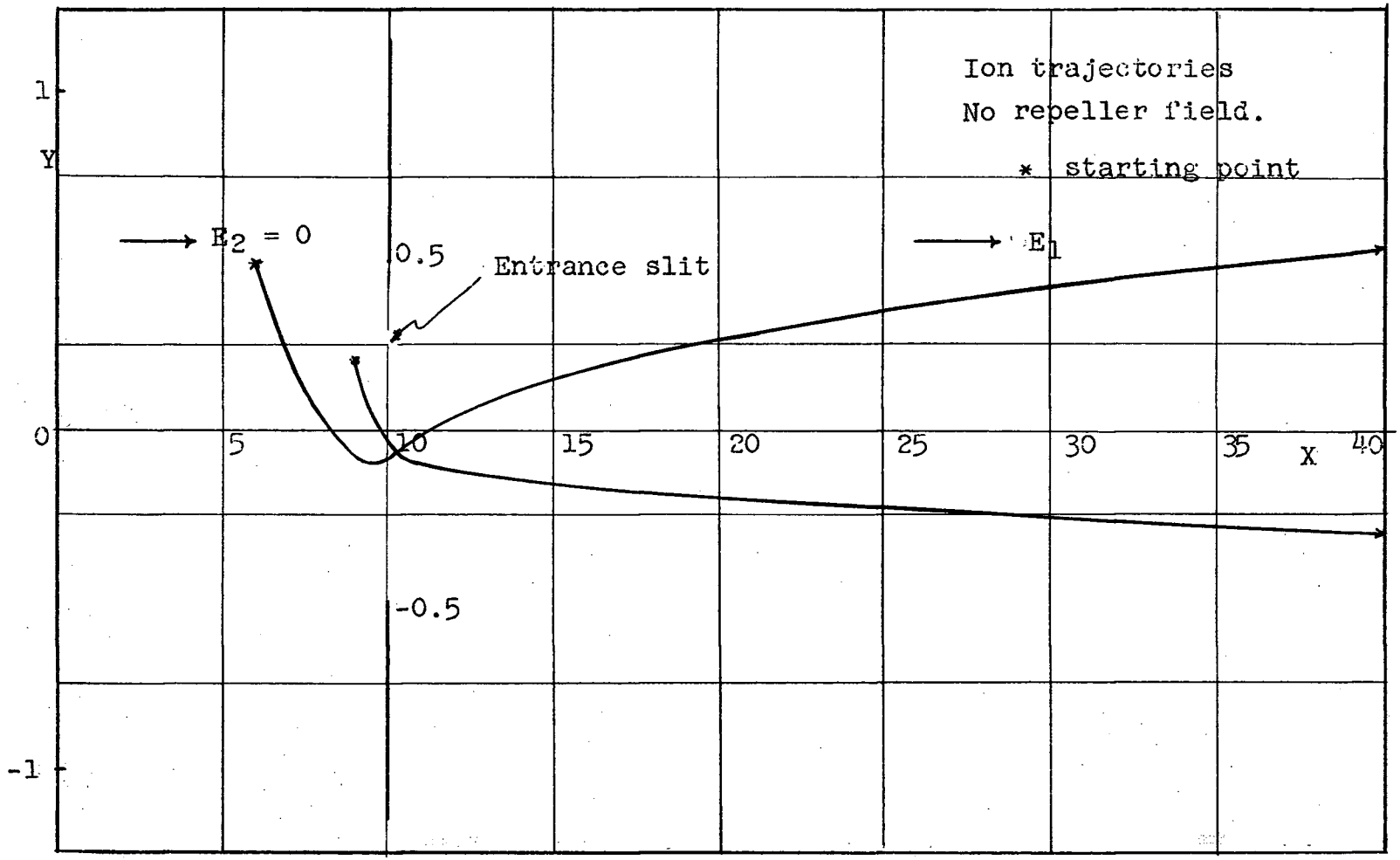
Ion trajectories
No repeller field.
* starting point
$E_2 = 0$
E_1
Entrance slit
0.5
-0.5
1
Y
0
-1
5
10
15
20
25
30
35
40
X

Fig. 2.3

from rest are shown in fig. (2.3). The general shape of the trajectories is illustrated in fig. (2.4). It has, as shown, two cross-overs x_{c_1} and x_{c_2}, the positions of which depend upon the starting plane $\rho(x_0)$ and the ratio E_2/E_1. Figures (2.5) and (2.6) illustrate the relationship between the position of cross-overs and the parameters x_0, the starting plane, and E_2/E_1, the ratio of repeller field to the accelerating field. We see from fig. (2.5) that, when most of the ions ($x_0 < -3$) are focused a short distance away from the slit. The portion of the trajectory from the second cross-over onwards may be approximated by a quadratic function

$$x = m y^2 + y/s + x_{c_2} \qquad (2.23)$$

where m is a constant depending upon x_0 and E_2/E_1, and s is the slope of the trajectory at the second cross-over and also a function of x_0 and E_2/E_1. It may be interesting to note that equation (2.23) is also the equation of trajectory in a uniform field; therefore, it appears that the effect of the slit width does not extend beyond a distance equal to a few slit widths.

In the presence of E_2, however, the ions are no longer focused a short distance from the slit, but, depending upon E_2/E_1, over a considerable length along the axis. (See section 2.5 for further discussion.)

The approximations made to linearize the trajectory equation giving the paraxial equation are usually very restrictive and are valid only within the close neighborhood of the axis. Most

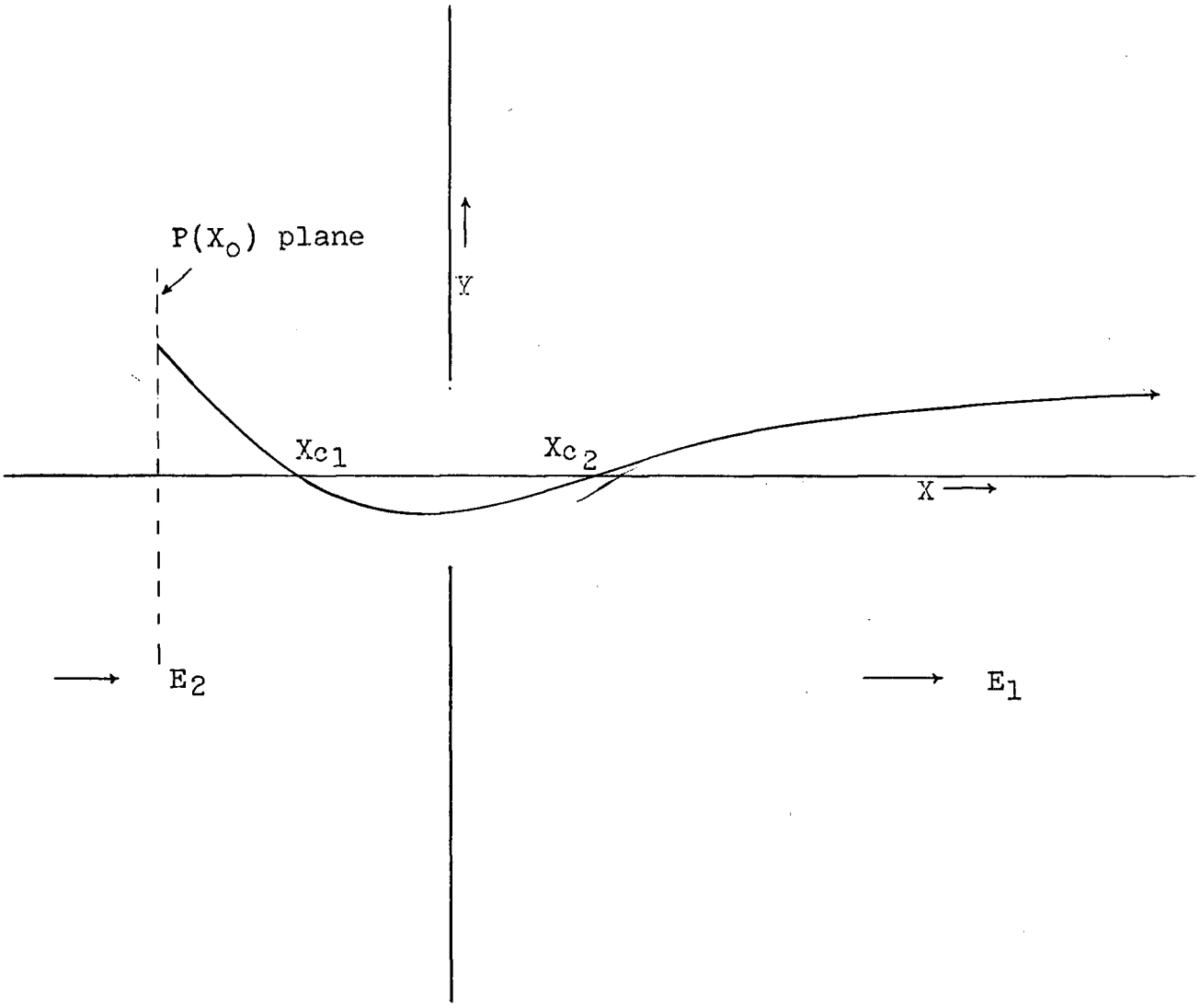

Fig. 2.4

Graphical illustration of a representative trajectory. The position of cross-over X_{c_1} and X_{c_2} depends upon the starting plane $P(X_o)$ and E_2/E_1.

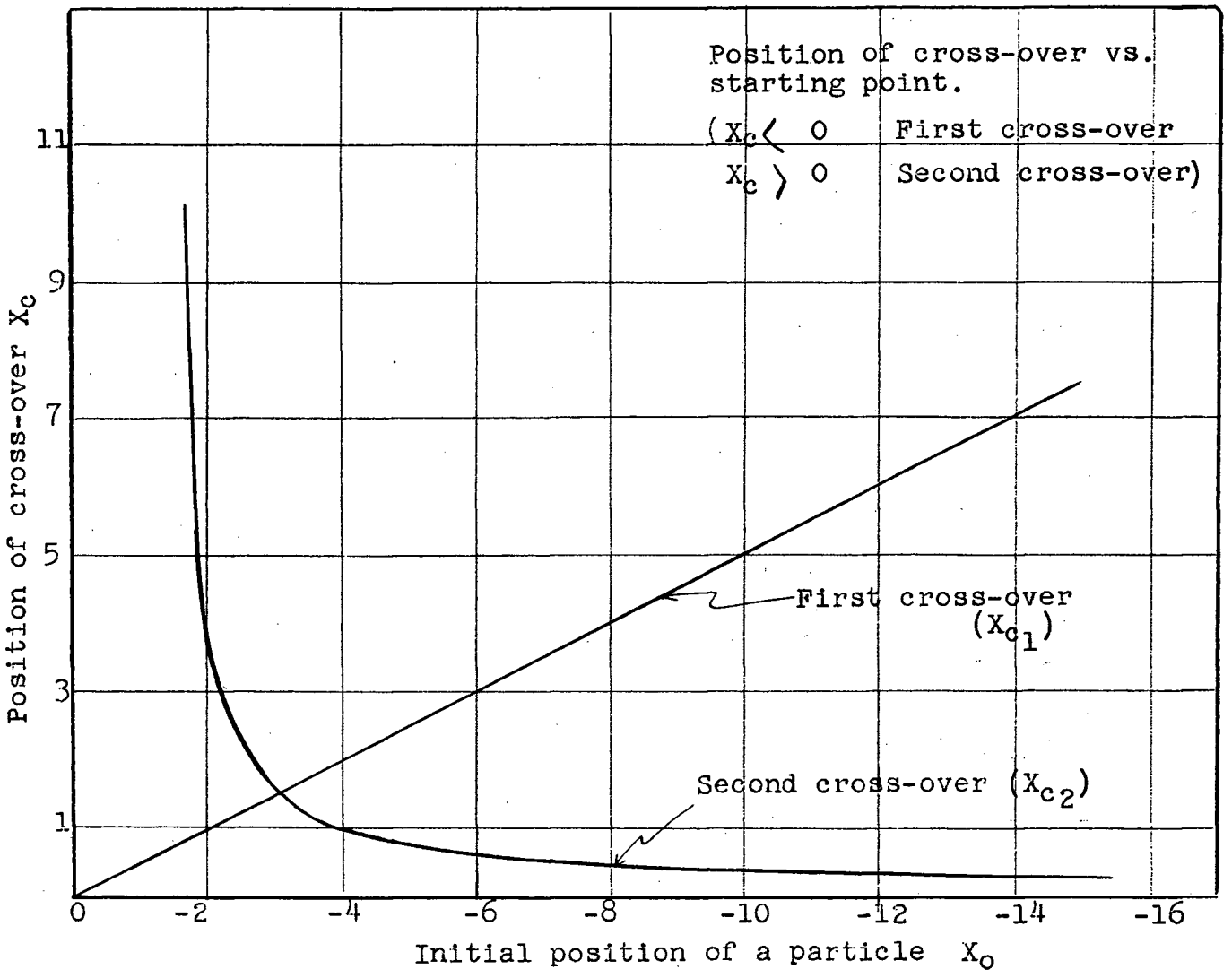
Position of cross-over vs. starting point.
(X_c < 0 First cross-over
X_c > 0 Second cross-over)
First cross-over (X_{c_1})
Second cross-over (X_{c_2})
Position of cross-over X_c
Initial position of a particle X_o
11
9
7
5
3
1
0
-2
-4
-6
-8
-10
-12
-14
-16

Fig. 2.5

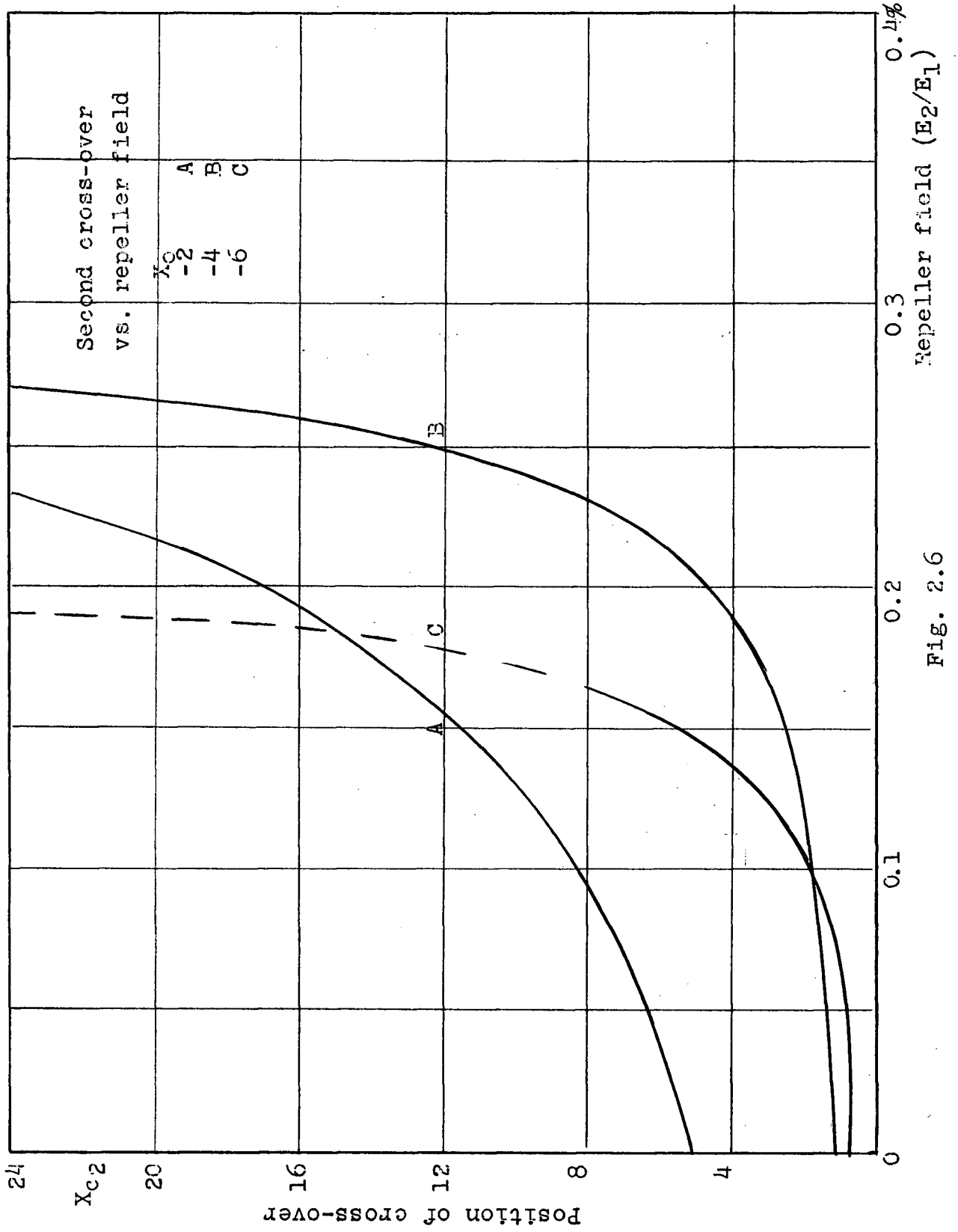
Second cross-over
vs. repeller field
X_o
-2 A
-4 B
-6 C
X_{c2}
24
20
16
12
8
4
0
0.1
0.2
0.3
0.4%
Repeller field (E_2/E_1)
Position of cross-over

Fig. 2.6

authors seem to be satisfied with the approximations without stating how far from the axis one can go without violating them. But we felt it necessary to sketch the region around the axis where the paraxial approximation will lead to an error less than a certain predetermined value.

The potential distribution around the axis is approximated by a series

$$V(x,Y) = V_0 - \frac{V_0''}{2!}Y^2 + \frac{V_0^{IV}}{4!}Y^4 \cdots (-1)^n \frac{V_0^{2n}}{(2n)!}Y^{2n} \cdots$$

The series is found to be convergent within a domain bounded by a curve A in fig. (2.17). If we take the first two terms only, as was done in the paraxial approximation, the region where the first two terms are adequate is shown by curve B in fig. (2.7). To test the net effect of the various approximations, and thus to determine the region of validity, we approximate the exact equation (2.16) to the increasing degree of severity:

(a) Exact equation

$$\frac{2\Phi Y''}{1+Y'^2} + \Phi_x Y' - \Phi_Y = 0 \qquad (2.24a)$$

(b) Taking the first two terms

$$\frac{2\left(V_0 - \frac{V_0''}{2}Y^2\right)Y''}{(1+Y'^2)} + \left(V_0' - \frac{1}{2}V_0'''Y^2\right)Y' + V_0''Y = 0 \qquad (2.24b)$$

(c) Non-linear paraxial equation

$$\frac{2\Phi_0 Y''}{(1+Y'^2)} + \Phi_0' Y' + \Phi_0'' Y = 0 \qquad (2.24c)$$

and (d) Linear paraxial equation

$$2\Phi_0 Y'' + \Phi_0' Y' + \Phi_0'' Y = 0 \qquad (2.24d)$$

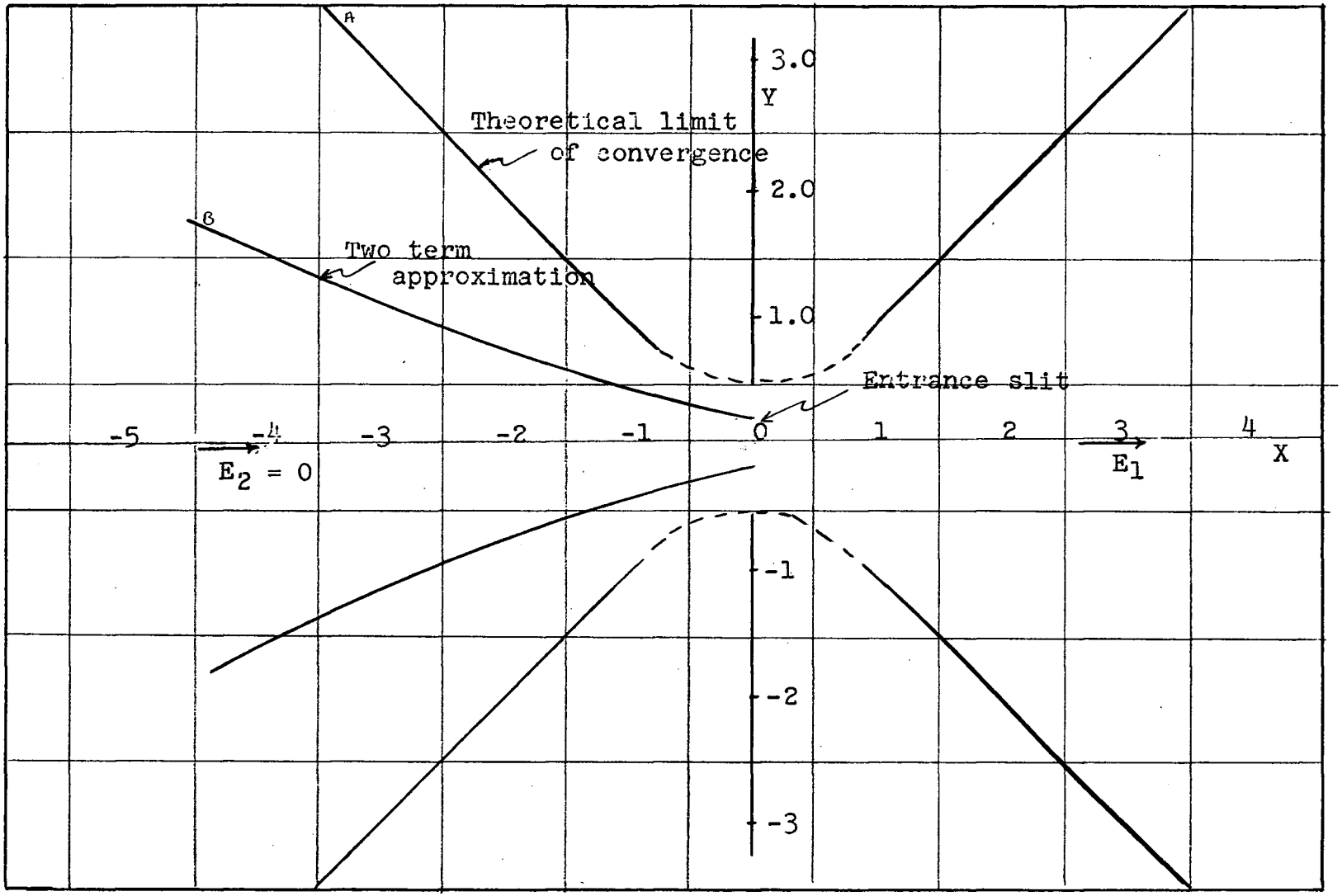

Fig. 2.7 - Domain of convergence of series expansion.

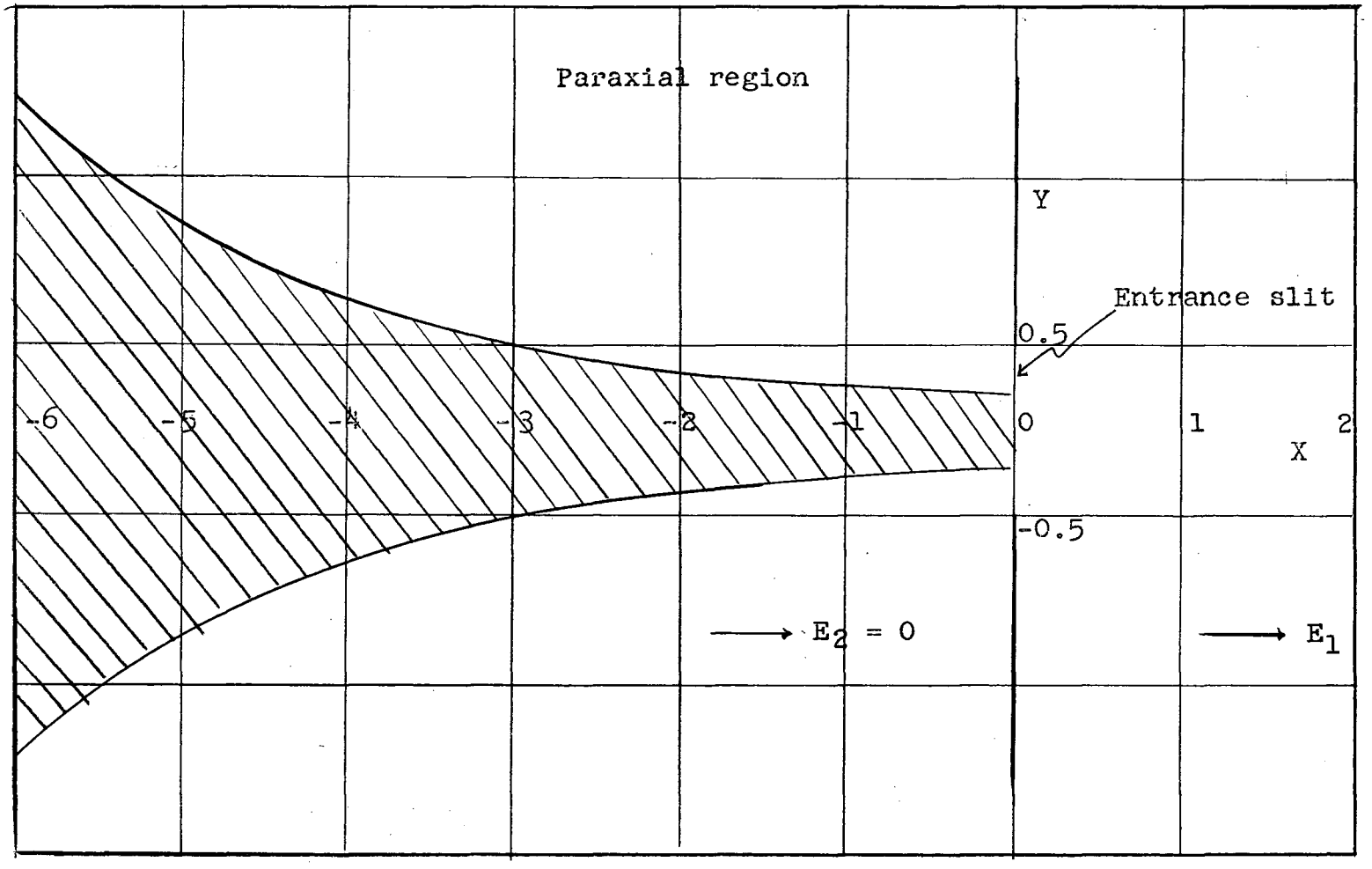

Fig. 2.8

The above equations were integrated numerically and the trajectories were compared for a simple case dealt with in this sub-problem. It was found that, if a particle were to start anywhere within the shaded region in figure (2.8), the resulting trajectory is within 5% of the exact trajectory obtained from equation (2.24a). Indeed, the linear paraxial equation gives better results as compared to the other two approximate equations in the paraxial region.

Subproblem (b)

In the previous subproblem we have considered a single slit and a 'uniform' field on either side (E_1 the accelerating field on the right hand side, and E_2 the repeller field on the left). Here we shall consider a repeller plate and the entrance slit plate as shown in fig 2.1b. It is interesting to know the effect of the repeller plate, particularly when it is close to the entrance slit plate, ie, when d is small; and how it differs from that of the uniform field (ie $d \to \infty$), which we considered in the previous subproblem.

In order to obtain the potential distribution, we use, as before, the method of Schwarz-Christoffel. The transformation function is given by

$$Z = -i P \left[\omega + \frac{a^2-1}{2a} \ln \left(\frac{\omega - a}{\omega + a} \right) \right] \qquad (2.25)$$

where the constants P and a are given implicitly by

$$\left.\begin{aligned} d &= \pi P \frac{1-a^2}{2a} \\ l &= 2P \left(1 - \frac{1-a^2}{2a} \ln \frac{1-a}{1+a} \right) \end{aligned}\right\} \qquad (2.26)$$

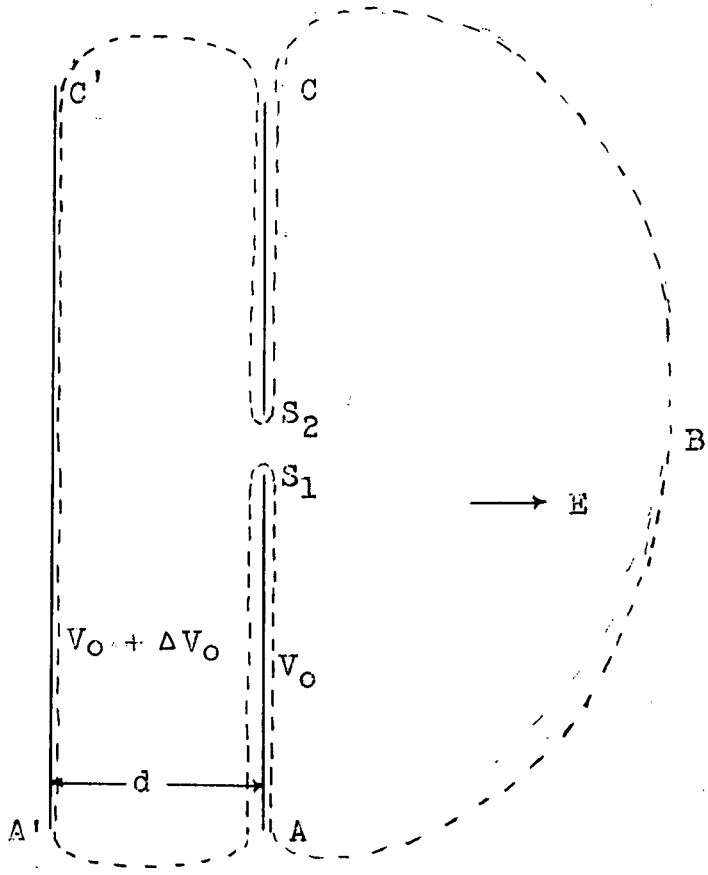

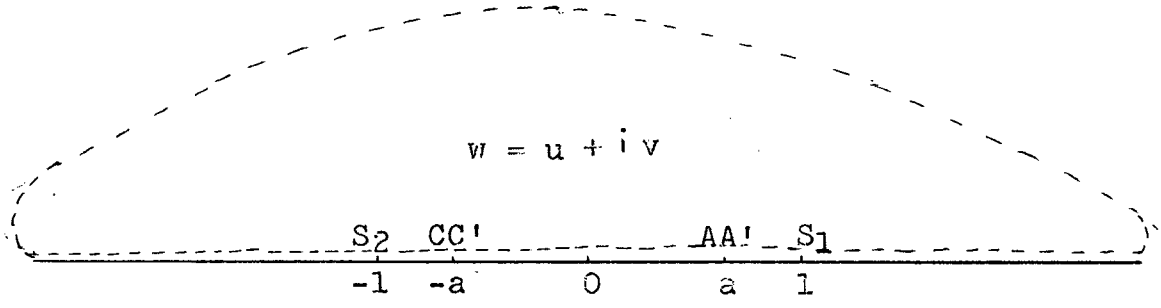

Fig. 2.9

Conformal mapping of the $w > o$ plane onto the whole of Z-plane by Schwarz-Christoffel method.

$$\frac{dz}{dw} = -ip(w-1)(w+1)(w+a)^{-1}(w-a)^{-1}$$

It is interesting to note that, if we let $d \to \infty$, $a \to 0$ and $P \to \frac{1}{4}$; then the transformation function (2.25) reduces to (2.19) as expected. And also as $d \to 0$, $a \to 1$ and $P \to \frac{1}{2}$, equation (2.25) reduces to

$$z = -i \frac{1}{2} w$$

which is just the linear transformation. To solve the system of equations (2.26), we shall eliminate P between them and rewrite

$$\frac{1}{d} = \frac{2}{\pi} \left(\frac{2a}{1-a^2} - \ln \frac{1-a}{1+a} \right) \qquad (2.27)$$

Let $$\xi = \frac{1}{d}$$

and $$\eta = a$$

The above equation becomes

$$\xi = \frac{2}{\pi} \left(\frac{2\eta}{1-\eta^2} - \ln \frac{1-\eta}{1+\eta} \right) \qquad (2.27')$$

The above equation may be solved in a number of ways; for instance, Newton-Rapson, Regula Falsi, etc; but here we shall adopt a different method which does not require us to guess at the initial approximation of the root. We shall express (2.27') in the form of a differential equation, viz.:

$$\frac{d\eta}{d\xi} = \frac{\pi}{8} (1-\eta^2)^2$$

and integrate numerically with the initial values

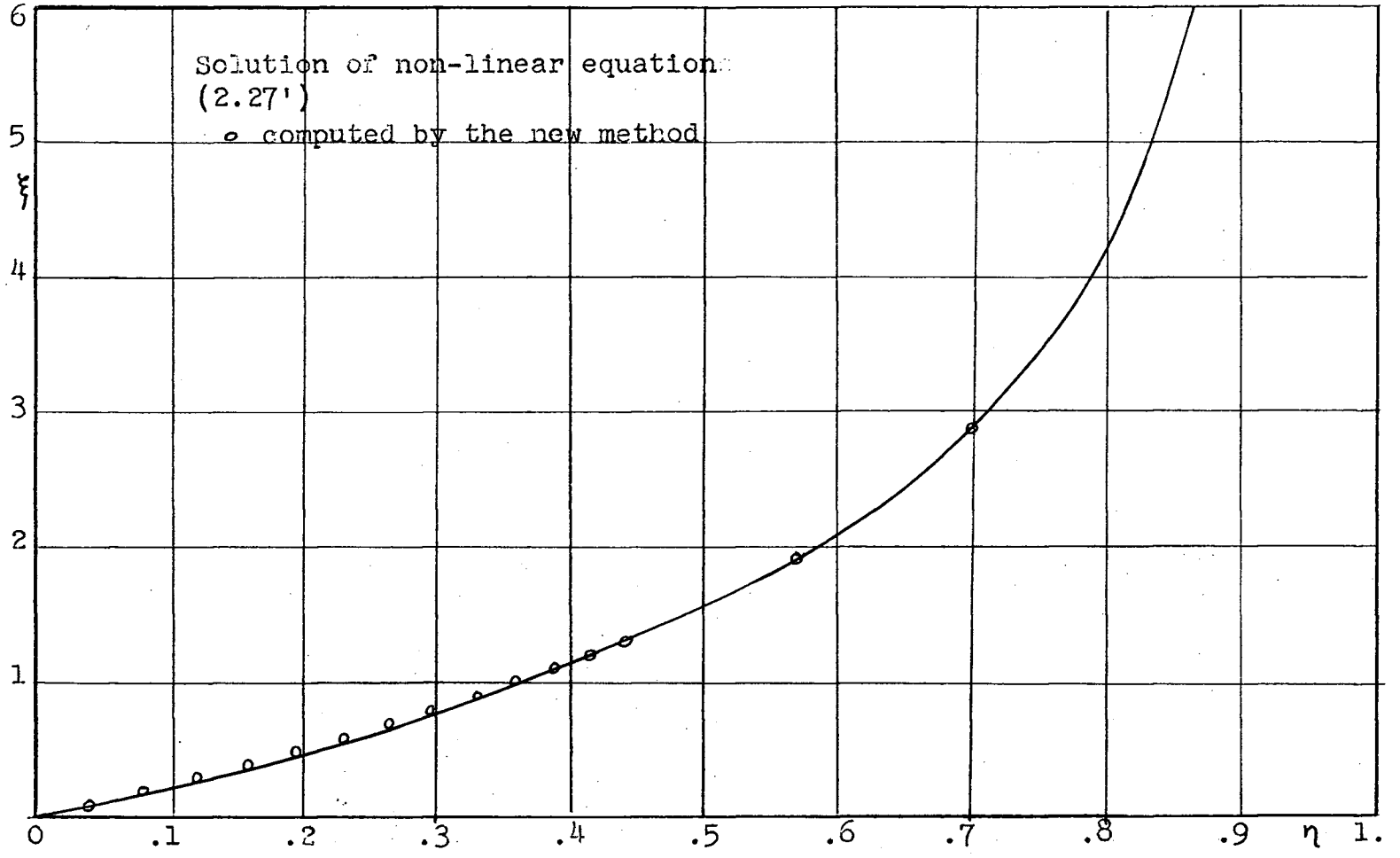
Solution of non-linear equation
(2.27')
o computed by the new method
6
5
4
3
2
1
ξ
0
.1
.2
.3
.4
.5
.6
.7
.8
.9
η
1.

Fig. 2.10

$$\xi = 0$$
$$\eta = 0$$

(this follows from the fact that as $d \to \infty$, $a \to 0$). The solution is shown in figure (2.10). Having obtained the transformation function, we proceed to solve for the potential distribution, first in the w-plane and then map onto the z-plane.

The boundary conditions to be satisfied are

$$V = V_0 \quad \text{on} \quad v = 0 \,, \; |u| > a$$

$$V = V_0 + \Delta V \quad \text{on} \quad v = 0 \,, \; |u| \leq a$$

$$V = E \rho v \quad w \to \infty$$

The last boundary condition follows from the fact that in the z-plane

$$V = E \, Re(z) \quad z \to \infty$$

From the transformation function (2.25) it follows that

$$z = -i \rho w \quad w \to \infty$$

$$V = E \, Re(-i \rho w) = E \rho v$$

To find the potential distribution in the w-plane, we consider the following cases and superpose them later:

(a) $V_A = V_0$ on the u-axis and uniform field in the $w>0$ plane

$$V_a = V_o + E\rho v$$

(b) $V_b = \Delta V$ on the u-axis $u > -a$ and zero on the rest of the u-axis.

$$V_b = \frac{\Delta V}{\pi}\left(\tan^{-1}\frac{v}{u-a}\right)$$

(c) $V_c = -\Delta V$ on the u-axis, $u > a$ and zero on the u-axis $(u < a)$

$$V_c = -\frac{\Delta V_o}{\pi}\left(\tan^{-1}\frac{v}{u+a}\right)$$

Therefore, the net potential in the w>0 plane is given by

$$V = V_a + V_b + V_c$$

$$\therefore \quad V = V_o + E\rho v + \frac{\Delta V_o}{\pi}\left[\tan^{-1}\frac{v}{u-a} - \tan^{-1}\frac{v}{u+a}\right] \qquad (2.28)$$

Now, in order to map the potential distribution onto the z-plane, we have to invert the transformation function (2.25), which is equivalent to the process of solving it as a nonlinear equation for a given value of z. It is then expressed as a system of two nonlinear equations

$$X = \rho v + \rho\frac{a^2-1}{2a}\left[\tan^{-1}\frac{v}{u-a} - \tan^{-1}\frac{v}{u+a}\right] \qquad (2.29a)$$

and

$$Y = -\rho u + \rho\frac{a^2-1}{2a}\left[\ln\frac{(u-1)^2+v^2}{(u+1)^2+v^2}\right] \qquad (2.29b)$$

Since $u = v = o$ it follows that $x = Y = o$; using these as initial conditions, we can solve the above system of equations by the

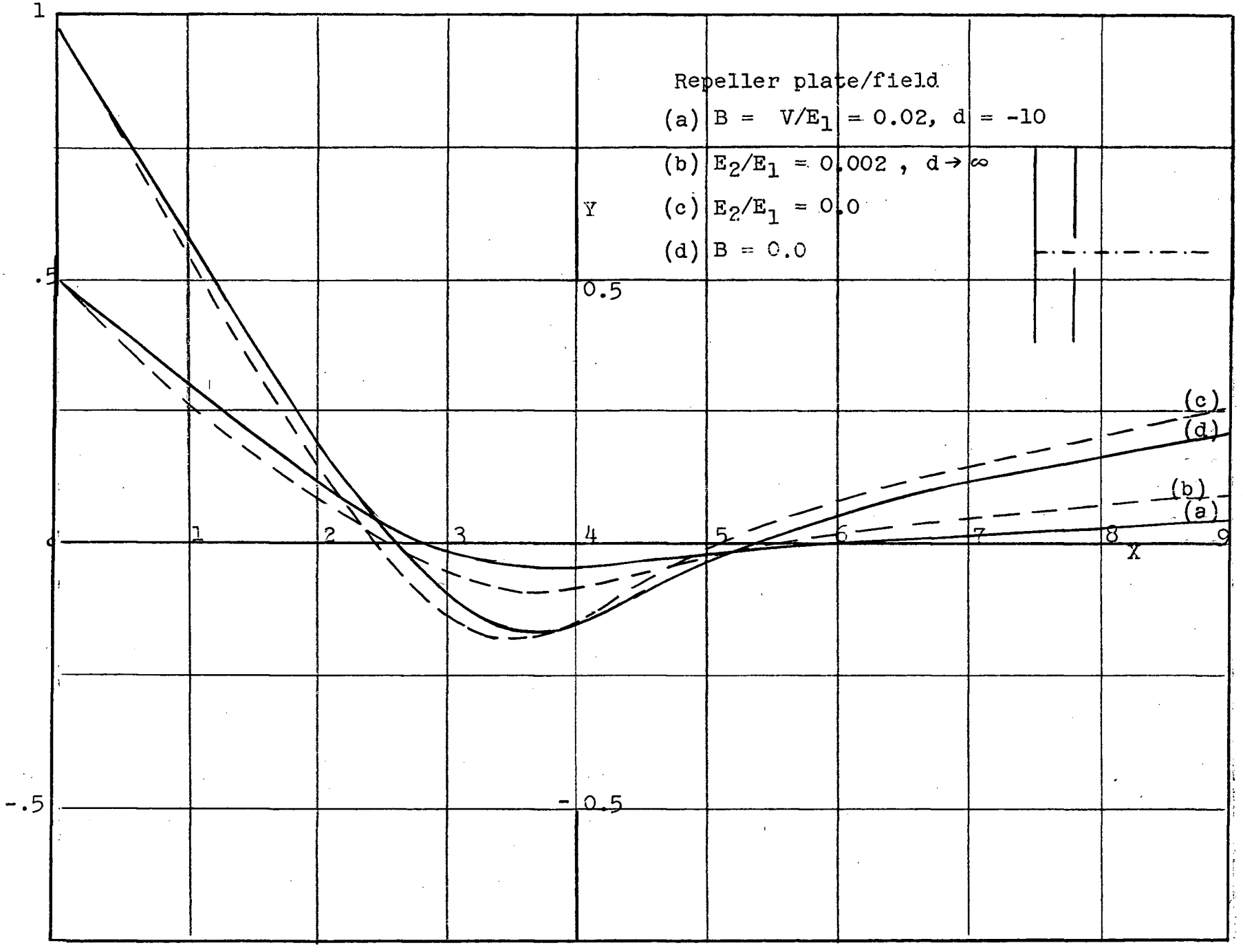
Repeller plate/field
(a) B = V/E1 = 0.02, d = -10
(b) E2/E1 = 0.002 , d → ∞
(c) E2/E1 = 0.0
(d) B = 0.0
Y
X
1
.5
0
-.5
0.5
- 0.5
1
2
3
4
5
6
7
8
9
(c)
(d)
(b)
(a)

Fig. 2.11

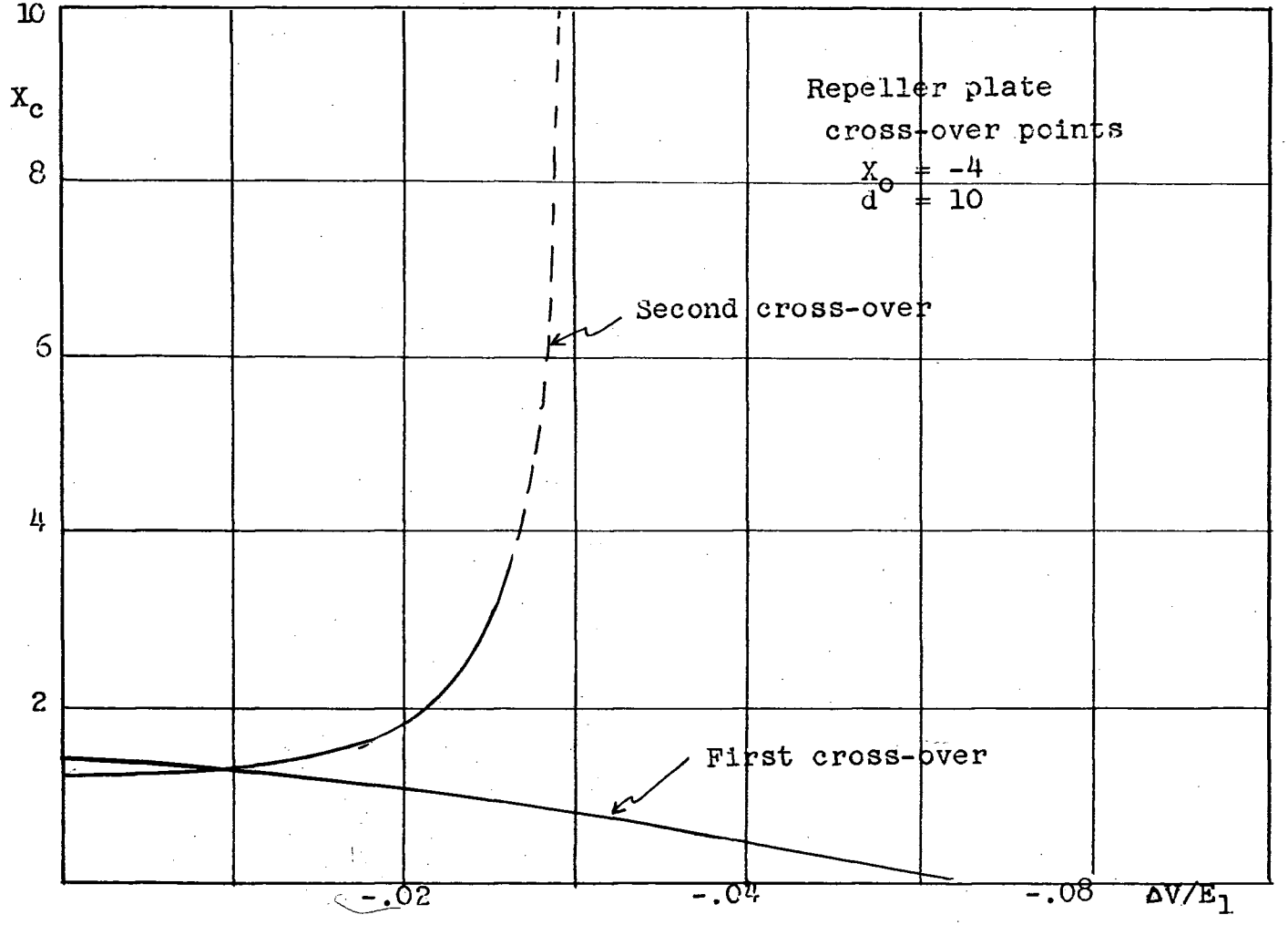
10
X_c
8
6
4
2
Repeller plate
cross-over points
$X_o = -4$
$d = 10$
Second cross-over
First cross-over
-.02
-.04
-.08
$\Delta V/E_1$

Fig. 2.12

method we have devised for (2.27'). However, since we are interested in the axial potential only (paraxial approximation), it is sufficient to consider (2.29a) and let $\mu \to 0$

$$X = \rho v + \rho \frac{1-a^2}{a} \tan^{-1}\left(\frac{v}{a}\right)$$

$$\therefore \quad \frac{dv}{dx} = \frac{1}{\rho\left(1 + \frac{1-a^2}{a^2+v^2}\right)}$$

which may be integrated numerically with the initial conditions $X = v = 0$. We are now in a position to integrate the paraxial trajectory equation.

The computer was programmed to accept the values of d and $\Delta V/E$ (ΔV repeller field, and E accelerating field), then to compute the constants ρ and a, and to invert the transformation function at each step. A few of the computed trajectories are shown in fig (2.11). The trajectories (a) and (b) are drawn to show the effect of proximity of the repeller plate; trajectory (a) is drawn for $d = -10$ and trajectory (b) for $d \to \infty$ keeping the repeller field the same, ie, $\frac{\Delta V}{E} = \frac{E_2}{E_1} = 0.002$ The mere presence of the repeller plate without any repeller voltage ($\Delta V = 0$) seems to affect the trajectory of the particle as shown by c and d in the same figure. This, of course, we would expect, because the repeller plate will distort the potential distribution. The relation between the position of the cross-overs (x_{c_1} and x_{c_2}) and the ratio $\Delta V/E$ is shown in figure 2.12. The relationship is very similar to that when the plate is at infinity (compare with fig 2.6)

To summarize, we see that the effect of a repeller voltage is in no way much different from that of a repeller field (i.e. when $d = -\infty$) unless it is close to the slit ($d < 10$). If d is very small ($d \longrightarrow 0$), the effect of the entrance slit plate is considerably masked by the repeller plate, and in the end, when $d = 0$, there is no perturbation field at all.

The principal effect of the repeller field is to shift the cross-over along the x-axis, thus to produce a linearly diffused focus which, in the absence of a repeller field, would have been sharp. Indeed, it is easy to adjust the repeller field such that some of the particles are focused just in front of the exit slit. If somehow all molecules are ionized within a small space, we could, by adjusting the repeller field, focus all the ions in front of the exit slit (see section 2.5 for further discussion).

Subproblem (c):

In this subproblem we shall consider the effect of the exit slit, particularly on the angle of divergence of the beam. The geometry of the problem is illustrated in fig. (2.13). Since $L >> 1$, the mutual coupling between the slits is negligible; therefore, each slit may be considered separately. The potential distribution in the three different regions, using (2.21), may be expressed by

region I $$V_I = Re\left[\tfrac{1}{2} E_1\left(z + \sqrt{z^2 + 0.25}\right)\right]$$

region II

$$V_{II} = Re\left[\tfrac{1}{2} E_1\left(z + \sqrt{z^2 + 0.25}\right) + \tfrac{1}{2} E_1\left((L - z) - \sqrt{(L-z)^2 + 0.25 \cdot 5^2}\right)\right]$$

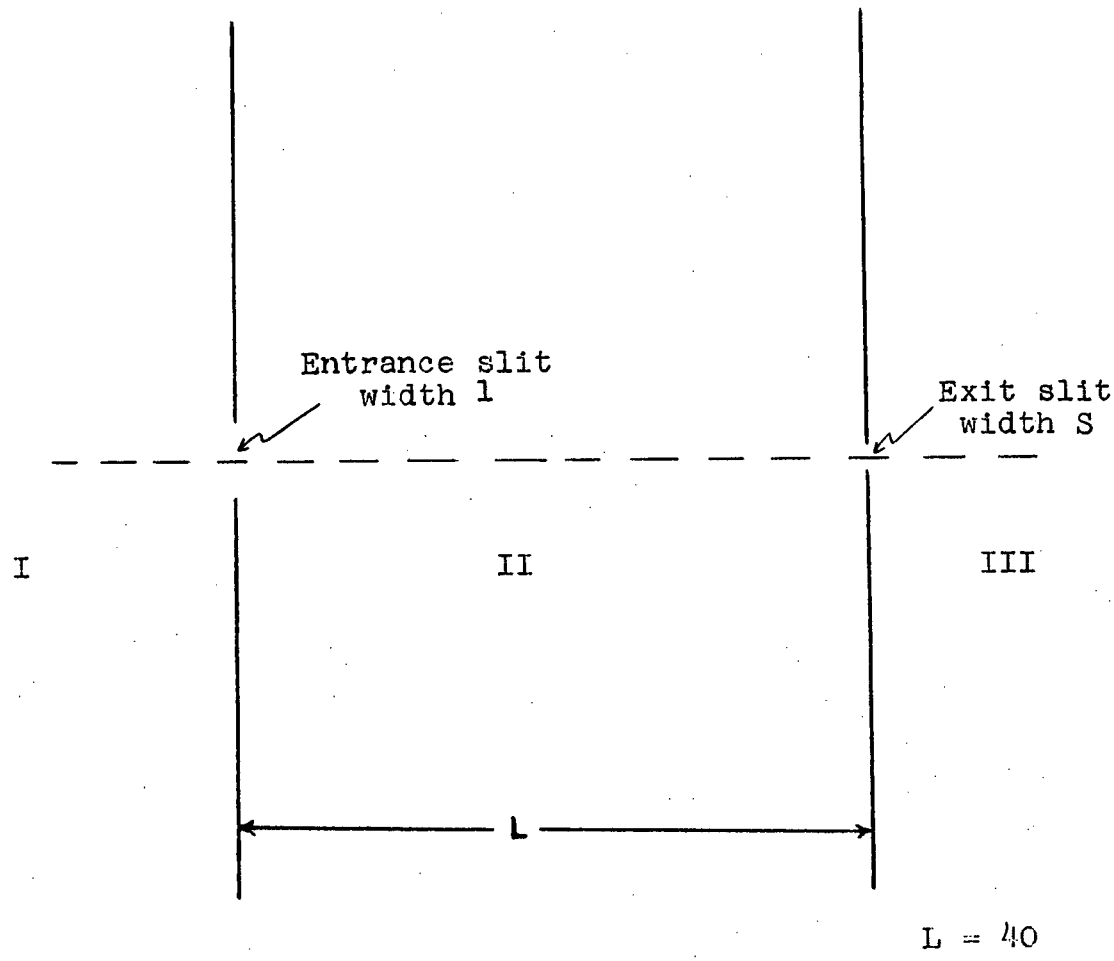

Fig. 2.13

Entrance and Exit slit plates.

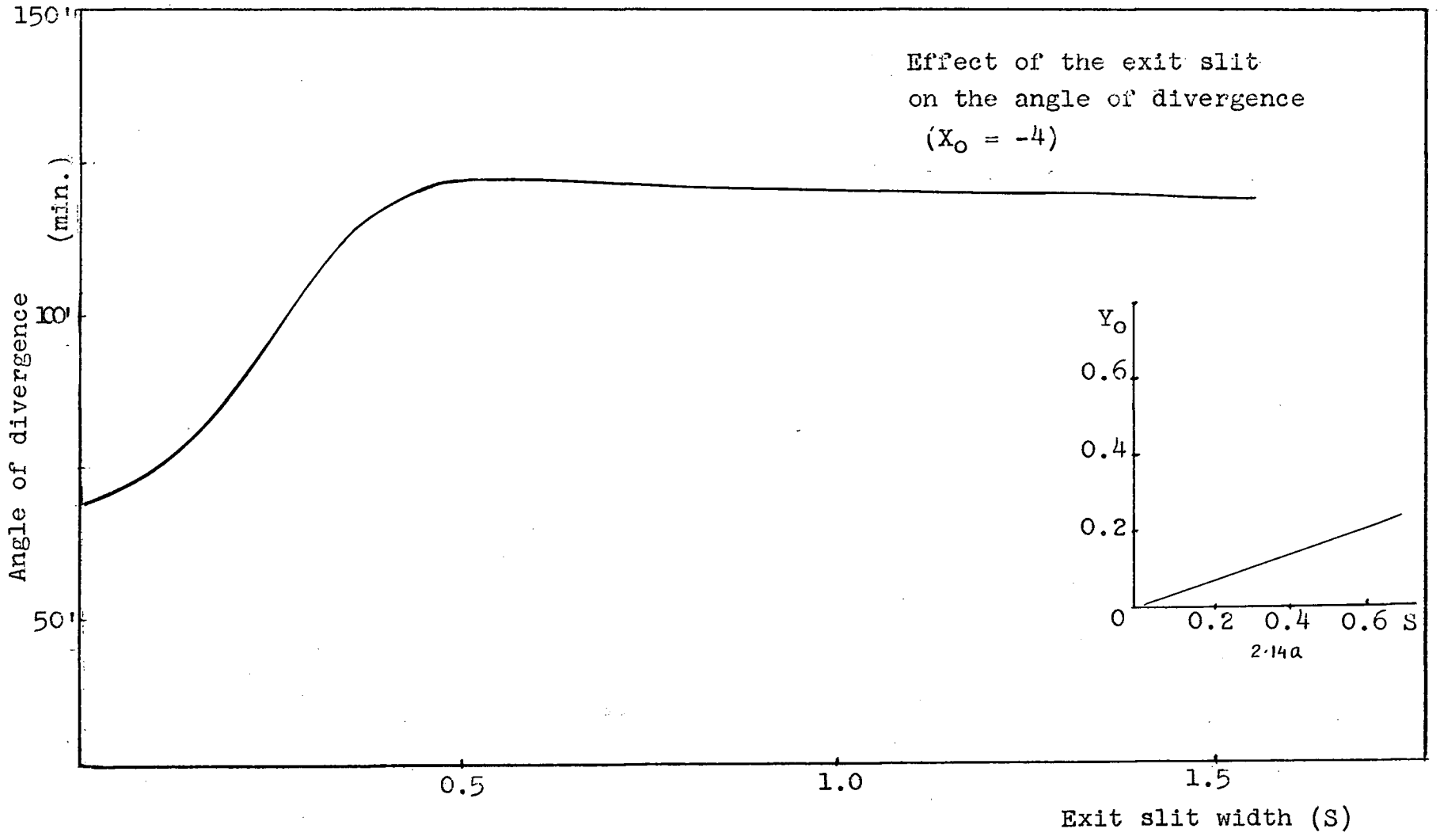
Effect of the exit slit
on the angle of divergence
(X_o = -4)
150'
(min.)
100'
50'
Angle of divergence
0.5
1.0
1.5
Exit slit width (S)
Y_o
0.6
0.4
0.2
0
0.2
0.4
0.6
S
2·14a

Fig. 2.14

region III

$$V_{III} = Re\left[\tfrac{1}{2}E_1(z-L) - \sqrt{(z-L)^2 + 0.25s^2}\right] + E_1 L \qquad (2.30)$$

(centre of co-ordinates at the centre of the entrance slit.) The paraxial trajectory equation is now integrated where the axial potential Φ is to be obtained from (2.30) depending upon the region.

The angle of divergence of the beam for the different values of the exit slit is shown in fig. (2.14) for a particle starting at $X_o = -4$, $Y_o = 1.0$. For any other particle, starting at a height, say $Y_o = \alpha$, the same relationship holds true except that the vertical scale is to be multiplied by α . The slope of the trajectory that just passes through the exit slit--grazing trajectory--can be determined from the figures (2.14a) and (2.14). Firstly, one determines Y_o of the grazing trajectory for a given exit slit width (s) from figure (2.14a) and finally, using figure (2.14), the slope of the trajectory.

Subproblem (d):

In this subproblem we shall consider the deflection of the beam passing between two plates, which are kept at different potentials (fig. 2.15). We shall assume a uniform field on both sides of the plates. A narrow monoenergetic beam enters the gap from left to right. First of all, we solve the boundary value problem to determine the potential distribution. It is again convenient to use the method of conformal transformation

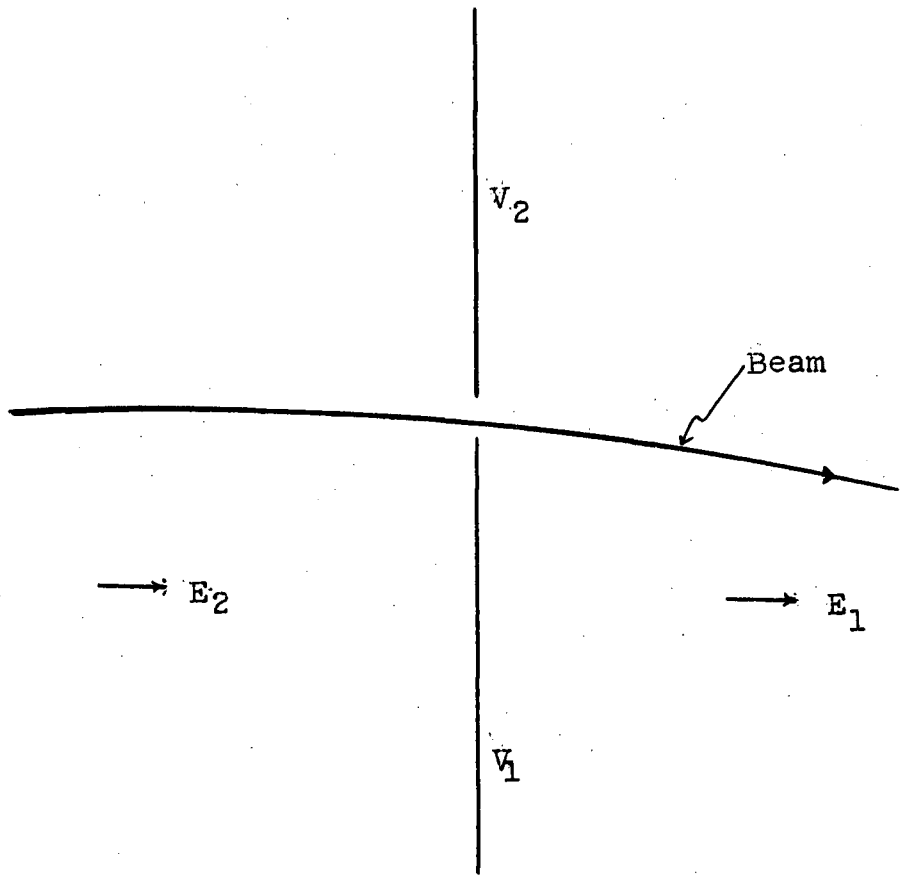

Fig. 2.15

Deflector plates kept at different potentials.

Beam passes from left to right.

Potential distribution around
the deflecting plates

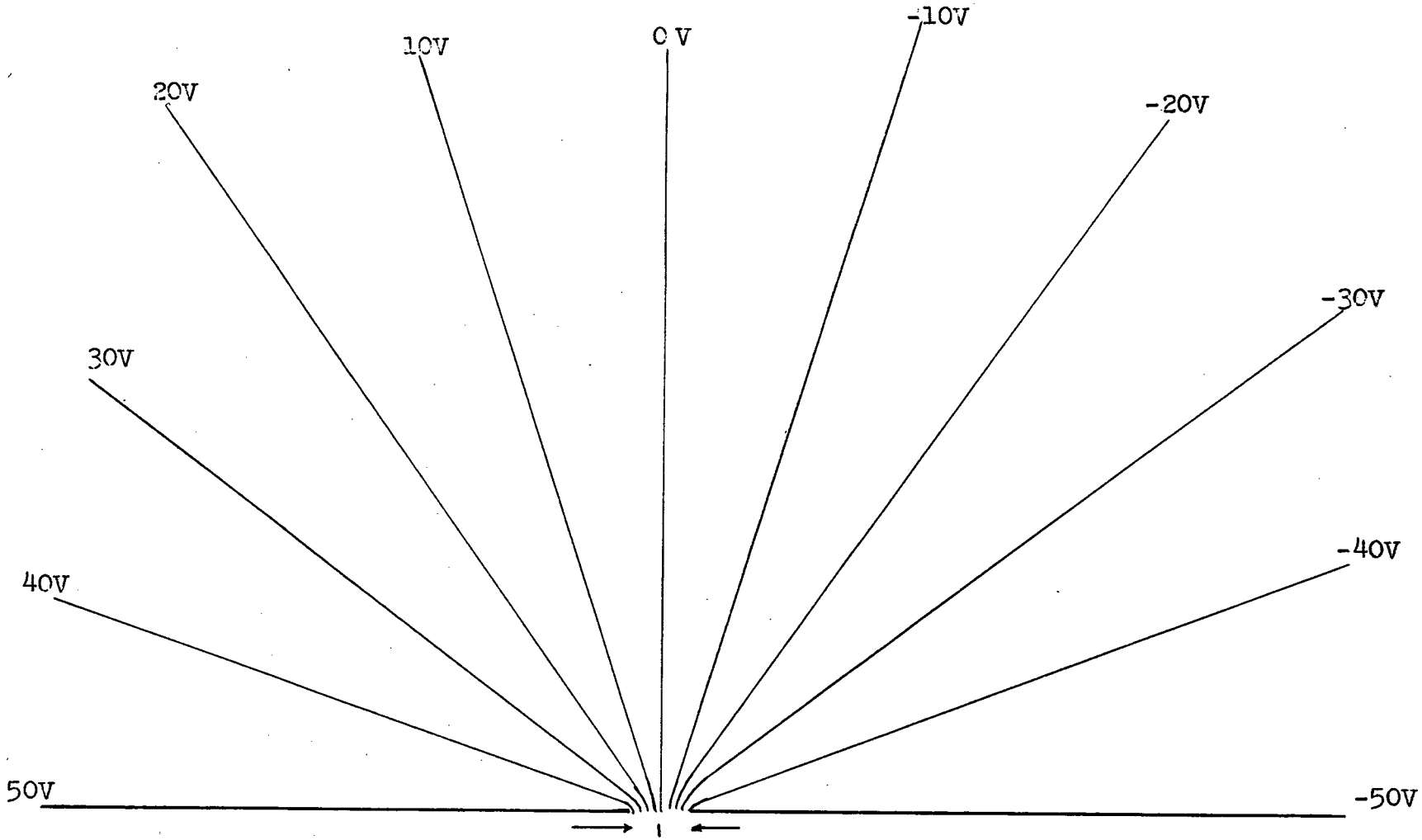

Fig. 2.16

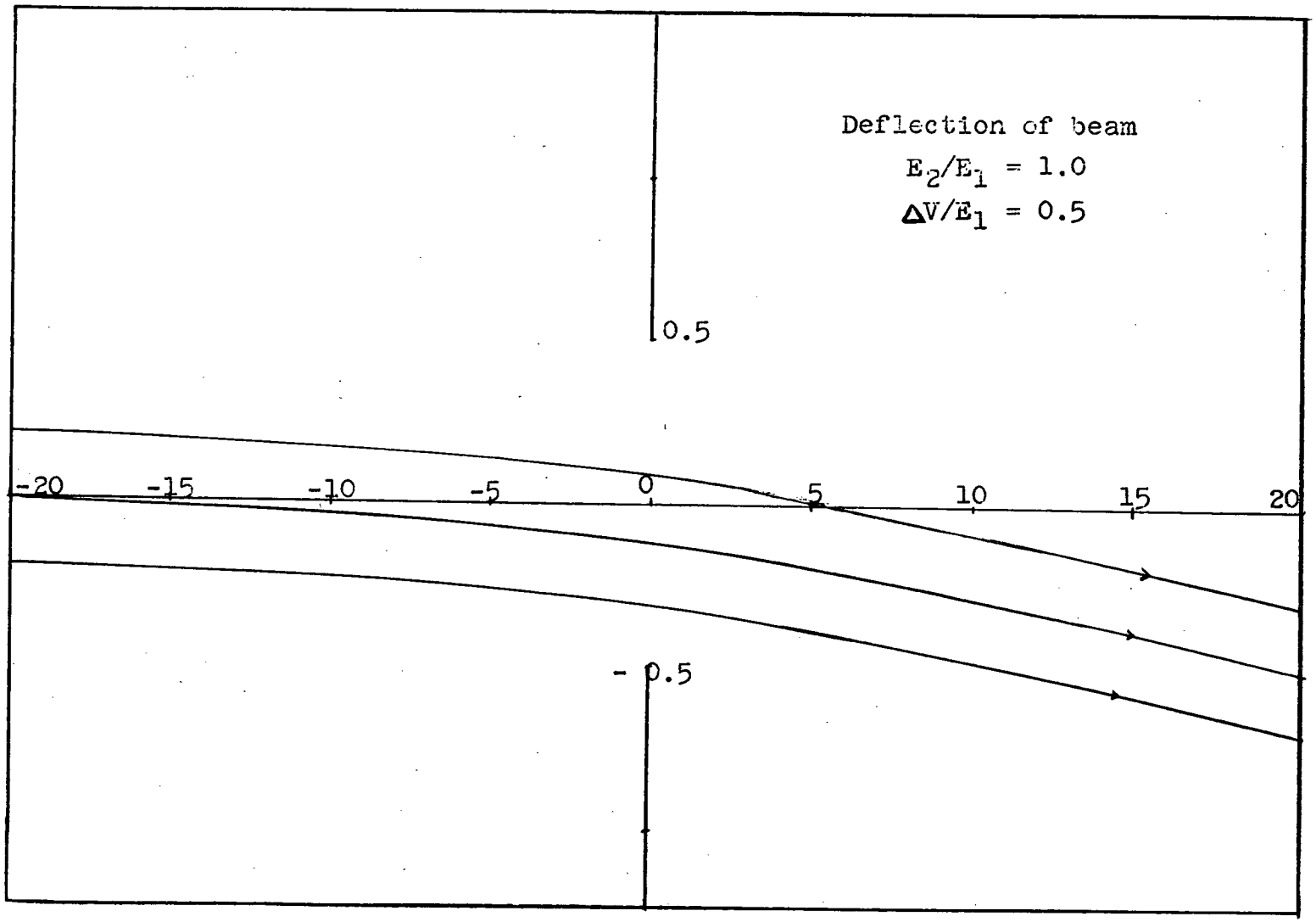
Deflection of beam
E_2/E_1 = 1.0
$\Delta V/E_1$ = 0.5
0.5
-20
-15
-10
-5
0
5
10
15
20
- 0.5

Fig. 2.17

which is illustrated in Fig. (2.2). The boundary conditions to be satisfied by the potential function are

$$V = V_2 \quad \text{on} \quad u < 0 \;, \; v = 0$$

$$V = V_1 \quad \text{on} \quad u > 0 \;, \; v = 0$$

$$V \rightarrow E\, Re(Pw)_{w \rightarrow \infty}$$

$$V \rightarrow E\, Re(P/w)_{w \rightarrow 0}$$

Such a function is given by

$$V(u,v) = V_1 + Re\left[P(E_1 w + E_2/w)\right] + \frac{(V_2 - V_1)}{\pi} \tan^{-1}\left(\frac{v}{u}\right) \qquad (2.31)$$

where

$$P = -i/4$$

Potential distribution may be mapped onto the z-plane using transformation function (2.19).

The paraxial approximations are no longer valid because the potential distribution is not symmetric about the axis (since $V_1 \neq V_2$); therefore, we shall have to integrate the exact equation (2.10). We may simplify the potential distribution considerably by letting $E_1 = E_2$, and thus we have the deflecting field given by

$$\Delta V = \frac{(V_2 - V_1)}{\pi} \tan^{-1}\left(\frac{v}{u}\right) \qquad (2.32)$$

which is illustrated in fig. (2.16). Except in the immediate vicinity of the gap, the field is normal to the radius vector and inversely proportional to the radial distance. Introducing the above approximation, the trajectory equation may be written as

$$2xY'' + Y' - \frac{\Delta V}{\pi E_1}\frac{1}{|x|} = 0 \qquad |x| > 0 \qquad (2.33)$$

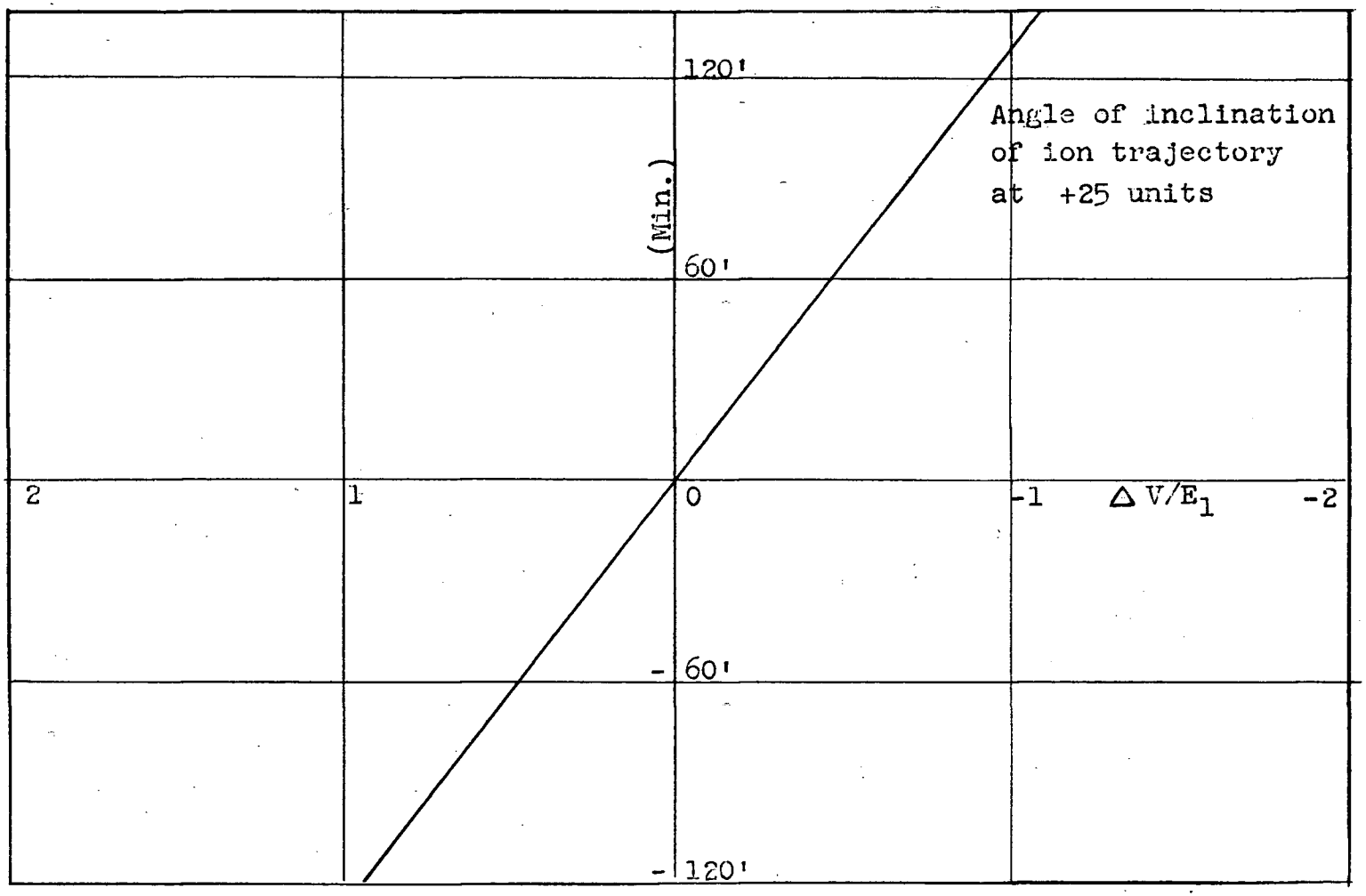
120'
Angle of inclination
of ion trajectory
at +25 units
(Min.)
60'
2
1
0
-1
$\Delta V/E_1$
-2
- 60'
- 120'

Fig. 2.18

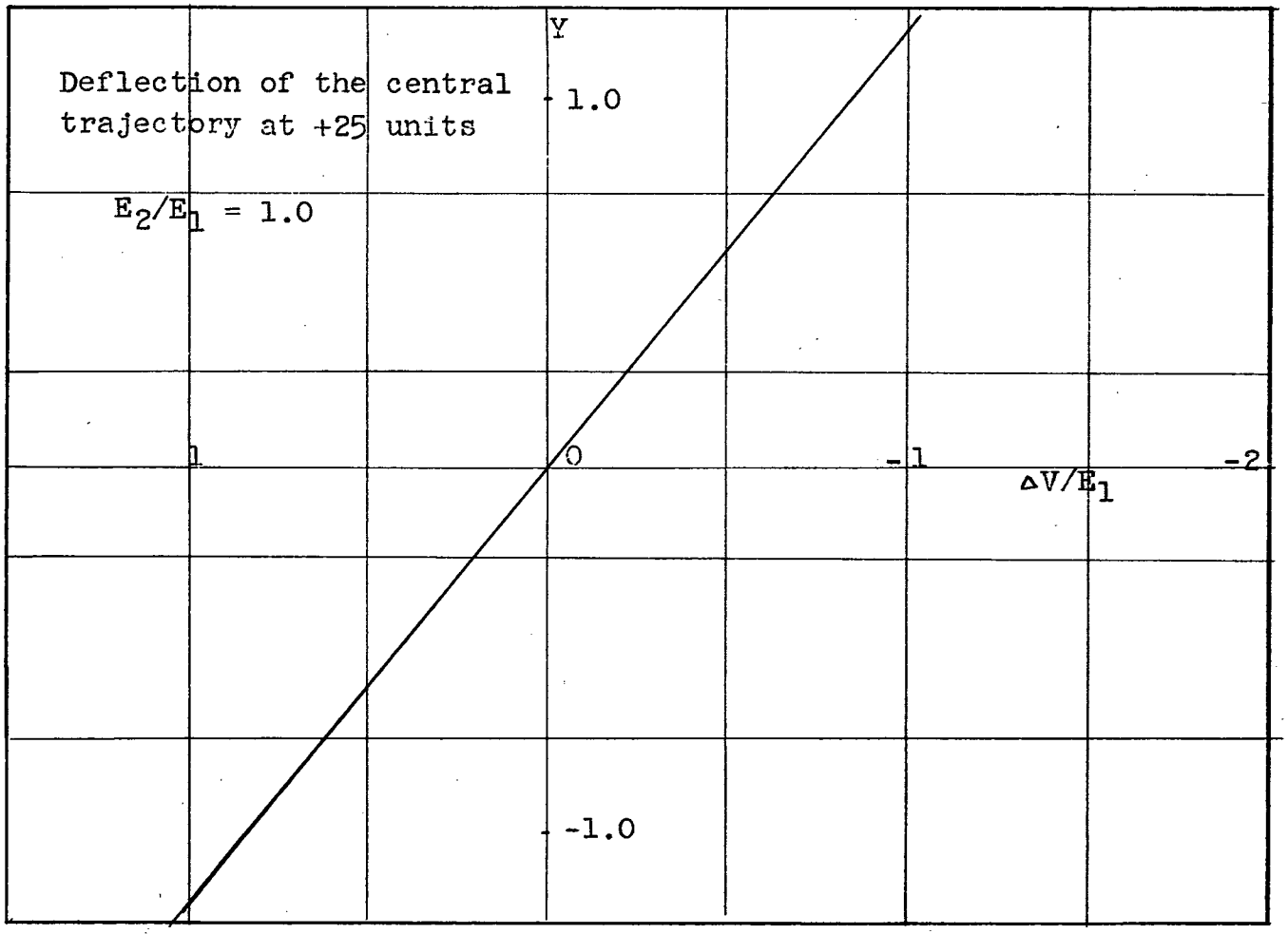
Deflection of the central trajectory at +25 units
E_2/E_1 = 1.0
Y
1.0
-1.0
1
0
-1
-2
$\Delta V/E_1$

Fig. 2.19

The equation (2.33), though simple, is not very useful when we have to trace the trajectory across the gap. We have, therefore, preferred to integrate the exact equation. A beam originally parallel to the x-axis is deflected by the plates as shown in fig. (2.17). It should be noted that the beam still remains parallel after its passage through the gap. The total deflection from the axis is linearly related to $\Delta V/E$ (fig. 2.18). One may compute the total deflection at any distance $X(X \rangle 1)$ for a given value of $\Delta V/E$ from the figures (2.17) and (2.18); as for example, suppose we wish to find the deflection at a distance $X = 10$ and $\Delta V/E = 1$. From fig. (2.17) we measure the deflection at $X = 10$ ($\Delta V/E = -0.5$). Plot this point on fig. (2.18) and draw a line joining to the centre of co-ordinates, thus giving a new relation between the deflection and $\Delta V/E$. Using the new relation, it is easy to determine the total effect for any value of $\Delta V/E$. Similarly, we can determine the angle of deflection at any point X from figures (2.17) and (2.19).

Subproblem (e):

In this subproblem we shall consider ion trajectories in the presence of a magnetic field. A magnetic field of the order of a few hundred gauss is often used to guide the ionizing electron beam in the source region. We shall assume a uniform magnetic field normal to the plane of a paper. The paraxial trajectory equation taking into account the magnetic field is given by

$$2\Phi_0 Y'' + \Phi_0' Y' + \Phi_0'' Y + \beta_z \cdot W\sqrt{\frac{2q}{\kappa m}}\,\Phi_0 = 0$$

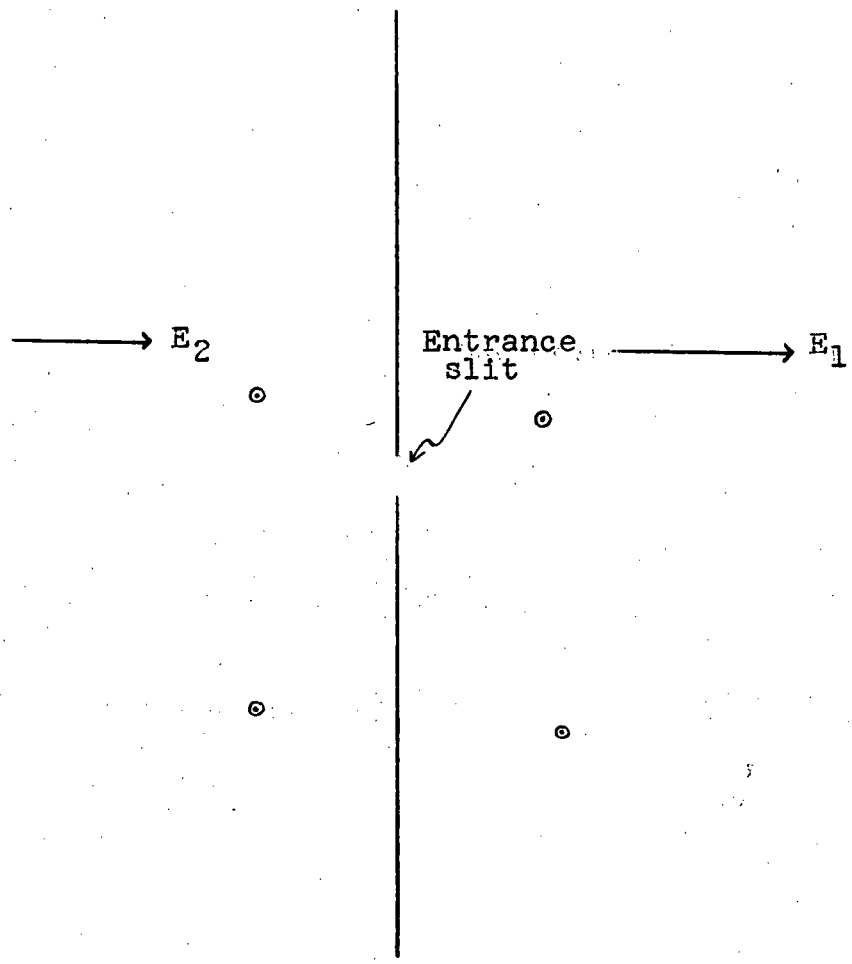

Fig. 2.20

⊙ Magnetic field normal to the plane of the paper (coming out)

(2.34)

(see p. 14)

where B_z stands for the magnetic field, and ω is equal to the entrance slit width. The presence of the magnetic field introduces an additional term into the paraxial equation and makes it inhomogeneous. If Y_1 and Y_2 are the fundamental solutions of the corresponding homogeneous equation, the particular solution may be given in terms of Y_1 and Y_2 as follows:

$$\Delta Y = Y_2 \int_{x_0}^{x} \frac{-Y_1 B_z \omega \sqrt{\frac{2q}{km}\Phi}}{\Delta(Y_1,Y_2)}\,dx - Y_1 \int_{x_0}^{x} \frac{-Y_2 B_z \omega \sqrt{\frac{2q}{km}\Phi}}{\Delta(Y_1,Y_2)}\,dx \qquad (2.35)$$

where

$$\Delta(Y_1,Y_2) = 2\Phi(Y_1Y_2' - Y_2Y')$$

Therefore, the effect of the magnetic field is given by (2.35). Since B_z is constant, it may be taken outside the integral sign; and hence the effect is proportional to the field strength. In practice, however, to obtain the particular solution, it is convenient to integrate the equation with the homogeneous initial conditions (i.e. $Y(0) = Y'(0) = 0$). There appears to exist a certain difficulty as pointed out before to initiate the numerical solution. The inhomogeneous part is singular at the starting point because $\Phi = 0$ at the starting point.

$$Y'' = -\frac{1}{2}\left(\frac{\Phi_0'}{\Phi_0}Y' + \frac{\Phi_0''}{\Phi_0}Y + \frac{B_z \cdot \omega}{1}\sqrt{\frac{2q}{km}}\frac{1}{\Phi_0}\right)$$

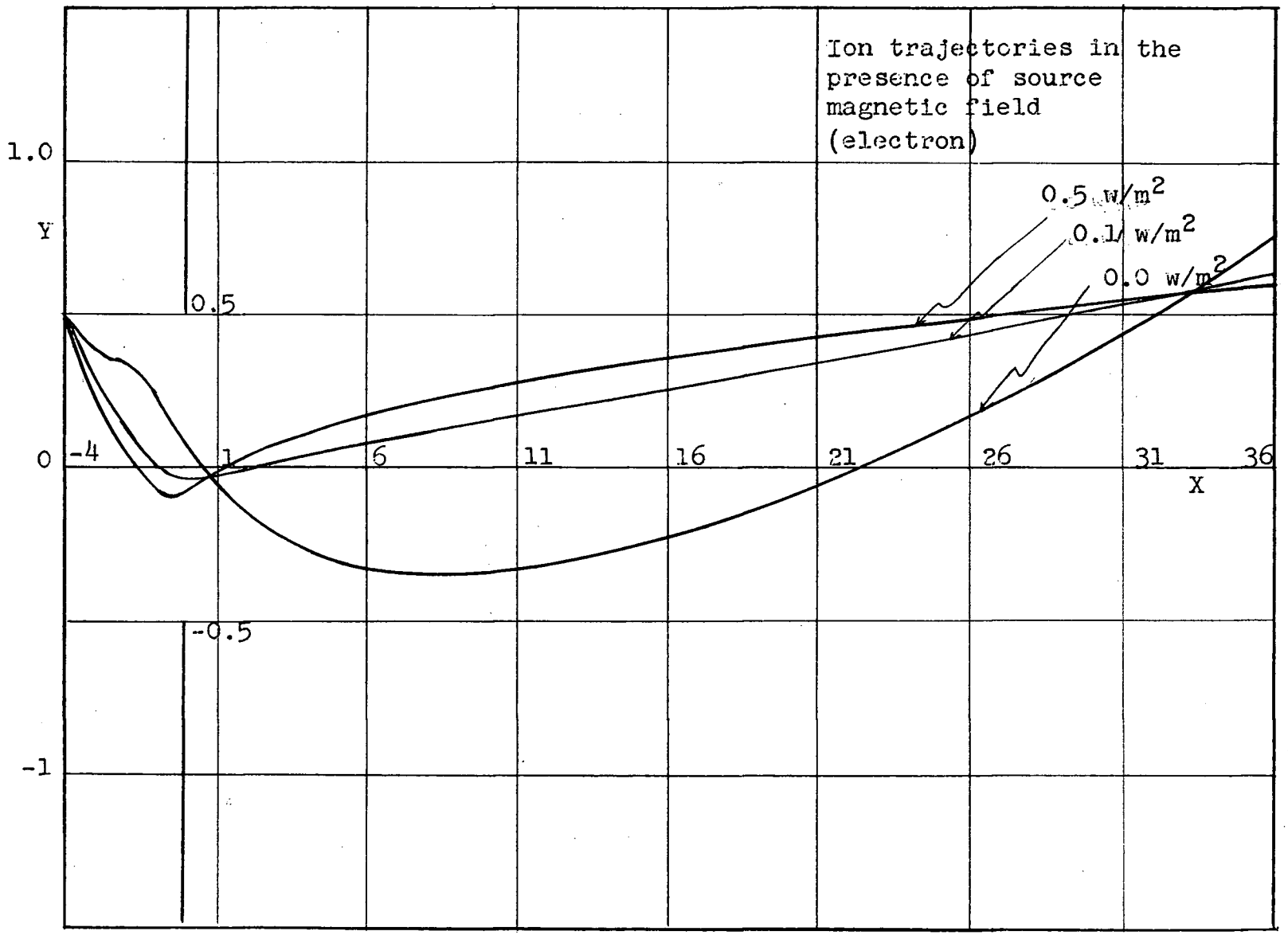
Ion trajectories in the presence of source magnetic field (electron)
0.5 w/m2
0.1 w/m2
0.0 w/m2
1.0
Y
0.5
0
-0.5
-1
-4
1
6
11
16
21
26
31
36
X

Fig. 2.21

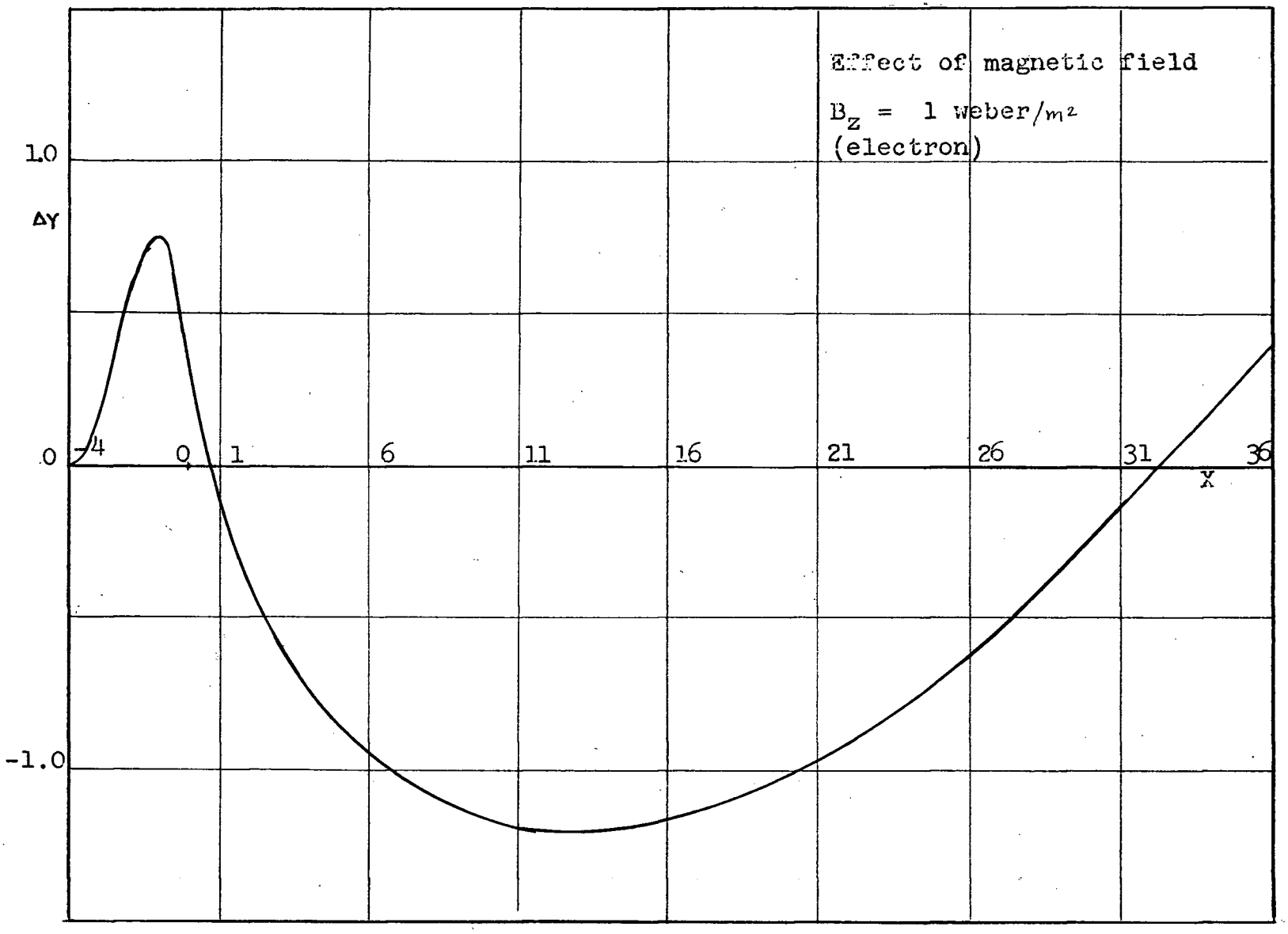
Effect of magnetic field
B_z = 1 weber/m^2
(electron)
1.0
ΔY
0
-1.0
-4
0
1
6
11
16
21
26
31
36
X

Fig. 2.22

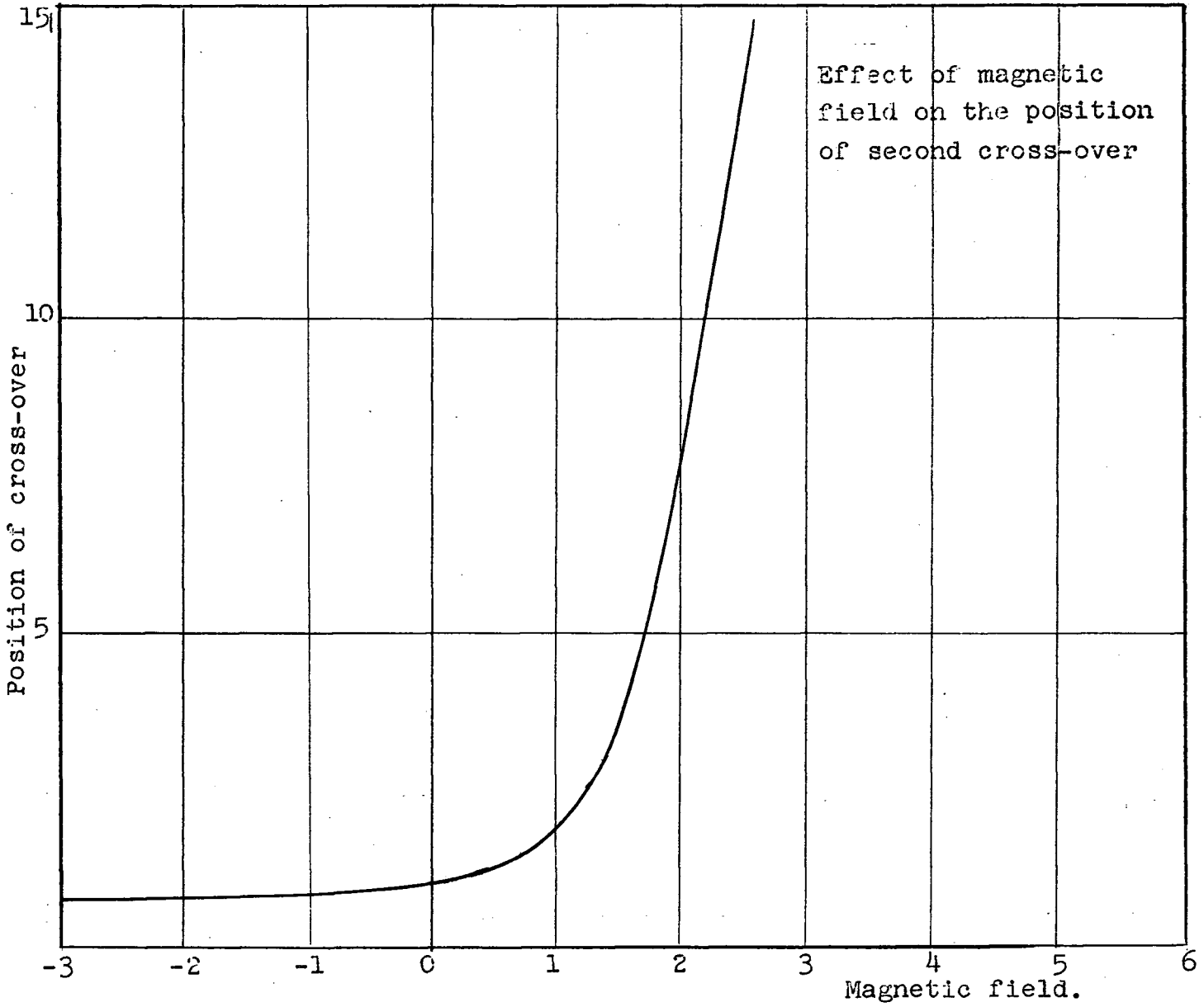
Effect of magnetic field on the position of second cross-over
Position of cross-over
15
10
5
-3
-2
-1
0
1
2
3
4
5
6
Magnetic field.

Fig. 2.23

By virtue of the initial conditions ($Y(0) = Y'(0) = 0$), the first two terms vanish, but the last term becomes infinite. If, however,

$$\Phi_0 \longrightarrow |x - x_0| \qquad x \longrightarrow x_0$$

the integral is convergent as shown by the Cauchy test (see Appendix B). This, however, does not help to initiate the numerical solution. We have to adopt a physical viewpoint: when the velocity of the ion is small ($\Phi \longrightarrow 0$), the force due to the magnetic field will be small, hence one may ignore the inhomogeneous part when initiating the numerical solution.

The equation (2.34) was integrated numerically for the following values of the constants:

$$B_z = .1, .5 \quad \text{webers/m}^2$$
$$E = 10^5 \quad \text{volt/meter}$$
$$W = 10^{-3} \quad \text{meter}$$
$$q/m = 1.7592 \times 10^5 \quad \text{coloumb/kilogram (electron)}$$

The trajectories are shown in fig. (2.21). The particular solution of (2.34) for $B_z = 1 \ \text{W/m}^2$ and other constants as above is in fig. (2.22). This figure may be used to compute the effect of the magnetic field for any other set of constants (e.g. for $Pb(CH_3)_3^+$ ion it may be obtained by multiplying by a factor 0.00145).

An important question is often asked regarding the mass discrimination due to the magnetic field in the source region. Consider two ions (isotopes) of masses m and $m + \Delta m$, so that

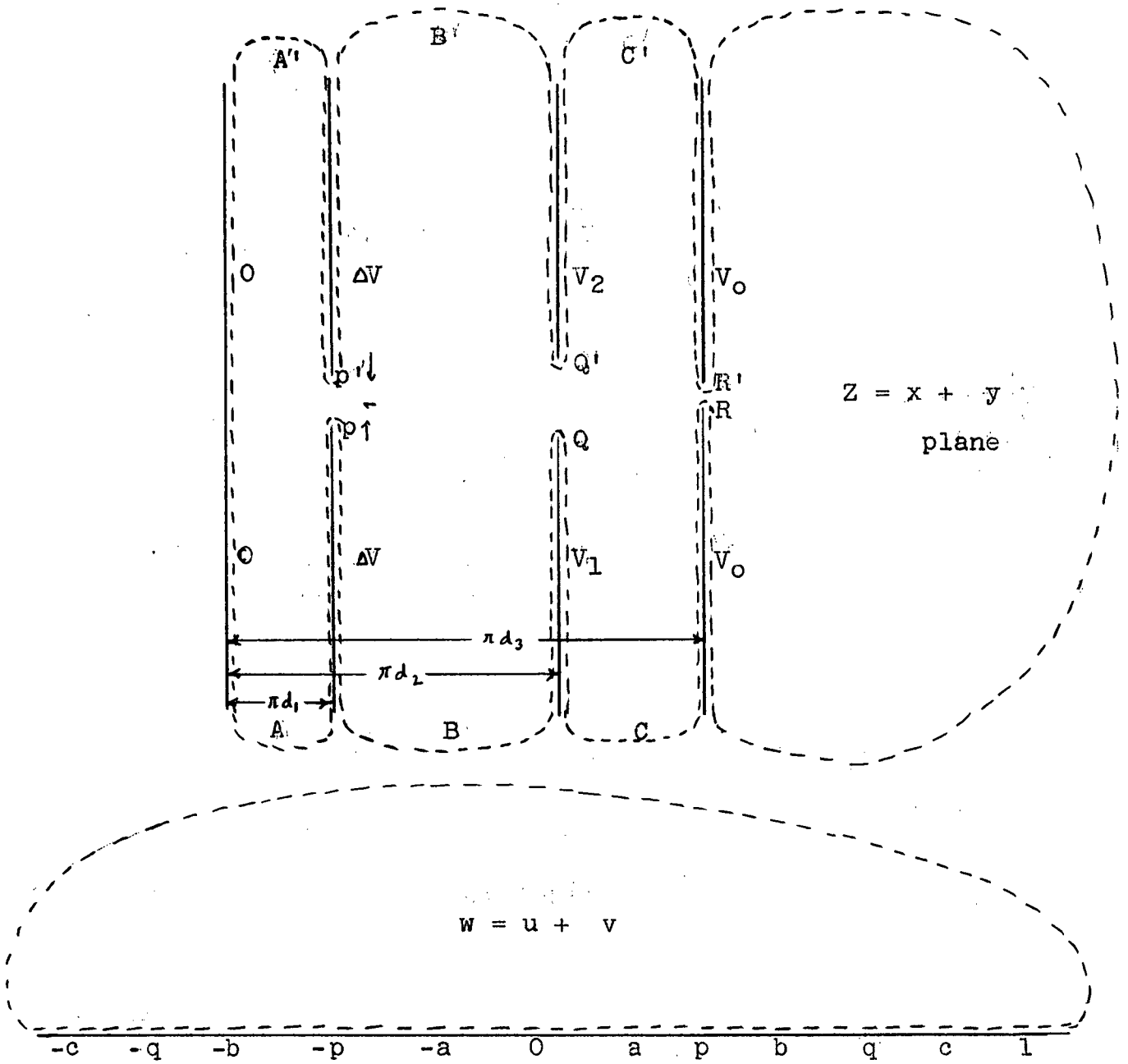

Fig.2.24

Conformal mapping of w $\rangle$ 0 plane onto the whole of the Z-plane.

$$\sqrt{q/m+\Delta m}\Big/\sqrt{q/m} \;=\; 1-\tfrac{1}{2}\frac{\Delta m}{m}$$

The trajectories of the two ions will be separated by ($\frac{\Delta m}{m}$ = 0.008 for $Pb^{204}(CH_3)_3^+$ and $Pb^{206}(CH_3)_3^+$ ions). Normally, the separation of heavy ions ($m >> 1$) is very small, and certainly much smaller than the exit slit even for the field of the order of 1 weber/m^2. Moreover, the separation may be minimized by placing the exit slit in the neighborhood of $\Delta Y = 0$. In some cases it may be possible to filter out the lighter ions by adjusting the magnetic field.

2.4 Global analysis:

In the previous section we analysed the ion optical system (fig. 1.2) considering each part separately. We now proceed to treat the problem on a global basis. The primary task is to find the potential distribution within the space bounded by the various plates. We assume as before the slits to extend to $\pm\infty$ in the direction of the y-axis. Boerboom (1957, 1959, 1960) considered a system of three such slits and obtained the axial potential. The following treatment is essentially based on his work and also gives a method of inverting the transformation function. We shall use the method of conformal mapping to solve the boundary value problem.

The mapping function is given in the differential form as

$$\frac{dz}{dw} = K(w-a)^{-1}\cdot(w-p)^{+1}(w-b)^{-1}(w-q)^{+1}(w-c)^{-1}(w-1)^{+1}$$

$$(w+a)^{-1}(w+p)^{+1}(w+b)^{-1}(w+q)^{+1}(w+c)^{-1}(w+1)^{+1} \qquad (2.36)$$

where a, p, b, q, c and K are constants and satisfy the relation

$$1 > c > q > b > p > a$$

Equation (2.36) may be written as

$$\frac{dz}{dw} = K\left[(AC + AD' + BC' + BD) + AC\left(\frac{a^2-p^2}{w^2-a^2}\right) + AD\left(\frac{b^2-p^2}{w^2-b^2}\right) + BC'\left(\frac{a^2-p^2}{w^2-a^2}\right) + BD'\left(\frac{c^2-p^2}{w^2-c^2}\right)\right] \tag{2.37}$$

where

$$A = \left(\frac{b^2-1}{b^2-c^2}\right)$$

$$B = \left(\frac{1-c^2}{b^2-c^2}\right)$$

$$C = \left(\frac{a^2-q^2}{a^2-b^2}\right)$$

$$D = \left(\frac{q^2-b^2}{a^2-b^2}\right)$$

$$C' = \left(\frac{a^2-q^2}{a^2-c^2}\right)$$

$$D' = \left(\frac{q^2-c^2}{a^2-c^2}\right) \tag{2.38}$$

Integration of equation (2.37) yields the transformation function.

$$z = K\left[(AC+AD+BC'+BD')w + AC\left(\frac{a^2-p^2}{2a}\right)\ln\left(\frac{w-a}{w+a}\right) + AD\left(\frac{b^2-p^2}{2b}\right)\ln\left(\frac{w-b}{w+b}\right) + BC'\left(\frac{a^2-p^2}{2a}\right)\ln\left(\frac{w-a}{w+a}\right) + BD'\left(\frac{c^2-p^2}{2c}\right)\ln\left(\frac{w-c}{w+c}\right)\right] \tag{2.39}$$

There are six unknowns, and therefore we seek six independent equations connecting them. We can get three of them by integrating equation (2.37) about a, b, and c over an infinitely small semicircle.

$$\pi d_1 = \frac{-iK(a^2-p^2)(a^2-q^2)(a^2-1)}{2a(a^2-b^2)(a^2-c^2)}\pi$$

$$\pi(d_2-d_1) = \frac{-iK(b^2-p^2)(b^2-q^2)(b^2-1^2)}{2b(a^2-b^2)(-b^2+c^2)}\pi$$

$$\pi(d_3-d_2) = \frac{-iK(c^2-p^2)(c^2-q^2)(c^2-1^2)}{2c(c^2-b^2)(c^2-a^2)}\pi \tag{2.40}$$

The remaining three relations we obtain by integrating equation (2.37) across the three slits. The three equations are

$$i = K\int_p^{-p} \frac{(w^2-p^2)(w^2-q^2)(w^2-1^2)}{(w^2-a^2)(w^2-b^2)(w^2-c^2)}dw$$

$$iw_1 = K\int_q^{-q} \frac{(w^2-p^2)(w^2-q^2)(w^2-1^2)}{(w^2-a^2)(w^2-b^2)(w^2-c^2)}dw$$

$$iw_2 = K\int_1^{-1} \frac{(w^2-p^2)(w^2-q^2)(w^2-1^2)}{(w^2-a^2)(w^2-b^2)(w^2-c^2)}dw \tag{2.41}$$

After integration equations (2.41) become

$$i = K\left[-2\alpha p + 2(\epsilon+\beta)\ln\frac{(a+p)}{(p-a)} + 2\gamma\ln\frac{(p+b)}{(b-p)} + 2\theta\ln\frac{(p+c)}{(c-p)}\right]$$

$$iw_1 = K\left[-2\alpha q + 2(\epsilon+\beta)\ln\frac{(a+q)}{(q-a)} + 2\gamma\ln\frac{(q+b)}{(q-b)} + 2\theta\ln\frac{(q+c)}{(c-q)}\right]$$

$$iw_2 = K\left[-2\alpha + 2(\epsilon+\beta)\ln\frac{(a+1)}{(1-a)} + 2\gamma\ln\frac{(1+b)}{(1-b)} + 2\theta\ln\frac{(1+c)}{(1-c)}\right] \tag{2.42}$$

where $$\alpha = AC + AB + BC' + BD'$$

$$\beta = AC\,\frac{(a^2-p^2)}{2a}$$

$$\gamma = AD\,\frac{(b^2-p^2)}{2b}$$

$$\epsilon = BC'\,\frac{(a^2-p^2)}{2a}$$

and

$$\theta = BD'\,\frac{(c^2-p^2)}{2c} \qquad (2.43)$$

In (2.40) to make the right hand side real and positive, we have to assume κ of the type

$$\kappa = -i\ell$$

where ℓ is a positive unknown constant. Substituting (2.38) in (2.43), we obtain

$$\begin{aligned} \alpha &= 1 \\ -d &= (\beta+\epsilon)\cdot\ell \\ -(d_2-d_1) &= \gamma\cdot\ell \\ -(d_3-d_2) &= \theta\cdot\ell \end{aligned} \qquad (2.44)$$

Making use of (2.44), we may write equations (2.40) and (2.42) as

$$d_1 = \ell\,\frac{(p^2-a^2)(q^2-a^2)(l^2-a^2)}{2a(b^2-a^2)(c^2-a^2)}$$

$$(d_2-d_1) = \ell\,\frac{(b^2-p^2)(q^2-b^2)(l^2-b^2)}{2b(b^2-a^2)(c^2-b^2)}$$

$$(d_3-d_2) = \ell\,\frac{(c^2-p^2)(c^2-q^2)(l^2-c^2)}{2c(c^2-a^2)(c^2-b^2)}$$

$$l = \left[2\ell p + 2d_1\ln\left(\frac{a+p}{p-a}\right) + 2(d_2-d_1)\ln\left(\frac{p+b}{b-p}\right) + 2(d_3-d_2)\ln\left(\frac{p+c}{c-p}\right)\right]$$

$$W_1 = \left[2lq + 2d_1 \ln\left(\frac{q+a}{q-a}\right) + 2(d_2-d_1)\ln\left(\frac{q+b}{q-b}\right) + 2(d_3-d_2)\ln\left(\frac{q+c}{c-q}\right)\right]$$

$$W_2 = \left[2L + 2d_1 \ln\left(\frac{1+a}{1-a}\right) + 2(d_2-d_1)\ln\left(\frac{1+b}{1-b}\right) + 2(d_3-d_2)\ln\left(\frac{1+c}{1-c}\right)\right] \tag{2.45}$$

The set of six nonlinear equations given by (2.45) may be solved for six unknowns. The transformation function (2.39) may now be written as

$$z = i\left[-lw + d_1 \ln\left(\frac{w-a}{w+a}\right) + (d_2-d_1)\ln\left(\frac{w-b}{w+b}\right) + (d_3-d_2)\ln\left(\frac{w+c}{w+c}\right)\right]$$

or

$$X = \left[v\cdot l - d_1\left(\tan^{-1}\frac{v}{u-a} - \tan^{-1}\frac{v}{u+a}\right) - (d_3-d_2)\left(\tan^{-1}\frac{v}{u-b} - \tan^{-1}\frac{v}{u+b}\right) - (d_3-d_2)\left(\tan^{-1}\frac{v}{u-c} - \tan^{-1}\frac{v}{u+c}\right)\right] \tag{2.46}$$

$$Y = \left[-ul + \frac{d_1}{2}\ln\frac{(u-a)^2+v^2}{(u+a)^2+v^2} + \left(\frac{d_2-d_1}{2}\right)\ln\frac{(u-b)^2+v^2}{(u+b)^2+v^2} + \left(\frac{d_3-d_2}{2}\right)\ln\frac{(u-c)^2+v^2}{(u+c)^2+v^2}\right] \tag{2.47}$$

From (2.46 and 2.47) it follows that the v -axis is mapped onto the x-axis and the u -axis onto the y-axis. To find the inverse transformation of (2.46) and (2.47), we express these equations as a system of two ordinary equations with x and y as independent variables and integrate them with the following

as initial conditions

$$X = Y = u = v = 0$$

Having obtained the transformation function, we proceed to solve the potential problem first in the w-plane and later map onto the z-plane using the inverse transformation. In the w-plane the potential function has to satisfy the following boundary conditions:

$$\begin{aligned} V &= 0 && \text{On } (a,-a) \\ V &= \Delta V && \text{On } (a,b) \text{ and } (-a,-b) \\ V &= V_2 && \text{On } (b,c) \\ V &= V_1 && \text{On } (-b,-c) \\ V &= V_0 && \text{On } (c,\infty) \text{ and } (-c,-\infty) \end{aligned} \tag{2.48}$$

(see figure 2.24)

To solve the boundary value problem, we consider only one of the boundary conditions at a time and assume $V = 0$ on the rest of the u-axis. These solutions are then to be added together to give the required solution. This kind of superposition is permissible for linear differential equation such as the Laplace equation. The solution is then given by

$$\begin{aligned} V(u,v) = {} & \frac{\Delta V}{\pi}\left[\left(\tan^{-1}\frac{v}{u-b} - \tan^{-1}\frac{v}{u+b}\right) - \left(\tan^{-1}\frac{v}{u-a} - \tan^{-1}\frac{v}{u+a}\right)\right] \\ & \frac{V_1}{\pi}\left[\tan^{-1}\frac{v}{u-c} - \tan^{-1}\frac{v}{u-b}\right] - \frac{V_2}{\pi}\left[\tan^{-1}\frac{v}{u+c} - \tan^{-1}\frac{v}{u+b}\right] \\ & \frac{V_0}{\pi}\left[\tan^{-1}\frac{v}{c-u} + \tan^{-1}\frac{v}{c+u}\right] \end{aligned} \tag{2.49}$$

This is valid everywhere except at certain points on the u-axis

(i.e. $a, b, c, \ldots, -a, -b, -c, \ldots$). This completes the formal solution of the boundary value problem.

2.5 Efficiency of ion beam transmission:

The present section is devoted to the drawing together of the results of the different subproblems discussed in section 2.3. We shall also discuss the ion optical properties of the system, particularly with reference to the ion beam transmission efficiency, that is, the fraction of the beam ultimately entering the magnetic analyser tube.

Since the slit widths are much smaller than the separation between the two consecutive plates, the mutual coupling is expected to be negligible. The repeller plate, however, is not always as far as is required ($d > 10$) for minimum coupling. The following discussion, nevertheless, is based on the assumption that the repeller plate is at a distance equal or greater than ten times the entrance slit width. Further, it was not felt necessary to compute the ion trajectories using the more precise potential distribution given by (2.49). The precision thus gained would be unmeaningful considering the errors introduced by the paraxial approximations and the assumption of zero initial energy.

The typical ion trajectories in the absence of a repeller field are shown in the figure (2.25). They have, in general, two cross-overs. Furthermore, all the ions starting from rest are bound to pass through the entrance slit* and cross the axis

*A particle will not strike the plates because they are at a higher potential than the surrounding space. If, however, the particle has finite initial energy, this will not be true for all particles.

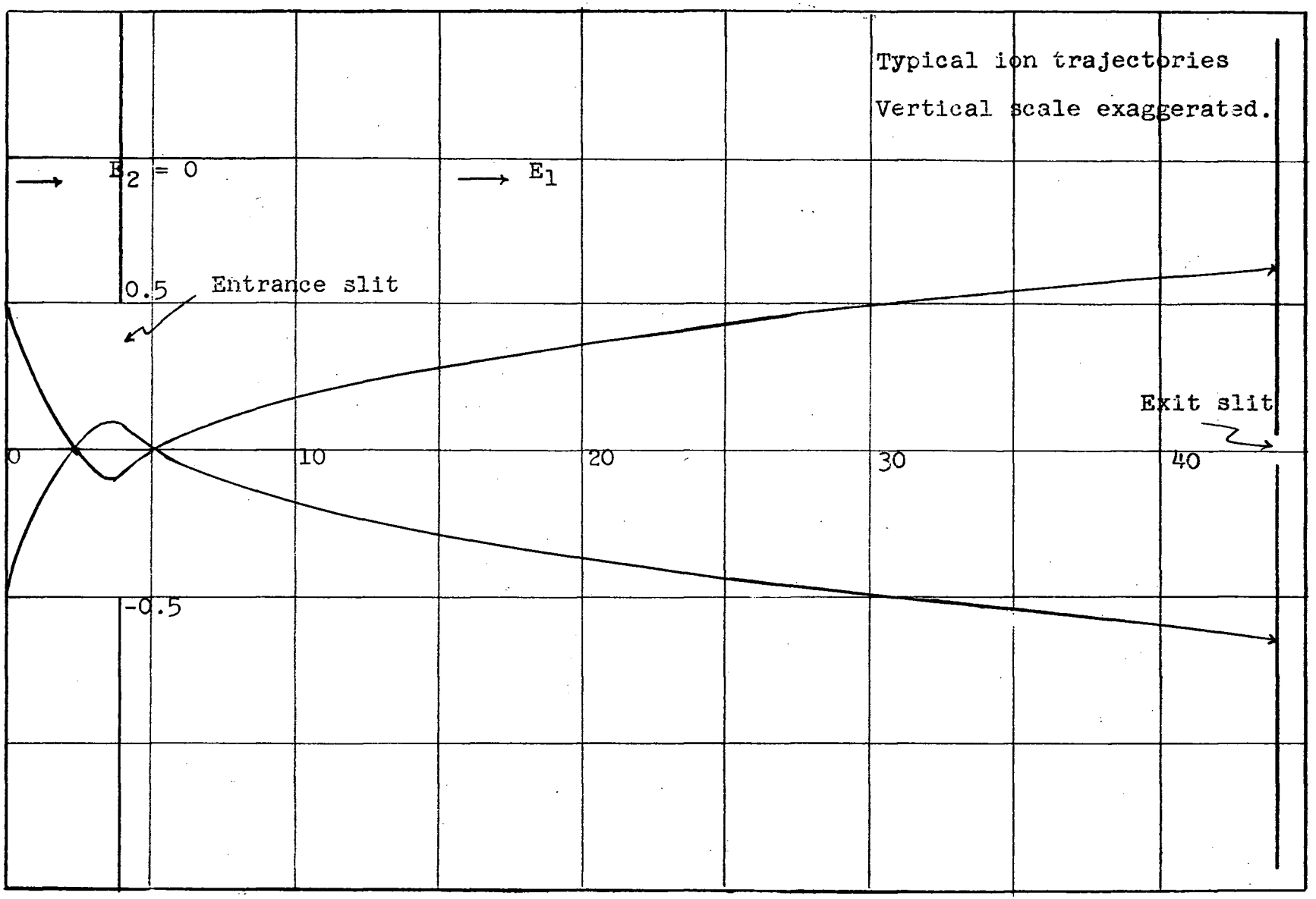
Typical ion trajectories
Vertical scale exaggerated.
$E_2 = 0$
E_1
0.5
Entrance slit
Exit slit
0
10
20
30
40
-0.5

Fig. 2.25

at a short distance ($x_{c_2} \simeq 1$) from the slit and thus produce a fairly sharp focus. The portion of the trajectory to the right of the second cross-over may be approximated by a simple quadratic expression (2.23), which is, incidently, the ion trajectory in a uniform field.

The trajectories are divergent; hence only a few particles are capable of passing through the exit slit which is often much smaller than the entrance slit (about a tenth of entrance slit width). By a process of actual observation whether a given trajectory starting at a point $P(x_0, y_0)$ passes through the exit slit kept at a distance of forty slit widths, we have sketched in fig. (2.26) a region -- a narrow horizontal strip of width approximately equal to the exit slit width. A particle starting anywhere within the region is bound to pass through the exit slit, and all ions formed outside the region are naturally lost completely. This is called the area of ion withdrawal.

However, the situation is somewhat different in the presence of a repeller field in the ionization space. Now the second cross-over is no longer sharp as before but linearly diffused along the axis. It is natural to expect to be able to adjust the repeller field such that the cross-over point lies just in the neighbourhood of the exit slit. Unfortunately, it is not possible to do so for all the ions as we see in fig. (2.27). Only a small fraction of ions coming from a certain specific region of the ionization space will cross the axis near the exit slit. In fig. (2.29) we have given a relation between the

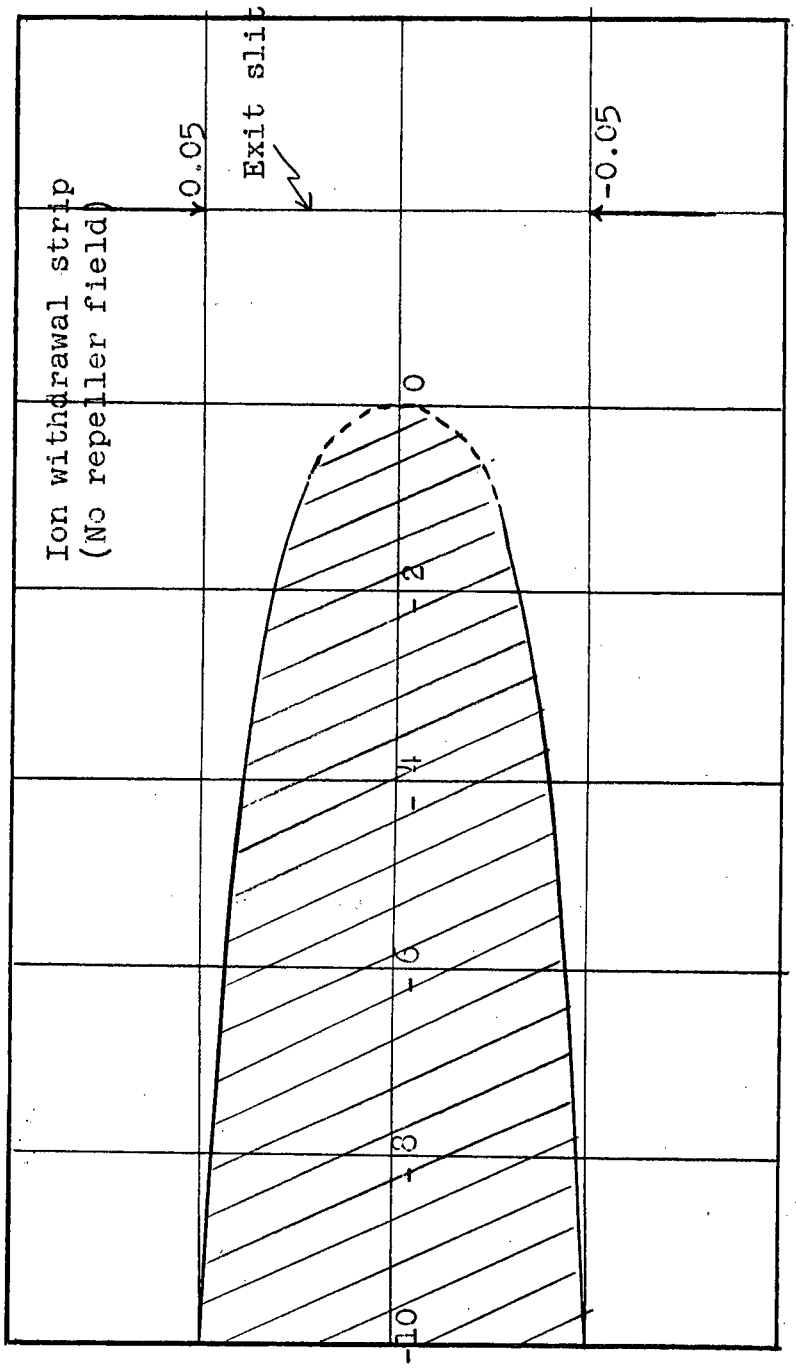
Ion withdrawal strip
(No repeller field)
0.05
Exit slit
-0.05
0
-2
-4
-6
-8
-10

Fig. 2.26

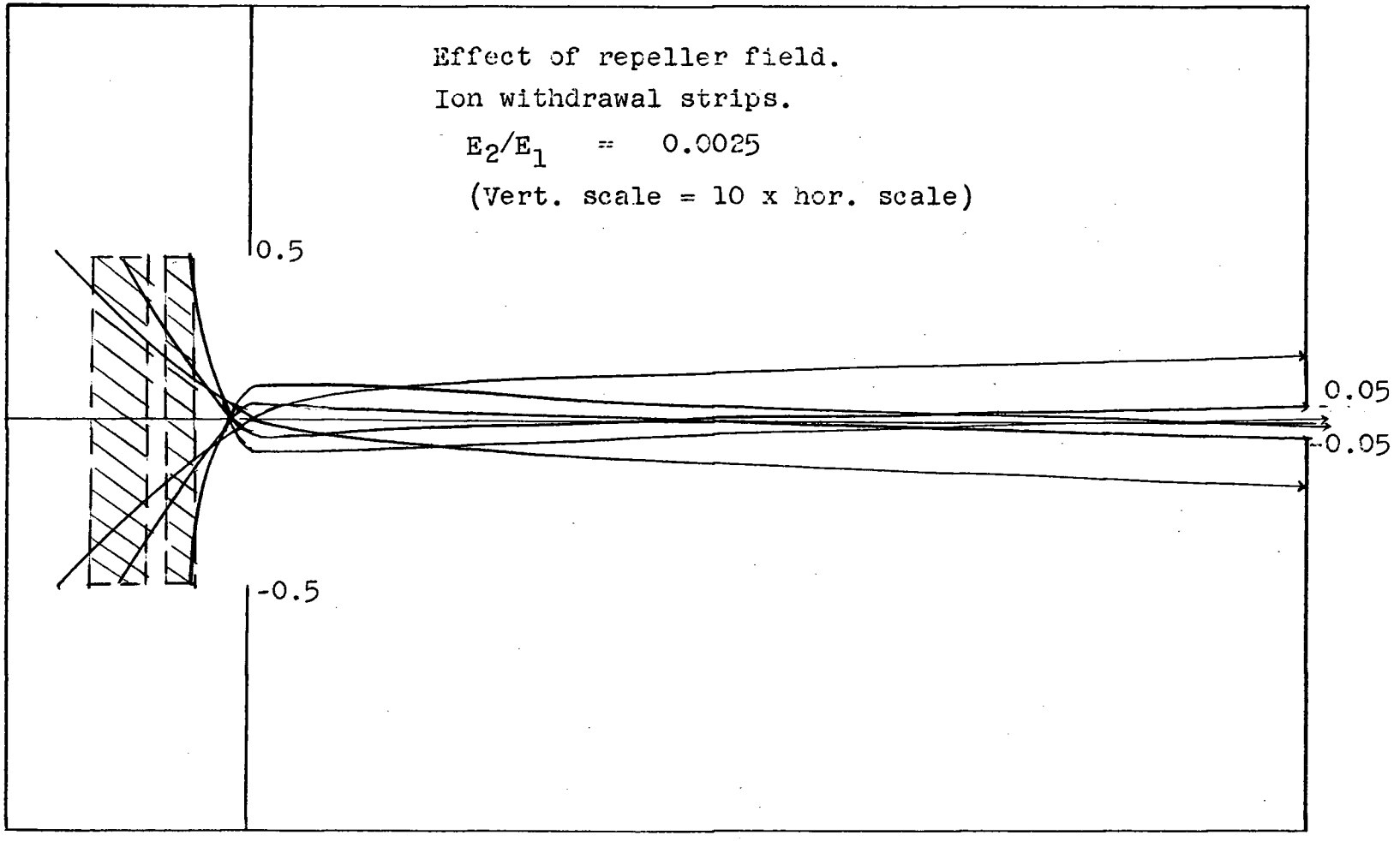
Effect of repeller field.
Ion withdrawal strips.
E_2/E_1 = 0.0025
(Vert. scale = 10 x hor. scale)
0.5
-0.5
0.05
-0.05

Fig. 2.27

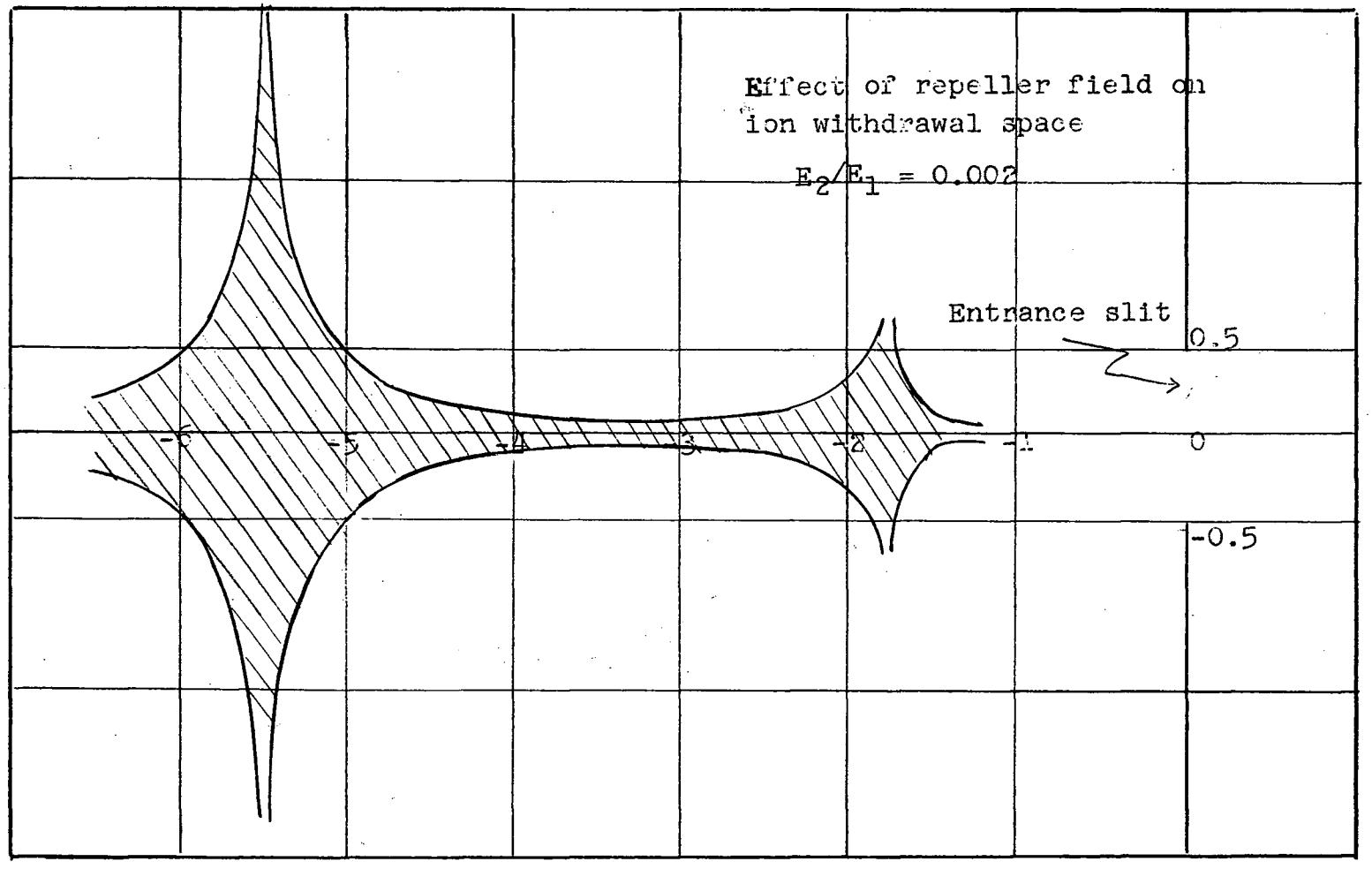
Effect of repeller field on
ion withdrawal space
$E_2/E_1 = 0.002$
Entrance slit
0.5
-0.5
-6
-5
-4
-3
-2
-1
0

Fig. 2.28

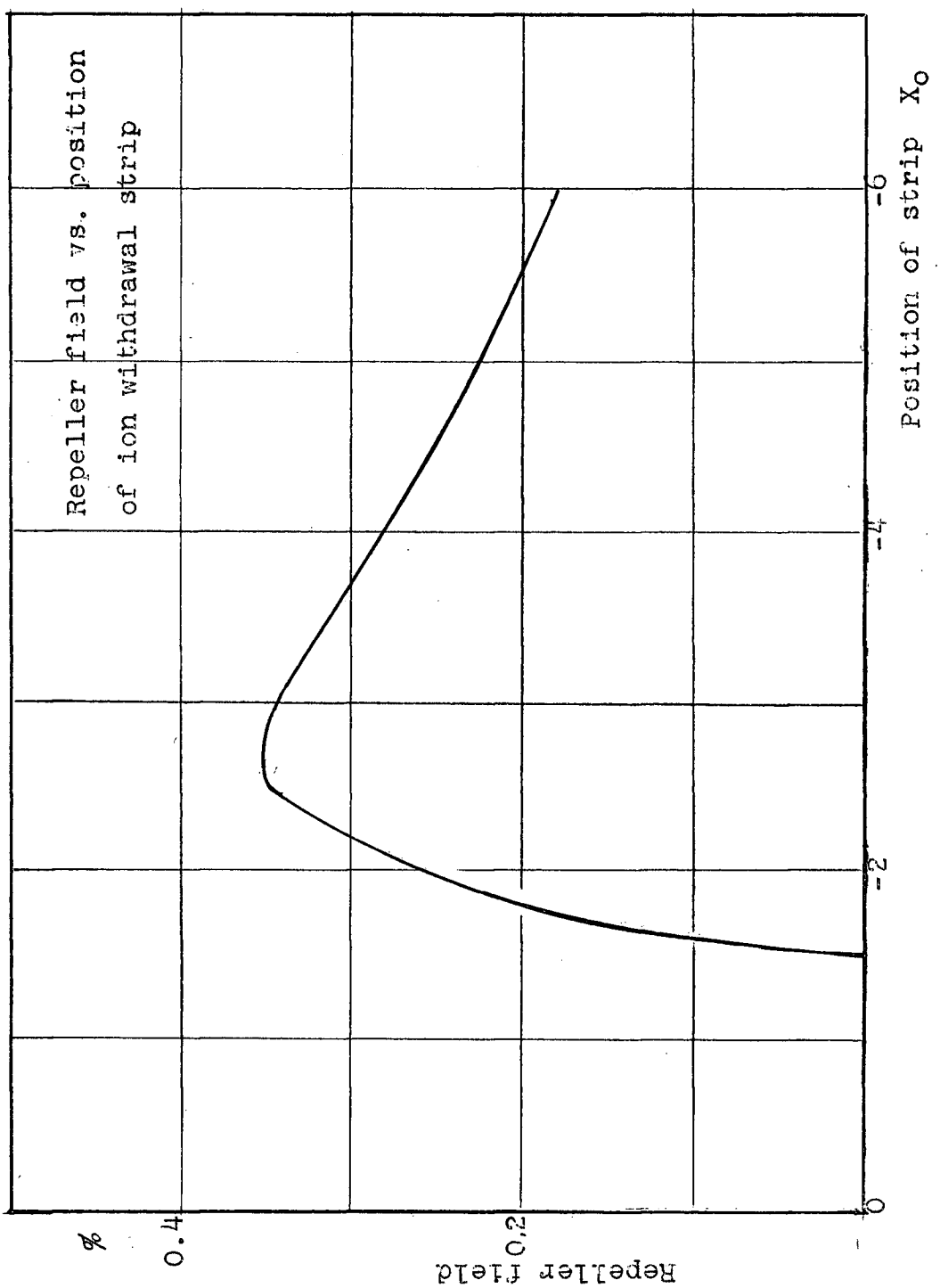
Repeller field vs. position
of ion withdrawal strip
%
0.4
0.2
Repeller field
0
-2
-4
-6
Position of strip X_o

Fig. 2.29

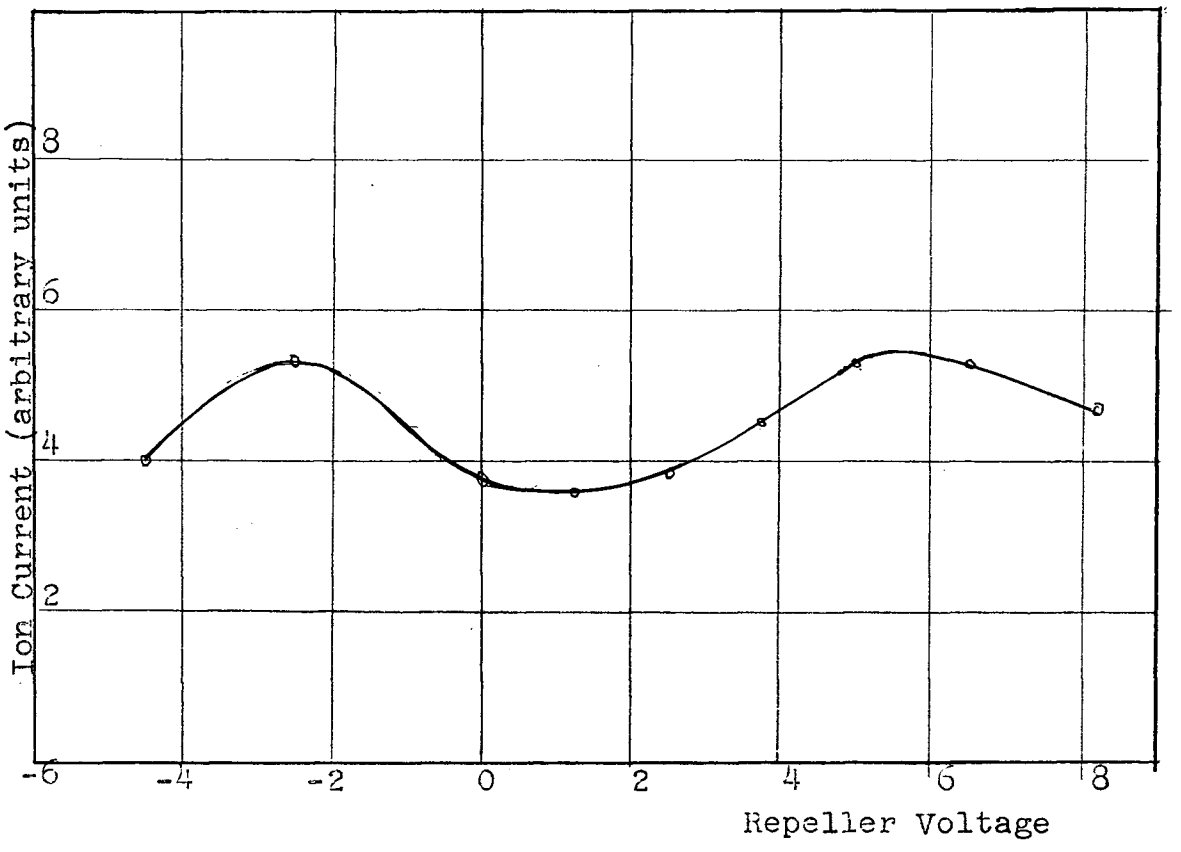

Fig. 2.30

Experimentally observed relationship between the repeller voltage and the ion current.

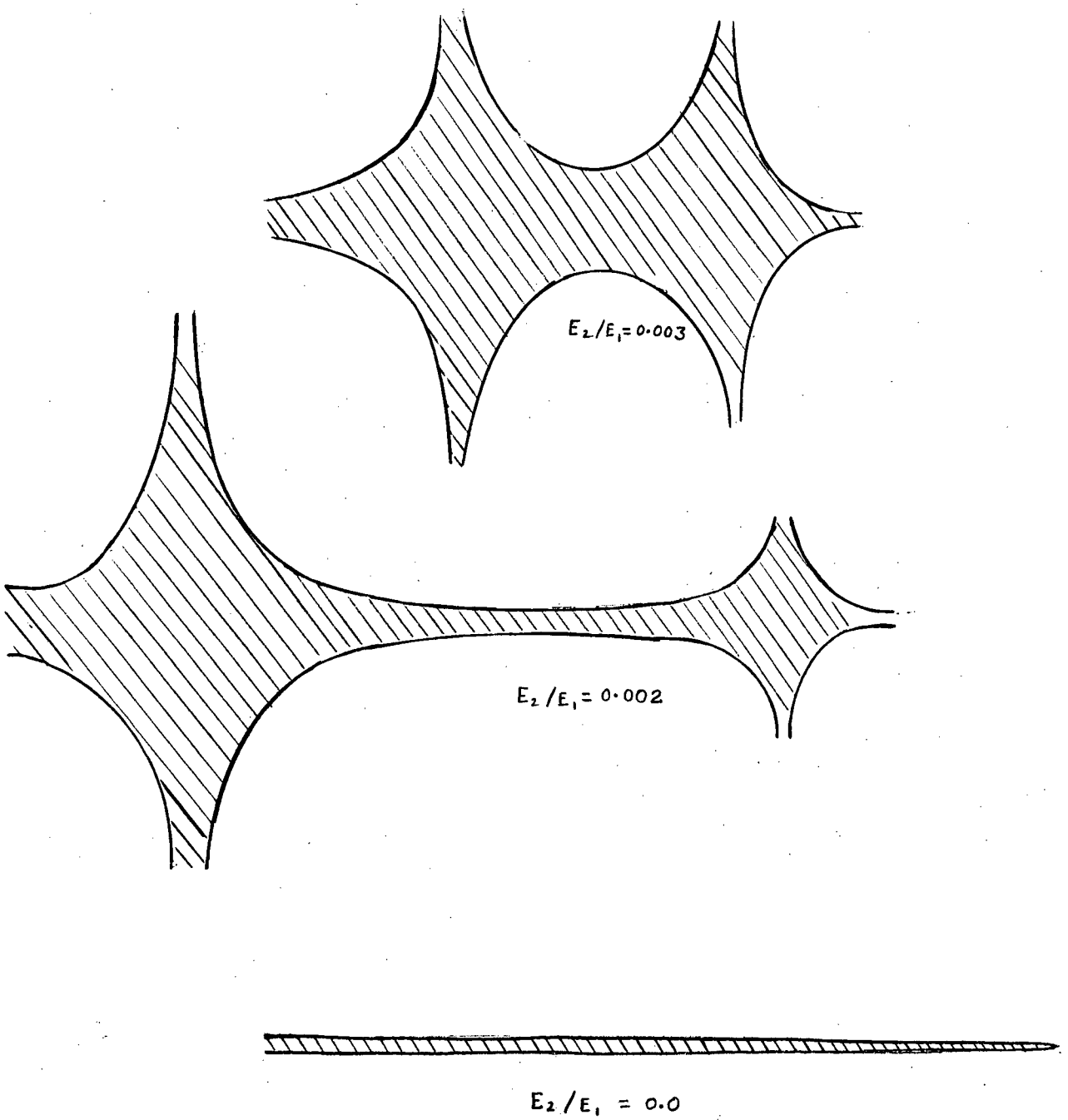

Fig. 2.31

Effect of repeller field on the shape of the strips.

repeller field and the position of the strip of ion withdrawal. For a given value of a repeller field, we see from fig. (2.29) that there are two values of X_0 , two strips of ion withdrawal (fig. (2.27)). The shape of the strips is shown in fig. 2.28 for $E_2/E_1 = 0.002$. Thus, in the presence of a repeller field the ions from a vertical strip are focused in the neighbourhood of the exit slit.

If somehow the ionization could be confined to the narrow strip, we should be able to withdraw almost all the ions. But unfortunately, in practice, it is difficult to confine the ionization to such a restricted space (2 to 3 mm). However, we can adjust the repeller field such that the region of withdrawal corresponds to the region of high ion density. The peaks in the experimentally observed relation between the repeller field and the ion current (fig. (2.30)) may be explained by the above conclusion based on the theoretical considerations.

The effect of the exit slit itself on the ion trajectory, especially the change in the angle of inclination as an ion passes through the exit slit is found to be very small (less than 10%). Also the effect of the magnetic field is small, unless the field is of the order of a few webers/m^2. Furthermore, there will be no perceptible mass discrimination due to the source magnetic field unless the field is large.

In summary, the ion beam transmission efficiency could be increased only if we could confine the ionization to a restricted space and adjust the repeller field accordingly.

Chapter III

The Inverse Problem of Particle Motion

Synopsis:

In this chapter we introduce the concept of the inverse problem of particle motion. In the usual problem we seek the trajectory of a particle, having been given the electrostatic potential distribution. In the inverse problem, we seek the potential distribution to guide a particle along a prescribed path.

Starting from the basic trajectory equation and Laplace equation we have shown that for any prescribed path a unique potential distribution can be obtained. Next, we generalize the problem: a unique potential distribution can be obtained for a set of prescribed paths satisfying certain geometrical relations.

Finally, using the theory, two types of ion sources are proposed. The stability analysis, however, shows that only one of them is stable, and therefore practical. The last section deals with the practical realization of the required potential distribution.

3.1 Theory of Inverse Problem:

Usually we are given a potential distribution and required to find the particle trajectories. But in the most applications we desire the particles to follow certain paths; for instance, certain desirable paths in the ion source of a mass spectrometer are shown in fig. 3.1. This gives rise to the inverse problem: that is, to find a potential distribution to guide the particles

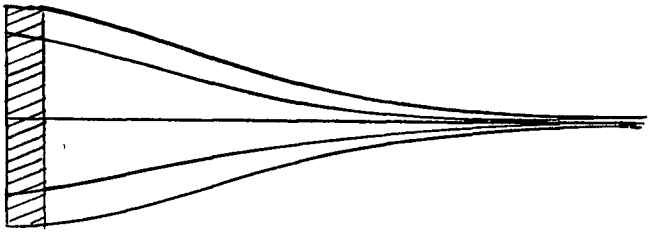

(a) Converging paths.
The shaded strip stands for the ionization space.
The ions are to be guided along a set of converging paths.

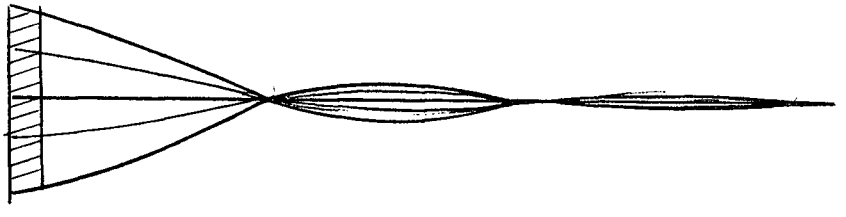

(b) Damped oscillatory paths.
The ions are to be guided along the paths.
The damped oscillatory paths are in a way complementary to converging paths. For more explanation see text p. 85 .

Fig. 3.1

along the prescribed paths. In this section we are going to develop the basic theory of the inverse problem of particle motion.

The author is unaware of any previous work on this problem except a suggestion, first made by Pierce (1954), that the paraxial equation (2.16) may be regarded as an equation for the potential on the axis if η and its derivatives are given.

The following are the two basic theorems in the theory of the inverse problem:

(a) There exists a potential distribution to guide a particle along any desired path.

(b) A group of particles may be guided along a set of paraxial paths.

The proof of the above theorems is given below. We shall confine ourselves to the two dimensional case; however, the arguments may be extended to the three dimensional case, too. In the trajectory equation η, η' and η'' are now known (or prescribed) functions of x. The trajectory equation and Laplace equation form a system of partial differential equations.

$$\eta' \Phi_x - \Phi_\eta + \frac{2\eta''}{1+\eta'^2} \Phi = 0 \qquad (3.1)$$

(The coefficients of Φ_x and Φ are functions of x only.)

$$\Phi_{xx} + \Phi_{\eta\eta} = 0 \qquad (3.2)$$

We have to solve the above system of equations for the potential Φ . The technique of solving the equations is as follows: The equation (3.1) is solved first, given the potential Φ along the prescribed path, to obtain Φ, Φ_x, and Φ_y in the neighbourhood of the path. Knowing Φ_x and Φ_y we can compute the normal derivative $\frac{\partial \Phi}{\partial n}$. The potential Φ and its normal derivative $\frac{\partial \Phi}{\partial n}$ constitute the Cauchy problem. Now in order to find the potential Φ everywhere in the x, y-plane, we have to solve the Cauchy problem for (3.2). The potential is assumed to be analytic as required for the uniqueness of the Cauchy problem (Hellwig, 1964).

The first order partial differential equation (3.1) is equivalent to a system of ordinary differential equations defining the characteristics of the equation (see Courant and Hilbert, p. 62). If we introduce a parameter s, arc length along the characteristics, the system of ordinary equations becomes

$$\frac{dx}{ds} = y'$$

$$\frac{dy}{ds} = -1$$

$$\frac{d\Phi}{ds} = \frac{-2by''}{1+y'^2} \qquad (3.3)$$

where, as usual, the prime indicates differentiation with respect to x. Every surface generated by (3.3) is an integral surface of (3.1). A unique surface, however, may be defined from the initial value problem for (3.3). Let us define a space curve C by

prescribing x, y, and Φ as a function of a parameter t (arc length) such that the projection C_0 of C on the x,y-plane coincides with the prescribed path of a particle. Now, in the neighbourhood of C_0, we seek an integral surface $\Phi(x,y)$ which passes through C, that is, a solution of (3.1) for which

$$\Phi(t) = \Phi(x(t), y(t))$$

holds identically in t. To solve the initial value problem, let us draw through each point of C a characteristic, that is, the solution of (3.3); this is possible in a unique way within a certain neighbourhood. We thus obtain a family of characteristics

$$\begin{aligned} x &= x(s,t) \\ y &= y(s,t) \\ \Phi &= \Phi(s,t) \end{aligned} \tag{3.4}$$

These curves will generate a surface $\Phi(x,y)$ if, using the first two functions, we can express s and t in terms of x and y. To be able to do this, we must show that the Jacobian

$$\Delta = \frac{\partial x}{\partial s} \cdot \frac{\partial y}{\partial t} - \frac{\partial y}{\partial s} \cdot \frac{\partial x}{\partial t}$$

is non-vanishing. Using equation (3.3) we obtain

$$\begin{aligned} \Delta &= y' y_t + x_t \\ &= y_t \left(\frac{1+y'^2}{y'} \right) \end{aligned}$$

which is non-vanishing for all values of y'. The geometrical

interpretation of the condition that the Jacobian is non-vanishing is that at every point on C_0 the projection of the tangent direction and characteristic direction on the x,y-plane are distinct. In fact in our case, since

$$\frac{dx}{ds} = y'_{(Path)}$$

$$\text{and} \quad \frac{dy}{ds} = -1$$

$$\therefore \quad \left(\frac{dy}{dx}\right)_{char} = -\frac{1}{y'}$$

$$\therefore \quad \left(\frac{dy}{dx}\right) \cdot \left(\frac{dy}{dx}\right)_{Path} = -1$$

the base characteristic and the path of a particle are orthogonal. We therefore conclude that for any simple * prescribed path a solution of equation (3.1) may be found in the neighbourhood of the path; and therefore, $\frac{\partial \Phi}{\partial n}$, the normal gradient may be found. The potential distribution in the x,y-plane may be obtained as a solution of the Cauchy problem for equation (3.2). This establishes theorem I. We next proceed to the second theorem.

We recall that in the solution of (3.1) as an initial value problem, the potential Φ was prescribed arbitrarily along the path of a particle. This may now be chosen such that a group of particles moves along a set of paraxial paths that are prescribed again arbitrarily. The trajectory equation of the neighbourhood particles in the paraxial approximations is given by Waters (1958):

$$2\Phi u'' + \Phi' u' + (4K^2\Phi + \Phi'')u = 0 \tag{3.5}$$

*The path may not have any double points.

where μ is the normal distance of a neighbouring particle from the central trajectory, and K the ~~radius of~~ curvature of the central trajectory at a given point. In equation (3.5) we may assume that μ and K are known (or prescribed) functions and solve the equation for Φ. Thus, one may obtain Φ for any prescribed path of a particle. But unless the set of paths is suitably chosen, the potential Φ will be different for each individual path. The condition that the set of paths must satisfy so that a unique potential function may be obtained is as follows:

Let

$$\mu = c\left(1 + a_1 t + a_2 t^2 + \cdots\cdots a_n t^n\right) \tag{3.6}$$

where t is arc length, and c a variable constant -- by varying c one may obtain a series of paths. If we substitute (3.6) into (3.5), we find that the resulting equation does not contain the variable constant c. Hence, a set of paths prescribed by varying c gives rise to a unique potential function Φ. Since in (3.6) $a_1, a_2, a_3 \cdots\cdots a_n$ are arbitrary, the set of paths represented by (3.6) is quite general; however, the function (3.6) must be continuous and must possess continuous derivatives up to the second order with respect to t.

A simple case of considerable importance is where the x-axis is the central path. Then, the equation (3.1) and (3.5) reduce to

$$\Phi_y = 0 \tag{3.7}$$

$$2\Phi_0 y'' + \Phi_0' y' + \Phi_0'' y = 0 \tag{3.8}$$

It may be noted that any potential distribution which is symmetric about the x-axis satisfies (3.7). To obtain the potential at any point $P(x,y)$, we solve the Cauchy problem, which in this case is particularly simple: Let $\Phi(x)$ be the axial potential, then the potential at any given point P is given by

$$\Phi(x,y) = Re\left(\Phi_0(x+iy)\right) \tag{3.9}$$

(see Morse and Feshbach, p. 689)

The Cauchy problem is known to be sensitive to the small fluctuations in Φ_0 and may give rise to large errors; but since we are basically interested in the paraxial region where the errors, if any, will not be large; this is not a very serious drawback.

3.2 Efficient ion source:

The sensitivity of a mass spectrometer is largely limited by the inefficient ion source. Only one molecule out of a million molecules reaches the analyser tube as an ion. In the previous chapter we have discussed the ion optical properties of the conventional source. There, we have seen that unless the ionization is confined to a very small region, we cannot improve the efficiency by merely adjusting the various geometrical and field parameters of the source. We feel that the entire design of the source may have to be discarded in favour of a more complex system. The question we now have to face is how are we going to devise a new system that would have high efficiency.

One way is to try a number of them until we hit upon a right one. This is obviously a tedious and uncertain process. The theory of the inverse problem, which we have developed in the last section, comes to our aid in obtaining a system that has the desired properties; thus, the long and laborious trial and error method can be avoided.

Imagine a set of paths slowly converging into a thin parallel beam as shown in fig. (3.1)* . Initially the paths are wide apart and therefore cover a large portion of the ionization space. The paths in fig. (3.1a) are exponentially converging while those in fig. (3.1b) are damped oscillatory. The central path is however, the x-axis. We now apply the theory developed in the previous section to find the potential distribution such that the particles are guided along these paths.

A class of converging paths may be represented by

$$y = a \exp(-b x^n)$$

where a is a variable constant, and b and n are fixed constants. Substituting in (3.8), we obtain

$$\Phi_0'' - b\,n\,x^{n-1}\,\Phi_0' + \frac{2(1+bnx^n-n)}{x^{2-n}}\,b\,n\,\Phi_0 = 0 \qquad (3.10)$$

The equation reduces to a particularly simple form for $b = 1$ and $n = 1$

$$\Phi_0'' - \Phi_0' + 2\Phi_0 = 0 \qquad (3.11)$$

*We are considering two different systems having the same properties. It will be clear later why we consider two systems.

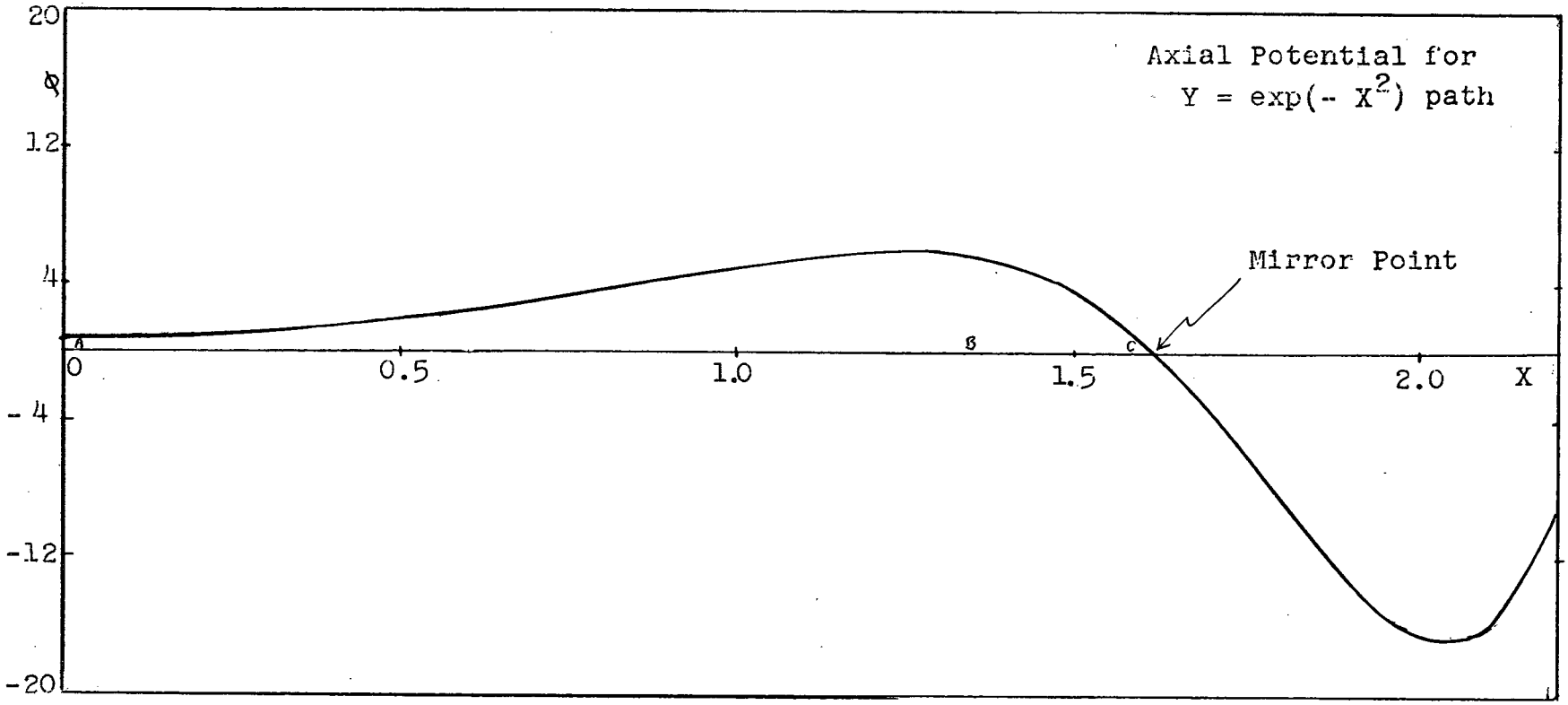
Axial Potential for
Y = exp(- X²) path
Mirror Point
20
12
4
- 4
-12
-20
0
0.5
1.0
1.5
2.0
X

Fig. 3.2

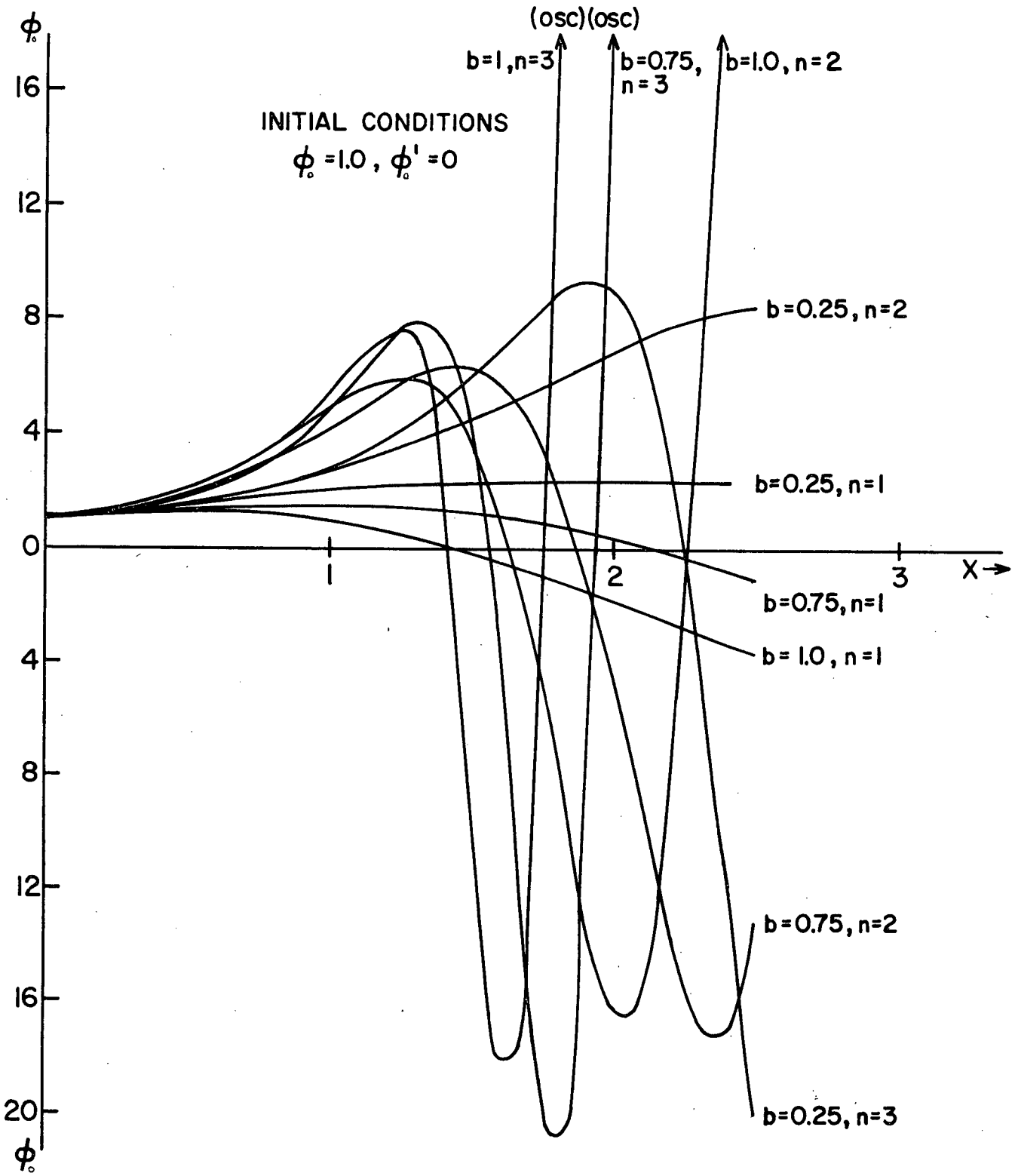

FIG. 3·3 AXIAL POTENTIAL FOR CONVERGING PATHS

$Y = a \exp(-bx^n)$

whose solution is given by

$$\Phi_0 = \exp(x/2)\,\sin\frac{\sqrt{7}}{2}(x-\beta)$$

(see Kamke, p. 412)

A series solution of (3.10) can be obtained for $b=1$ and $n=2$. Then the equation reduces to

$$\Phi_0'' - 2x\Phi_0' + 4(2x^2+1)\Phi_0 = 0 \tag{3.12}$$

Consider the series

$$\Phi_0 = a_0 + a_1 x + a_2 x^2 + \cdots$$

Substituting in (3.12) and letting the coefficients of x and its higher powers go to zero, we obtain the recurrence relation

$$(n+1)(n+2)\,a_{n+2} - 2n\,a_n + 8\,a_{n-2} - 4\,a_n = 0$$

which enables us to find the constants $a_2, a_3, \cdots\cdots a_n$ having been given a_0 and a_1. The series is convergent (though the number of terms required to attain an accuracy within $\pm$ 0.001% increases rapidly for $x > 2$). For large intervals, that is $x > 2$, and for other values of b and n it is convenient (and efficient from the point of machine time) to solve (3.10) numerically. These solutions are shown in fig. (3.3).

From fig. (3.3) it is obvious that the solutions are oscillatory and unstable. The potential along the path is oscillatory and hence alternatively positive and negative. Let us imagine a particle starting at A in fig. (3.2) with a unit

initial energy and moving along the axis. The particle is accelerated until it reaches the point B and thereafter decelerated until it reaches the point C where its energy goes to zero. It cannot proceed any further unless the sign of the charge on the particle is changed. Since this is not physically possible, it goes back to B and then to A . The point C may be called a mirror point. There are as many mirror points as the number of zeros of equation (3.10). Therefore, the converging paths are not necessarily accelerating paths nor complete paths, i.e., free of mirror points. Such a behaviour is quite consistent with the properties of the equation of motion (Chapter II, eq. (2.16).

The equation (3.8) is almost symmetric for Φ_0 and y . It may be written as

$$\Phi'' = -\left[\frac{y'}{y}\Phi_0' + \frac{2y''}{y}\Phi_0\right] \tag{3.12}$$

or

$$y'' = -\tfrac{1}{2}\left[\frac{\Phi_0'}{\Phi_0}y' + \frac{\Phi_0''}{\Phi_0}y\right] \tag{3.13}$$

They would have been exactly symmetrical but for the figure 2 in the equation. By exact symmetry we mean, if $y = g(x)$ in (3.12) and $\Phi_0 = g(x)$ in (3.13), we would have obtained exactly the same solutions. In any case the presence of the figure 2 does not completely destroy the symmetry for if in eq. (3.9)

$$\Phi_0 = \exp(-b x^n)$$

the trajectories will be unstable oscillatory functions; but such trajectories are not of interest. On the other hand, if

$$\Phi_0 = \exp(b x^n)$$

we should obtain oscillatory trajectories. Let us consider a simple function

$$\Phi_0 = \exp(b x^n) \tag{3.14}$$

The equation (3.8) reduces to

$$y'' = -\tfrac{1}{2}(y' + y)$$

whose solution is given by

$$y = A\, e^{-x/4} \cdot \sin \frac{\sqrt{7}}{4}(x - B) \tag{3.15}$$

where A and B are arbitrary constants. Since Φ is a monotonically increasing function, the resulting paths are both accelerating and complete, that is, without any mirror points.

Though the first system is not of much practical importance (because of the presence of the mirror points) as compared to the second system with the damped oscillatory paths, it is interesting to consider both for comparison. Furthermore, we shall show in the next section that the first system is essentially unstable.

The Cauchy boundary value problem was solved as shown in Section (3.1). The potential distribution in the x,y-plane is shown in figures (3.4) and (3.5). A typical ion trajectory is shown by the dashed curve in each of these figures.

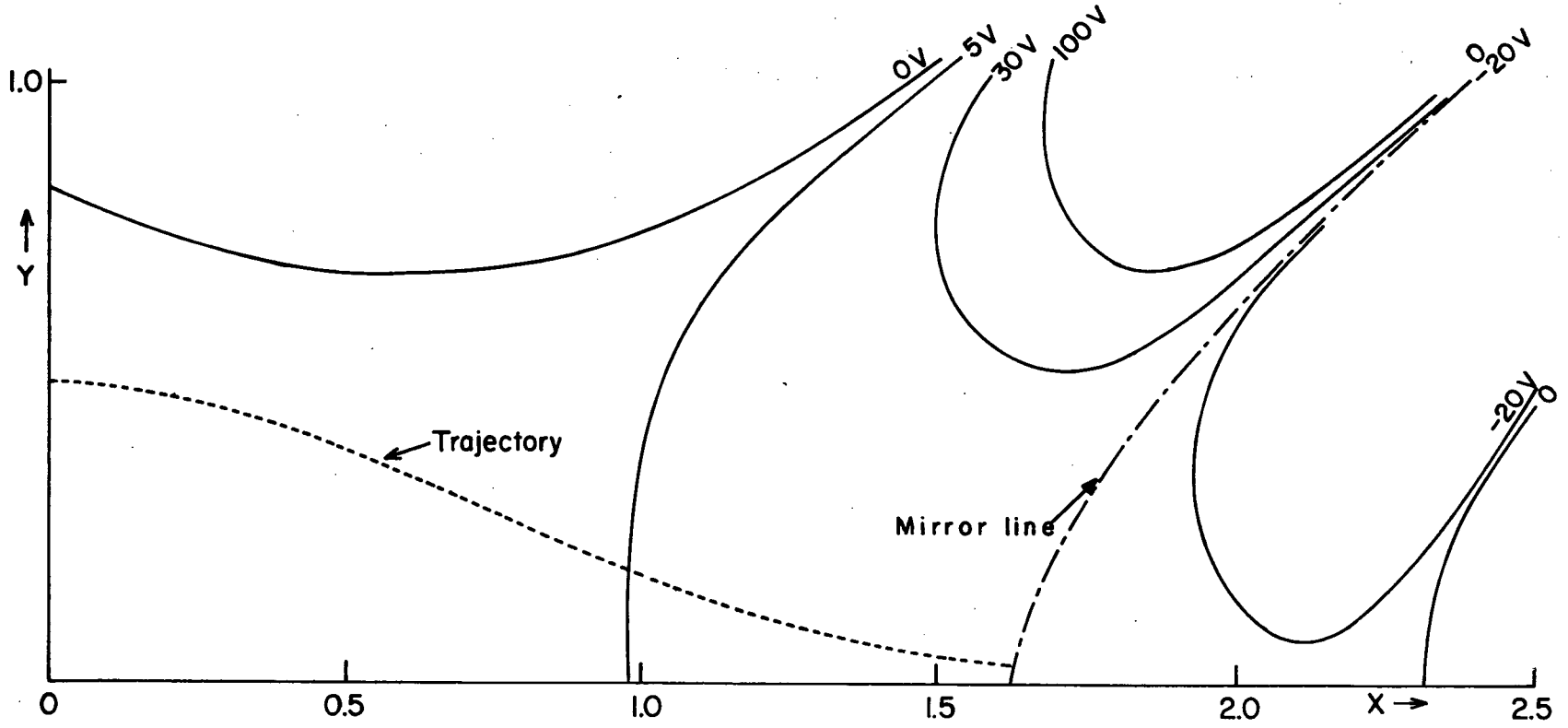

FIG. 3-4 SYSTEM I POTENTIAL DISTRIBUTION FOR CONVERGING PATHS

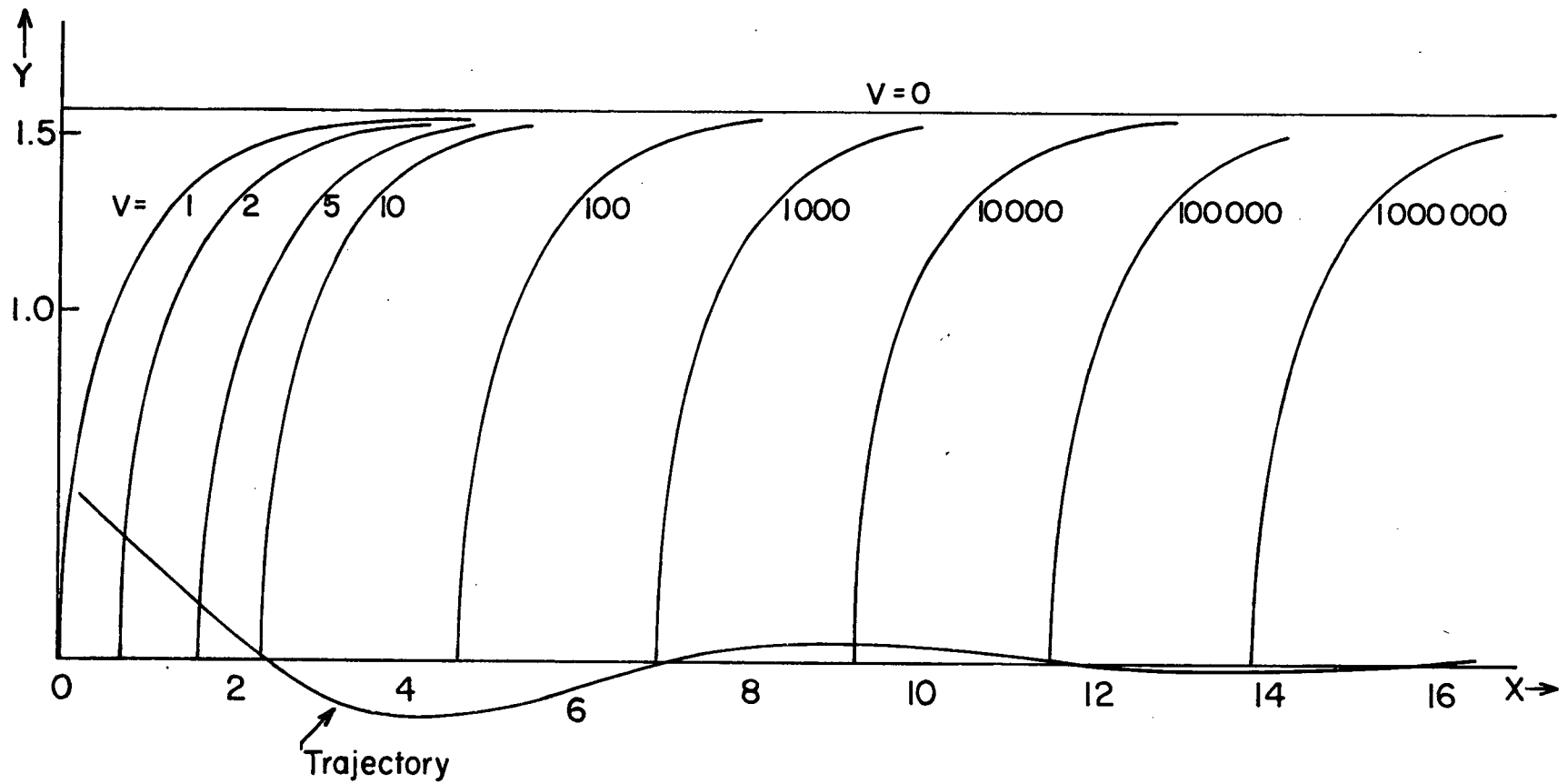

FIG. 3·5 SYSTEM II POTENTIAL DISTRIBUTION FOR DAMPED OSCILLATORY PATHS

3.3 Stability analysis:

The basic assumptions in the theory of the inverse problem are that a particle starts with the same initial energy and in a direction proportional to the height of the starting point. These assumptions are, however, rarely satisfied in a 'real' source, for the thermal energy spread is bound to exist and also the probability of emission in all directions is equal. The present section is, therefore, devoted to the study of the effects of more realistic initial conditions, conditions not satisfying the requirements of the theory. One consequence is that some of the particles may deviate considerably from their projected paths, leading to an unstable situation. The systems leading to unstable paths are impractical, and therefore, every proposed system must be carefully examined. The two cases we have studied here present an example of a stable and an unstable system. The gross effect of the thermal energy spread has been considered by several authors: Pierce (1954), Cutler and Hines (1955), and Kirsteinen (1963). Assuming the Maxwellian velocity distribution and equal probability of emission in all directions at the cathode, these authors attempted to find the longitudinal current density distribution at any plane x = const. But, such a method is not very useful to study the stability of a system because the stability information could be obtained easily by considering just one particle instead of a whole ensemble of particles as in their method. We shall, therefore, adopt a method due to Poincaré (1905) and Moulton (1926) with certain modifications to suit our needs.

The paraxial trajectory equation of an ion whose initial energy differs from the mean by ϵ is given by

$$2(\Phi_0+\epsilon)y'' + \Phi_0' y' + \Phi_0'' y = 0 \tag{3.16}$$

where Φ is the solution of

$$2\Phi_0 y_0'' + \Phi_0' y_0' + \Phi_0'' y_0 = 0 \tag{3.16'}$$

where y_0 is the path of a normal particle. We can express the solution of (3.16) in terms of

$$y = y_0 + \epsilon y_1 + \epsilon^2 y_2 + \epsilon^3 y_3 + \cdots\cdots \epsilon^n y_n \tag{3.17}$$

where $y_1, y_2, y_3 \cdots\cdots y_n$ are the perturbation functions. Substituting (3.17) into (3.16) and letting the coefficients of ϵ and its higher powers tend to zero, we obtain a system of differential equations:

$$2\Phi_0 y_1'' + \Phi_0' y_1' + \Phi_0'' y_1 + 2y_0'' = 0$$

$$2\Phi_0 y_2'' + \Phi_0' y_2' + \Phi_0'' y_2 + 2y_1'' = 0$$

- - - - - - - - - - - - - - -

- - - - - - - - - - - - - - - - -

$$2\Phi_0 y_n'' + \Phi_0' y_n' + \Phi_0'' y_n + 2y_{n-1}'' = 0 \tag{3.18}$$

All perturbation functions may be required to satisfy the initial conditions

$$y_n = 0$$

$$y_n' = 0 \qquad \text{at } x = 0$$

for all n $(n \neq 0)$

while the principal solution y_0 satisfies the given initial conditions. Let u_0 and v_0 be the fundamental solutions of (3.16′) satisfying the initial conditions

$$u_0 = 1$$

$$u_0' = 0$$

$$v_0 = 0$$

$$v_0' = 1$$

so that we may write

$$y_0 = a u_0 + b v_0$$

where a and b are the initial conditions. The first perturbation function may be written as*

$$y_1 = -v_0 \int \frac{2 y_0'' u_0}{\Delta(u_0, v_0)}\, dx + u_0 \int \frac{2 y_0'' v_0}{\Delta(u_0, v_0)}\, dx \qquad (3.19)$$

where

$$\Delta(u_0, v_0) = 2\pi (u_0 v_0' - u_0' v_0) \quad \text{(Wronskian)}$$

* To obtain this refer to Morse and Feshbach, p. 530; in 5.2.19 let $c_1 = c_2 = 0$, because of our initial conditions.

Substituting for y_0 in (3.19) we obtain

$$y_1 = +v_0 \int -2\frac{(a u_0'' + b v_0'')u_0}{\Delta(u_0, v_0)}dx + u_0 \int -2\frac{(a u_0'' + b v_0'')v_0}{\Delta(u_0, v_0)}dx \tag{3.20}$$

or

$$y_1 = a\left[+v_0 \int -\frac{2u_0'' u_0}{\Delta(u_0, v_0)}dx + u_0 \int -\frac{2u_0'' v_0}{\Delta(u_0, v_0)}dx\right]$$

$$+ b\left[+v_0 \int -\frac{2v_0'' u_0}{\Delta(u_0, v_0)} + u_0 \int -\frac{2v_0'' v_0}{\Delta(u_0, v_0)}dx\right] \tag{3.21}$$

Compare each of the brackets on the right-hand side of (3.21) with (3.19). Each of them represents a perturbation function corresponding to one of the fundamental solutions, u_0 and v_0 ; hence we may write

$$y_1 = a u_1 + b v_1$$

where u_1 and v_1 are the first order fundamental perturbation functions corresponding to the fundamental solutions u_0 and v_0 respectively. Following a similar procedure, we can show that

$$y_n = a u_n + b v_n$$

for all values of n . The fundamental perturbation functions may be obtained by solving the equation (3.16′) and (3.18) numerically, treating them as a system of $(n+1)$ equations. This

approach to finding the perturbation functions overcomes the necessity of evaluating them for each set of initial conditions; in this respect this method is superior to that of Poincaré and Moulton.

For the sake of simplicity let us specify the normal initial conditions as

$$y_0 = a$$
$$y_0' = 0 \qquad \text{at } x = 0$$

and the initial energy as unity ($\Phi(0) = 1$). The normal trajectory of a particle with more realistic initial conditions is then given by

$$\tilde{y} = a u_0 + b v_0 + a \sum_1^n \epsilon^n u_n + b \sum_1^n \epsilon^n v_n \tag{3.22}$$

The fundamental solutions u_0, v_0 and the first three fundamental perturbation functions for both the systems are illustrated in figures (3.6) to (3.13). These may be used to compute the total perturbation for any given set of more realistic initial conditions.

The fundamental perturbation functions for the system I increase monotonically in the region where the particles are being accelerated, and outside this region they tend to oscillate (not shown in the figures). Hence it is expected that the more realistic initial conditions will be amplified to such a stage where the particles deviate so much from their projected paths that it leads to what we have called instability. Therefore,

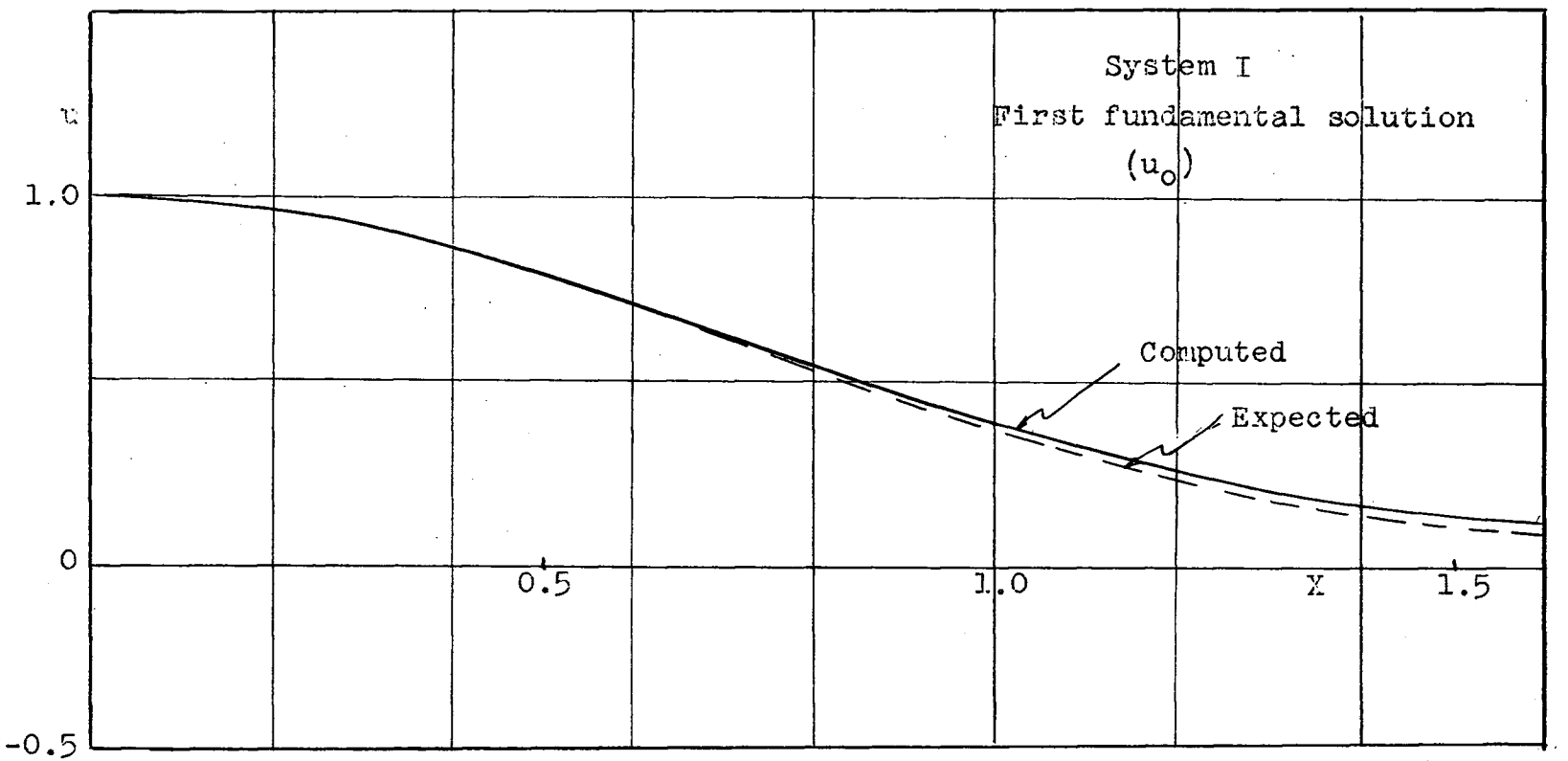
System I
First fundamental solution
(u_o)
u
1.0
0
-0.5
0.5
1.0
1.5
X
Computed
Expected

Fig. 3.6

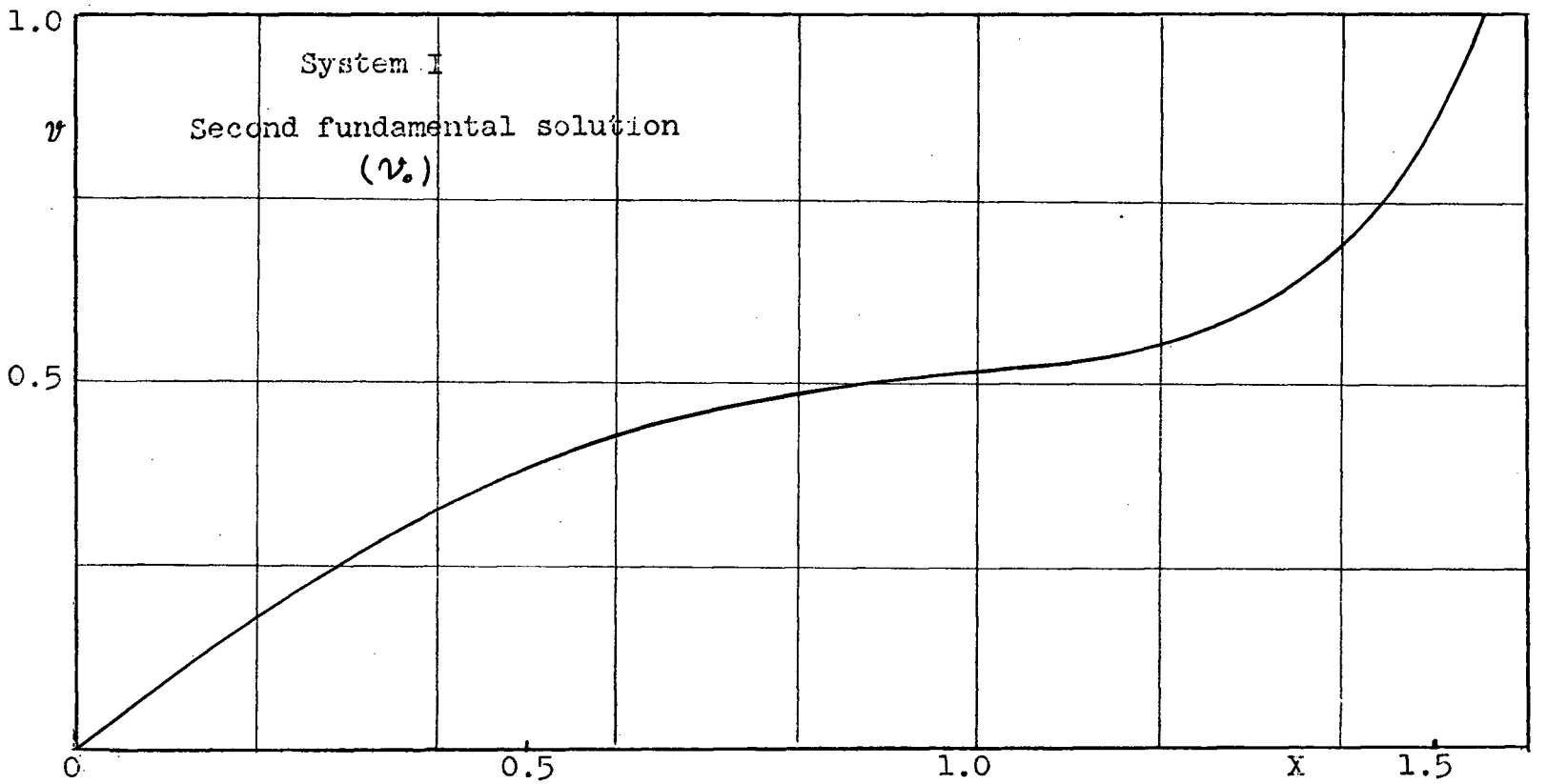

Fig. 3.7

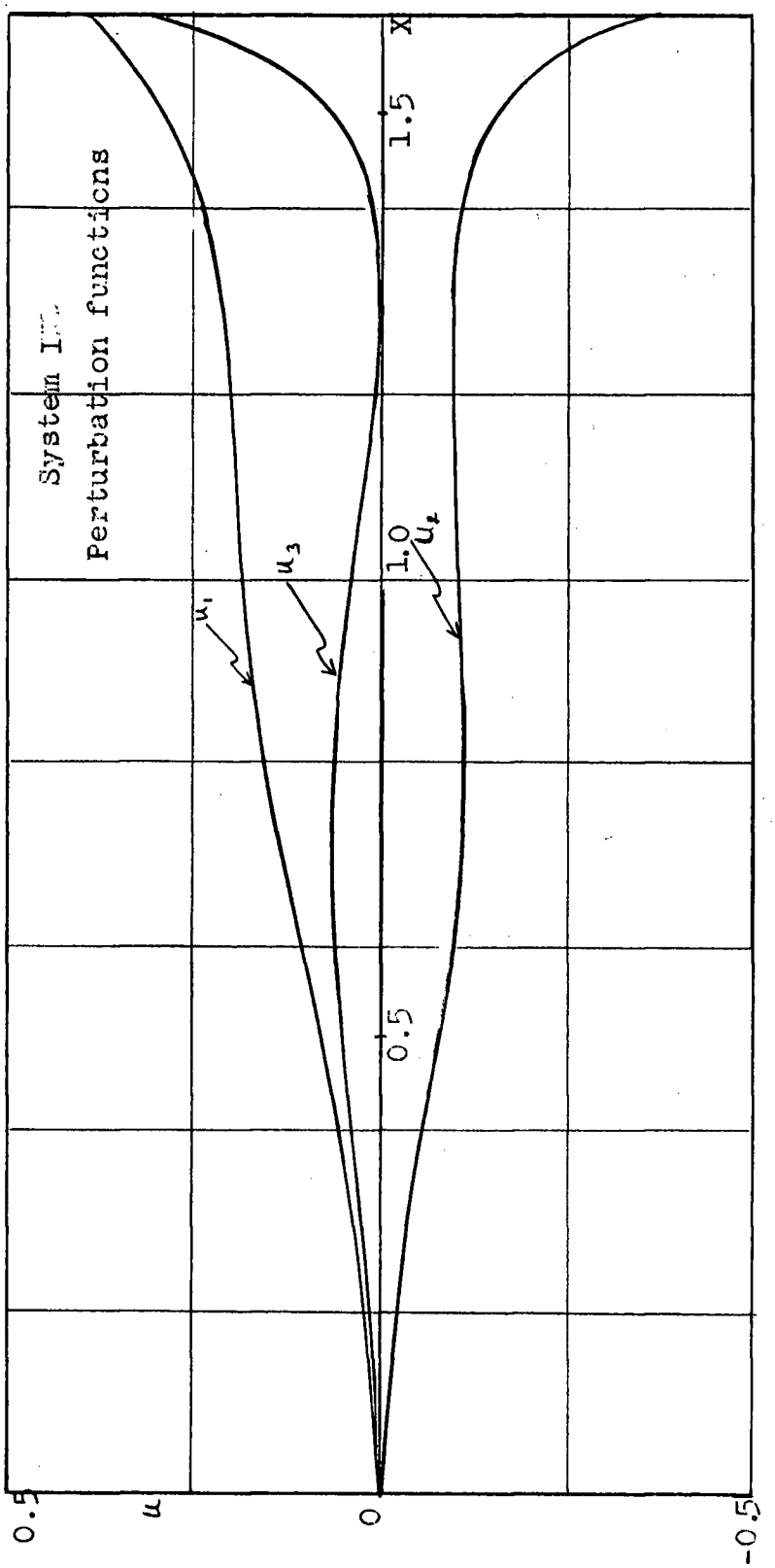

Fig. 3.8

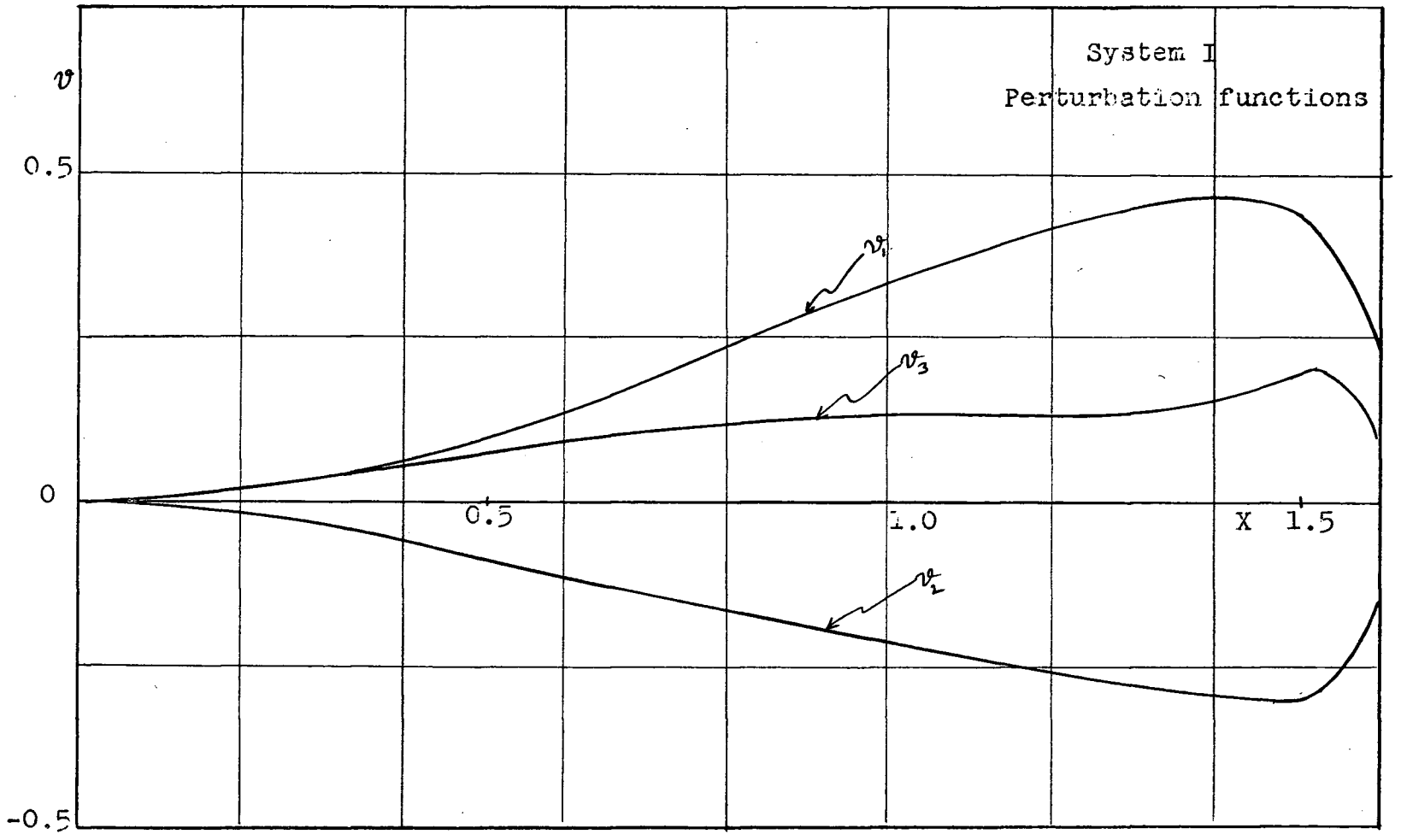

Fig. 3.9

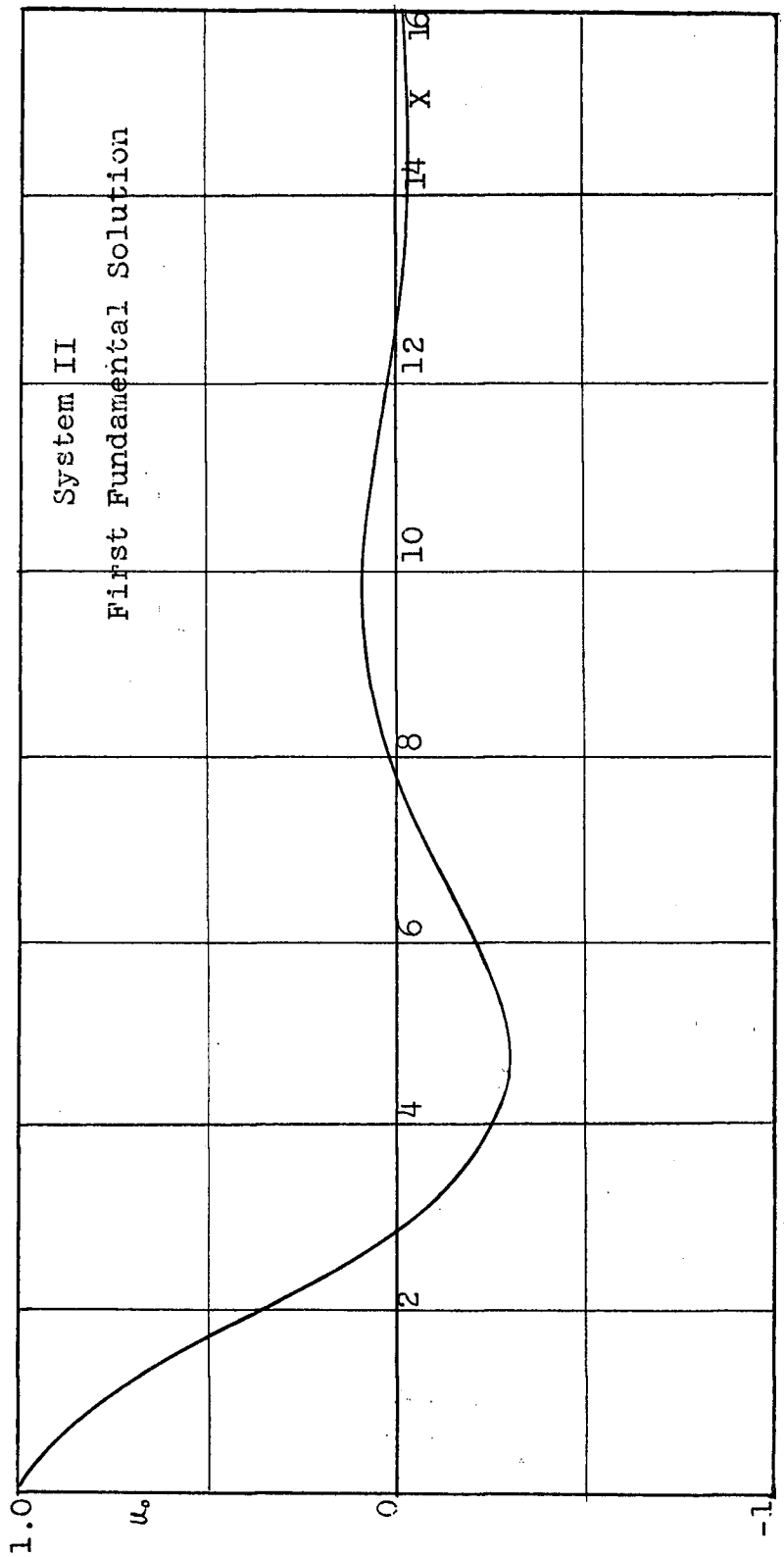
System II
First Fundamental Solution
1.0
u_o
0
-1
2
4
6
8
10
12
14
16
x

Fig. 3.10

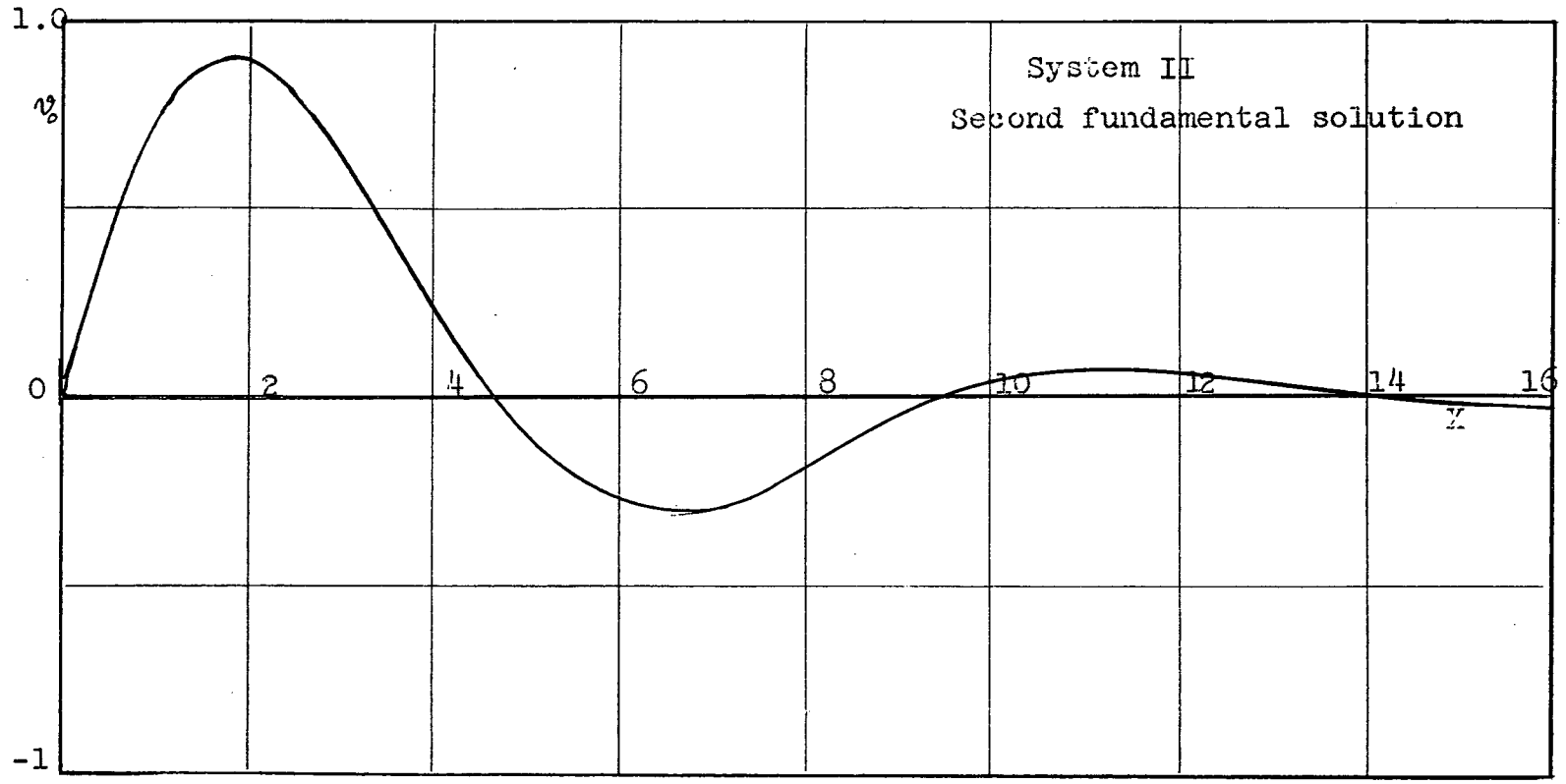
1.0
v_0
0
-1
2
4
6
8
10
12
14
16
x
System II
Second fundamental solution

Fig. 3.11

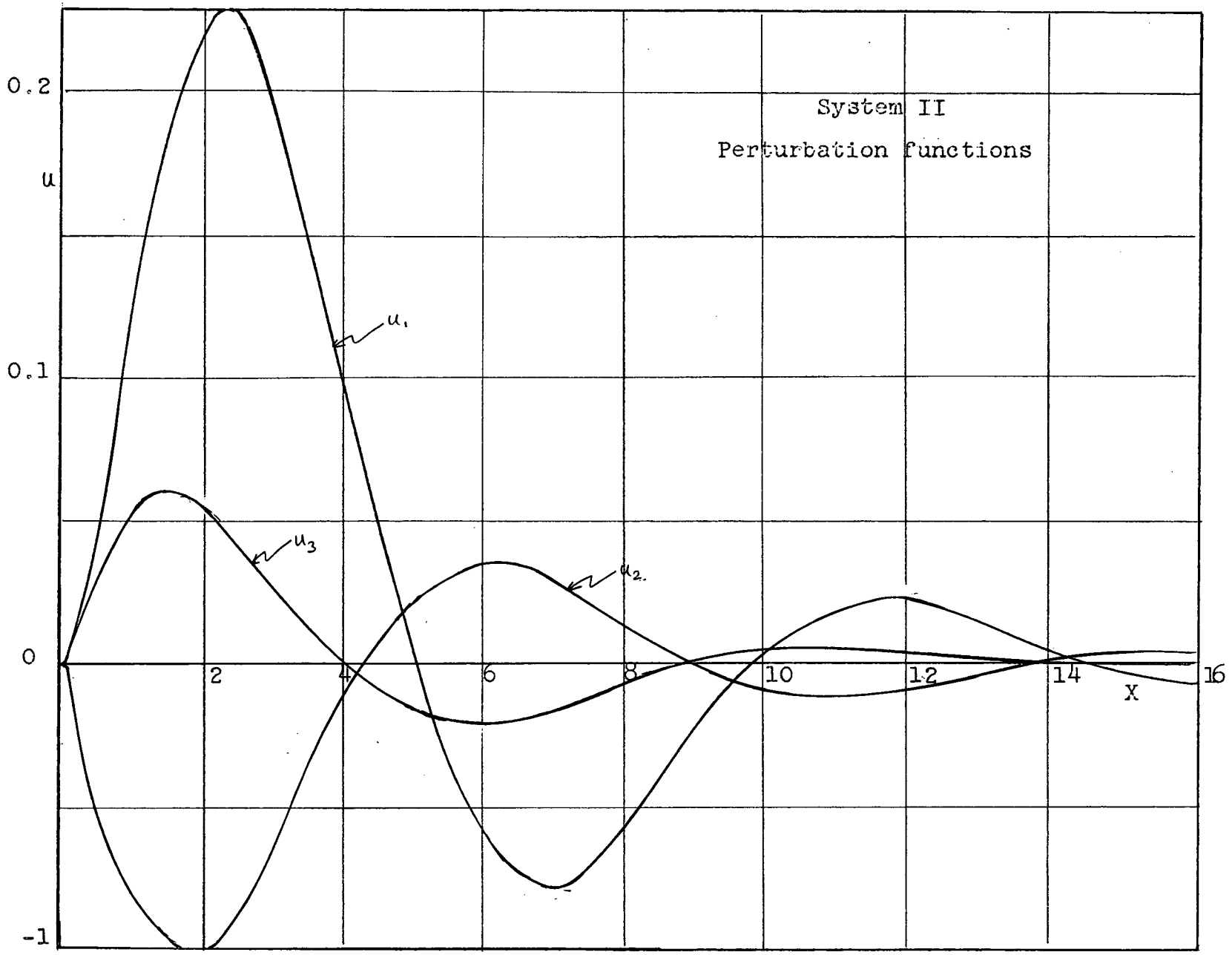
System II
Perturbation functions
0.2
u
0.1
0
-1
2
4
6
8
10
12
14
16
X
u_1
u_2
u_3

Fig. 3.12

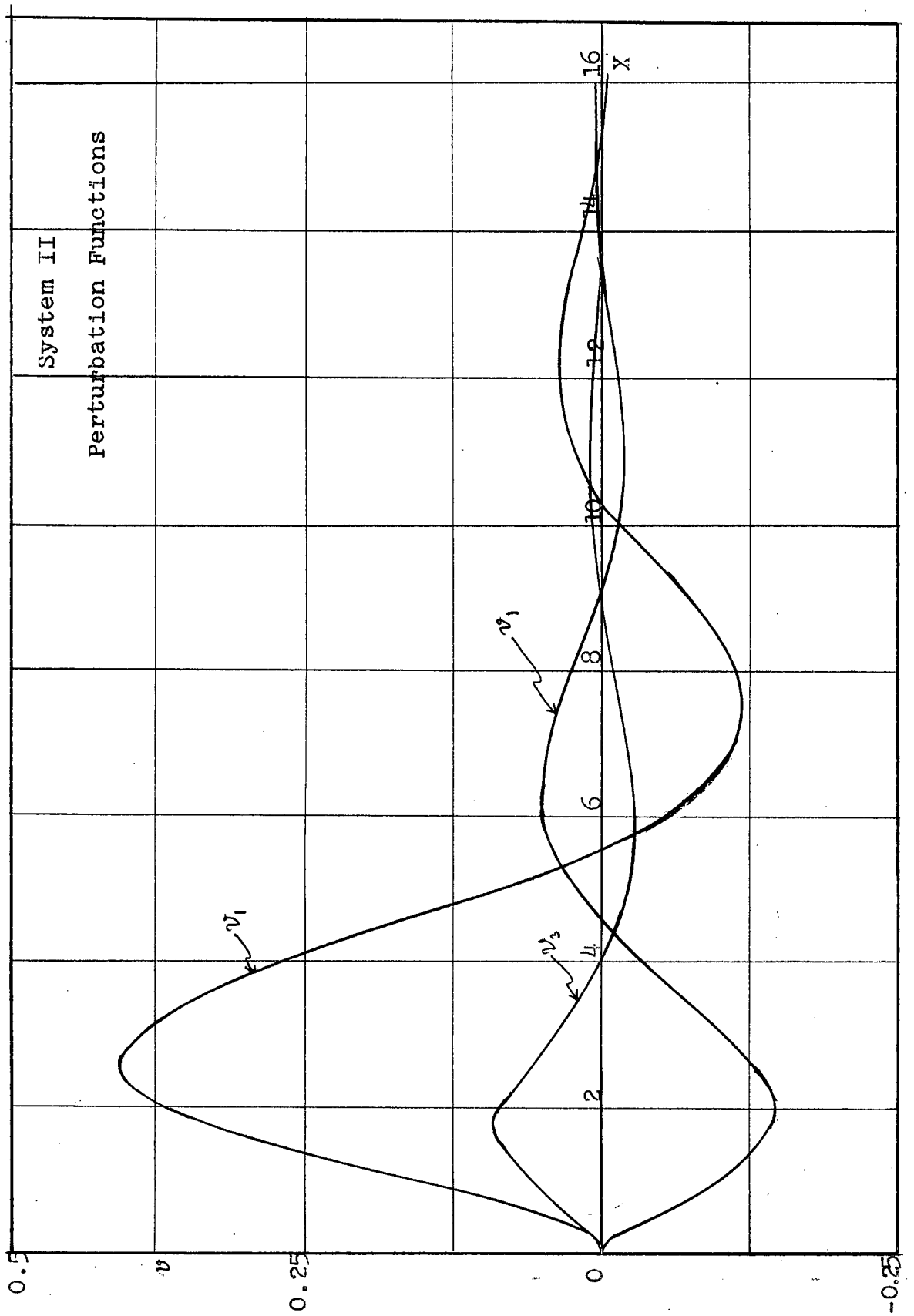
System II
Perturbation Functions
0.5
0.25
0
-0.25
v
2
4
6
8
10
12
14
16
x
v_1
v_1
v_3

Fig. 3.13

the system I is basically unstable. The system II, on the other hand, is characterized by damped oscillating perturbation functions (fig. 3.11 to 3.13) so that the more realistic initial conditions are damped out, leading to a stable system.

The system I,besides being unstable,is not useful as an ion source without an additional accelerating system as it itself does not accelerate the ions. This, however, is not necessary in the system II.

It may be noted that the field in the ionization space is very weak; therefore we expect a small energy spread (apart from the thermal energy spread) in the resulting ion beam.

3.4 Electrode configuration:

There are in practice at least two ways to realize the prescribed potential distribution:

(a) set up a system of electrodes having the shape of the equipotential lines (planes in three dimensions),

(b) set up the potential distribution on the faces of a rectangular box as done by Orr (1963).

The dimensions of the system could be quite arbitrary. However, to satisfy the paraxial approximations involved in the theory (see page 9), we must restrict the actual zone of ionization to a strip of height less than unity on any chosen scale. Note that this does not put any restrictions on the actual dimensions so long as we choose the proper scale, but the potentials have to be properly scaled. All potentials given here are with

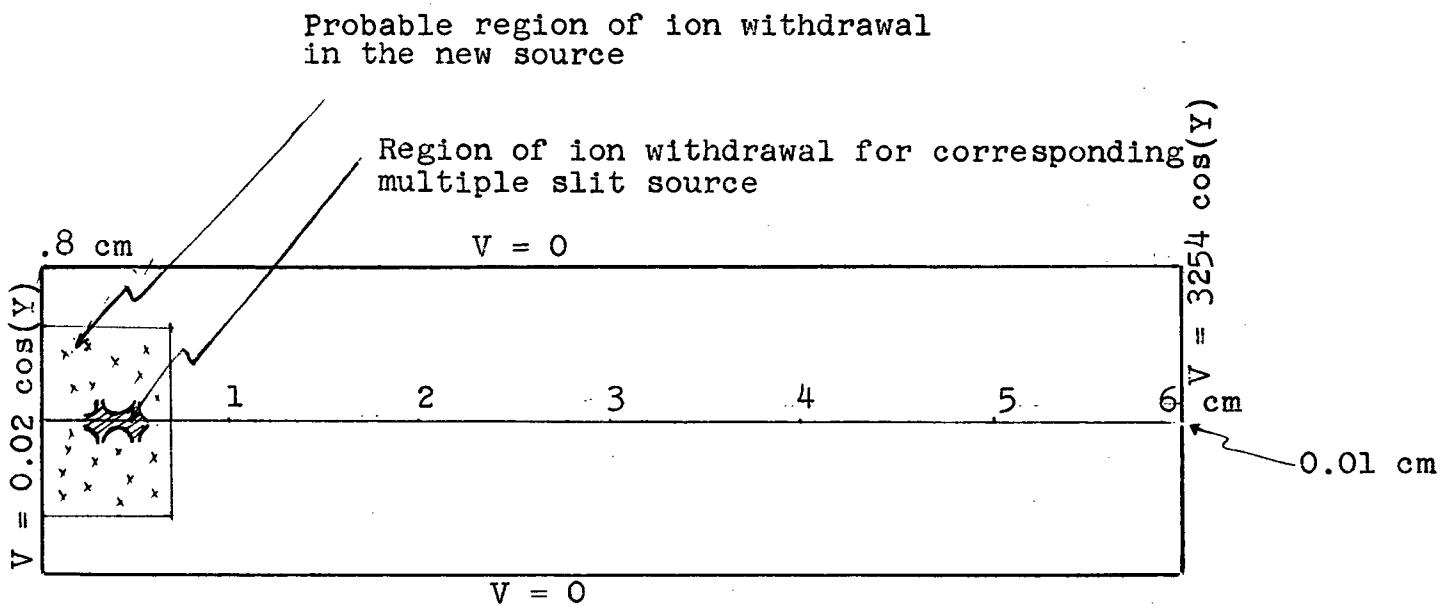

Fig. 3.14

The relative merit of the new source and the multiple slit source. Compare the regions of ion withdrawal.

respect to the initial energy, which was taken as unity for simplicity. If the source is to be operated say at 100° when the average energy is 0.01 volt, the potentials should be scaled down by a factor of 10^2.

Chapter IV

Summary and contributions of the present writer

4.1 Summary:

The sensitivity of a mass spectrometer is a function of the sensitivity of the current measuring system and of the ion source. The latter can be expressed as the product of the efficiency of ionization and the efficiency of ion beam transmission. The preliminary examination of the various sources of limitations has indicated that the low efficiency of ion beam transmission may be a factor limiting the sensitivity of the ion source.

A detailed mathematical analysis of the ion optical properties of the source was undertaken with the aim of evaluating the efficiency of ion beam transmission. A mathematical model representing an average source--a stack of plates carrying parallel and coplaner slits--was investigated. First we developed the equation of trajectory in the generalized two dimensional electric and normal magnetic field. Series of approximations--paraxial approximations--were introduced to linearize the equation of trajectory. Further, the initial energy of the ions was assumed to be zero for the sake of simplicity.

The problem was approached in two different ways:

(a) part-by-part approach

(b) global approach

The part-by-part approach, though not very precise, provides considerable insight into the mechanism of ion beam transmission. On the other hand, the global approach is far more precise but the precision thus gained would be meaningless considering the errors introduced by the paraxial approximations and the assumption of zero initial energy. The model was broken down into several parts and the effect of each part on the ion trajectory was studied.

The combination of repeller plate and the entrance slit plate plays an important role in the mechanism of ion beam transmission. All the ions formed within the limits of these two plates pass through the entrance slit and form a divergent beam. If the repeller plate is at a distance greater than ten times the entrance slit width ($d \geqslant 10$), it is as if being at infinity and may be replaced by a uniform field, the repeller field.

In the absence of the repeller field a divergent beam is formed with its apex at a short distance (about one slit width) from the entrance slit. The width of the beam grows on and is several slit widths (entrance slit width) at the exit slit; hence only a small fraction of the total beam can pass through the exit slit, which is normally a tenth of the entrance slit and the rest of the beam is, therefore, lost completely. We have shown that the ions which pass through the exit slit are drawn from a small horizontal strip of width equal to the exit slit (fig. 2.26).

When the repeller field is present, the situation is dif-

ferent. The beam is still divergent, but the apex is not sharp but diffused along the axis. By adjusting the repeller field, we can focus the ions from a certain part of the ionization space in the neighbourhood of the exit slit. Such a strip of ion withdrawal is, for example, shown in fig. (2.28). The position of the strip may be moved to and fro by varying the repeller field according to the relationship shown in fig. (2.27).

The effect of the exit slit, particularly on the angle of divergence of an ion trajectory as it passes through the exit slit is very small--about 10% of the normal angle of divergence in the absence of the exit slit.

The deflection of the ion beam produced by the deflecting plates is linearly related to the deflecting potential (i.e., the potential difference between the plates). It is found that, for small deflections, the shape of the beam remains unchanged after deflection.

The presence of the magnetic field in the ion source region, if the field is weak (a few tens of gauss), is merely to slightly perturb the shape of the ion trajectory. In the weak field no perceptible mass discrimination is observed.

To increase the efficiency of the ion beam transmission of the present source, we will have to confine the region of ionization to the region of ion withdrawal (2-3 mm wide strip), which in practice, is very difficult to attain. However, we can maximize the efficiency by letting the region of ion withdrawal fall exactly over the region of highest ion density.

A system producing a divergent beam, as is the present multiple slit source, is basically inefficient. On the other hand, a system capable of producing a convergent beam will be more efficient. Instead of pursuing a trial and error method until we hit upon the desired system, we posed to ourselves an inverse problem, that is, given any path, to find the potential distribution so as to guide a particle along the prescribed path. In this connection we have proved the following two basic theorems:

(a) There exists a potential distribution to guide a particle along any desired path.

(b) A group of particles may be guided along a set of paraxial paths.

A case of considerable importance is where the central trajectory is the x-axis. We have considered two types of convergent paths as shown in fig. (3.1) -- exponentially converging and damped oscillatory paths. Although, in principle, we may choose the paths of any shape (but always paraxial) quite arbitrarily, there are certain limitations:

(a) incomplete paths -- a particle may be turned back at a certain point.

(b) unstable system -- abnormal particles, i.e. those not satisfying certain initial conditions of uniform energy and direction deviate considerably from their projected paths.

The two systems we have considered here illustrate the above

limitations. The paths shown in fig. (3.1a) are incomplete and the system is also unstable; while the damped oscillatory paths shown in fig. (3.1b) are complete and the corresponding system is stable, therefore practical.

4.2 Contributions of the present writer:

Following are the contributions of the present writer:

(a) Complete analysis of the ion optical properties of the multiple slit source. That the efficiency of the source is low on account of the small region of ion withdrawal was shown for the first time.

(b) Theory of the inverse problem and its application to efficient ion source. This is considered to be the major contribution.

(c) Mathematical tools such as the solution of certain algebraic equations and the inversion of transformation functions expressing them as differential equations, and the development of a method to take into account the effect of the thermal energy and random initial direction may also be considered as contributions of the present writer.

Appendix A

1. An example of ion source efficiency calculation:

The following are the observations made on the mass spectrometer at the Geophysics Laboratory of the University of British Columbia (A.B.L. Whittles, personal communication):

Total ion current	2.4×10^{-11} amp. (1.5×10^{8} ion/sec)
Mass flow	0.3×10^{-6} gm/hr (2.4×10^{14} mol/sec)
Efficiency of the ion source	0.6×10^{-6}

2. Theoretically expected ion currents:

$$i^{+} = L \times \sigma \times p \times i^{-}$$

where

i^{+}	positive ion current
L	path length of electrons
p	gas pressure
i^{-}	electron beam intensity
σ	Townsend's coefficient of ionization

Reasonable estimates of these parameters are

L	=	2 cm.
σ	=	10 electron/cm/mm Hg
p	=	10^{-4} mm Hg
i^{-}	=	500×10^{-6} amp
i^{+}	=	10^{-6} amp.

3. Effect of the source magnetic field on the electron path lengths:

Let V_z and V_r be the velocity components in the z- and r-directions respectively.

$$B_z \cdot e \cdot V_r = V_r^2 \cdot \frac{m}{r_0}$$

where B_z is the magnetic field in the source region and r_0 the radius of the spiral orbit.

$$dz = V_z \cdot dt$$

$$d\theta = \frac{v_r}{r_0} dt$$

$$dL' = \sqrt{(dz)^2 + (r_0\, d\theta)^2}$$

$$\therefore \quad dL' = \sqrt{V_r^2 + V_z^2}\, dt$$

$$dL' = \sqrt{\left(1 + \frac{V_r^2}{V_z^2}\right)}\, dL$$

where dL' is the electron path length in time interval dt.

$$L' = \int \sqrt{\left(1 + \frac{V_r^2}{V_z^2}\right)}\, dL$$

$$L'/L = \sqrt{\left(1 + \frac{V_r^2}{V_z^2}\right)}$$

where L' is the total path length.

Since $V_r < V_z$ for a well collimated beam, $L'/L = 1$ and also the total path length is independent of the magnetic field.

Appendix B

1. Numerical error estimation:

The commonly used numerical method of solving a set of ordinary differential equations is after Runge (1895) and Kutte (1901). For this method the bounds on the total error committed at the end of each step, though difficult to evaluate an exact expression for, may be estimated from the data obtained at several consecutive steps (Scraton, 1964) or obtained by considering different step sizes. If at three consecutive steps, ΔY_1, ΔY_2 and ΔY_3 are computed with constant step size, an estimate of error is given by Scraton (1964)

$$\text{Error} = \left(10\,\Delta Y_1 + 19\,\Delta Y_2 + \Delta Y_3 - 3h\,y_1' - 18h\,y_2' - 9h\,y_3' \right) / 30$$

On the other hand, if ΔY_1 and $\Delta \bar{Y}_1$ are the computed values at a certain point with step sizes h and $2h$ respectively, the approximate total error is given by Hildebrand (1956)

$$\text{Error} = \left| \Delta Y_1 - \Delta \bar{Y}_1 \right| / 30$$

A few numerical experiments were carried out to estimate the truncation and round-off errors. The round-off error was estimated by carrying out the computation with different number of significant digits: 4, 8, 12 and 16 on a variable word length machine, IBM 1620. The table below shows the results of the computation.

Significant digits	Relative round-off error
4	4%
8	1%
12	10^{-5} %
16	0 (reference zero)

The bulk of computation was, however, carried out on the IBM 7040 with single precision, that is, 9 digits. The round-off error, therefore, is presumed to be less than one percent.

To obtain the above accuracy, it is not necessary to have the step size small everywhere but only close to the slit where the trajectory undergoes rapid changes, and away from it we can take larger steps. The Runge-Kutte process allows the variation of step size at any step; therefore, we have linearly increased the step size -- the smallest step is equal to 0.05 at the slit and increases to 2 at 40 units from the slit.

2. Mathematical complications introduced when the magnetic field is taken into consideration:

For numerical integration of equation (2.15), we write in the form

$$Y'' = -\frac{1}{2}\,\frac{\Phi''(x)\cdot Y(x) + \Phi'(x)\cdot Y'(x) + c\sqrt{\Phi}}{\Phi(x)}$$

where $$C = B_z \cdot \omega \cdot \sqrt{\frac{2q}{mK}}$$

Since at $$x = x_0$$

$$\Phi = 0$$

and $$\Phi'' Y + \Phi' Y' = 0$$

the above equation reduces to

$$Y'' \longrightarrow \frac{1}{2} \frac{C}{\sqrt{\Phi}} \longrightarrow \infty$$

in other words, the equation has a singularity at $x = x_0$. Assuming, however, $\Phi \doteq ax$ as $x \to 0$, it is easy to see from the Cauchy's convergence test that the integral

$$Y = \iint -\frac{1}{2} C \frac{1}{\sqrt{\Phi}} dx$$

is convergent, but the numerical process cannot be initiated at that point. This difficulty can be overcome by adopting a physical view--the force due to the magnetic field tends to zero as velocity tends to zero; therefore, we may drop off completely the term containing the magnetic field when initiating the numerical process.

Bibliography

Allard, J. L. and Russell, R. D. (1963) The electric potential in the region of a thin slit. Brit. J. Appl. Phys., Vol. 14, 800.

Boerboom, A. J. H. (1957) De Ionenoptik Van de Massaspectrometer, Unpublished Ph.D. thesis, Rijksuniversiteit te Leiden.

Boerboom, A. J. H. (1959) Numerical calculation of the potential distribution in ion slit lens system I. Z. für Naturforschung, Vol. 14, 809.

Boerboom, A. J. H. (1960) Numerical calculation of the potential distribution in ion slit lens system II. Z. für Naturforschung, Vol. 15, 244.

Boerboom, A. J. H. (1960) Numerical calculation of the potential distribution in ion slit lens system III. Z. für Naturforschung, Vol. 15, 253.

Boerboom, A. J. H. (1960) Modified ion slit lens for virtual variation of slit width. Z. für Naturforschung, Vol. 15, 350.

Courant, R. and Hilbert, D. (1953) Methods of mathematical physics. Vol. II, Interscience Publishers, Inc.

Cutler, C. C. and Hines, M. E. (1955) Thermal velocity effects in electron guns. Inst. of Radio Engineers Proc., Vol. 43, 307.

Dietz, L. F. (1959) Ion optics for V-type surface ionization filament used in mass spectrometer. Rev. Scientific Instruments, Vol. 30, 235.

Einstein, P. A. and Jacob, L. (1948) On some focal properties of an electron optical immersion objective. Phil. Magazine, 39, 20.

Hellwig, G. (1964) Partial differential equations, An introduction. Blaisdell Publishing Co., Chap. III.

Hildebrand, F. B. (1956) Introduction to Numerical Analysis. McGraw-Hill Book Co.

Jacob, L. (1950) Some cross-over properties in the electron immersion objectives. J. Appl. Phys., Vol. 21, 966.

Jacob, L. (1951) An introduction to electron optics. Mathuen Publications.

Kamke, E. (1959) Differentialgleichungen Lösungsmethoden und Lösungen. Band I, Chelsea Publishing Company.

Kirsteinen, P. T. (1963) Thermal velocity effects in axially symmetric solid beams. J. Appl. Phys., Vol. 34, 3479.

Mayne, K. I. (1960) Stable isotope geochemistry and mass spectrometric analysis, in Methods in Geochemistry. Edited by Smales, A. A. and Wager, L. R., Interscience Publishers Inc.

Morse, P. M. and Feshbach, H. (1953) Methods of theoretical physics. Vol. I, McGraw-Hill Book Co.

Moulton, F. R. (1926) Methods in exterior ballistics. Dover Publications Inc., Chap.IV.

Naidu, P. S. (1962) Studies on the telluric field response of some geological inhomogeneities. Unpublished M. Tech. thesis, Indian Institute of Technology, Khargpur, Calcutta.

Orr, D. (1963) Aberrations in electrostatic quadrupoles. Nuclear Instruments and Methods, Vol. 24, 377.

Pierce, J. R. (1954) Theory and design of electron beams. D. van Nostrand Company Inc., Chapter II.

Poincaré, H. (1905) Les methodes nouvelle de la mecanique celestia I, Chap. II, Gautheir-Villars, Paris.

Scraton, R. E. (1964) Estimation of truncation error in Runge-Kutte method and allied processes. The Computer Journal, Vol. 7, 246.

Shibata, N. (1960) On a solution of the paraxial ray equation in an axially symmetrical electrostatic field. J. Phys. Soc. Japan, 15, 200.

Stacey, J. S. (1962) Method of ratio recording for lead isotopes in mass spectrometer. Unpublished Ph.D. thesis, University of British Columbia.

Vauthier, R. (1955) Applications de l'optique des chargé electriques a la spectrometrie de masse. Annales de Physique, Vol. 10, 968.

Waters, W. E. (1958) Rippling of thin electron ribbons. J. Appl. Phys., Vol. 29, 100.